Integrated Control System for Frequency and Voltage support via Type-3 Wind Turbines equipped with Energy Storage System

Christos M. Nikolakakos

Delft University of Technology

TU Delft Delft University of Technology

Challenge the future

Integrated Control System for Frequency and Voltage support via Type-3 Wind Turbines equipped with Energy Storage System

by

Christos M. Nikolakakos

in partial fulfillment of the requirements for the degree of

Master of Science
in Electrical Engineering

at the Delft University of Technology,
to be defended publicly on Friday July 5, 2019 at 3:00 PM.

Supervisor:	Dr. ir. M. Cvetkovic	
Thesis committee:	Prof. dr. P. Palensky,	TU Delft
	Dr. ir. M. Cvetkovic,	TU Delft
	Dr. Z. Qin	TU Delft

TU Delft Delft University of Technology

Acknowledgements

"Κάνταῦθα, ὦ ξένε, τὸ νικᾶν αὐτὸν αὐτὸν πασῶν νικῶν πρώτη τε καὶ ἀρίστη, τὸ δὲ ἡττᾶσθαι αὐτὸν ὑφ᾽ ἑαυτοῦ πάντων αἴσχιστόν τε ἅμα καὶ κάκιστον. ταῦτα γὰρ ὡς πολέμου ἐν ἑκάστοις ἡμῶν ὄντος πρὸς ἡμᾶς αὐτοὺς σημαίνει"

– Πλάτων, «Νόμοι, 626.e. 2 – 5»

This thesis closes my circle as a student, since it is my last obligation to obtain the Master's degree in Electrical Engineering. It is necessary to express my gratitude to all those people who contributed towards this cause.

I would like to thank Dr. Milos Cvetkovic for his help during my studies and the opportunity that gave me to contribute in a research project like this. Without his trust and guidance during those 9 months the completion of this thesis could not be possible. Moreover, I want to thank Assoc. Professor Peter Palensky and Dr. Z. Qin for their time and accepting being part of my thesis committee. I feel also the need to express my gratitude to PhD Candidate Umer Mushtaq for being my daily supervisor and helping me overcome any arising research problem.

The presented thesis is performed in collaboration with EASY-RES project of European Union Horizon 2020 initiative with Grant agreement: 764090.

It would be an omission, not to thank my friends, who stood by me at my ups and downs, especially during the last two years. Thanks for your patience and understanding during my struggles.

Moreover, I would like to express my gratitude to my beloved Elli, for her love and support, while patiently tolerating me during Delft's "Blue days". She was the remedy for all my difficulties. The best is yet to come.

Last but not least, I would like to thank my family for being next to me in every step I decide to make and their support. This accomplishment would not have been possible without them. Thank you from the depths of my heart.

Christos M. Nikolakakos
Delft, July 2019

Abstract

During previous centuries, humanity had relied on fossil fuels to generate the demanded energy. Nowadays, the extensive use of oil, gas and coal for energy production is becoming a major problem which concerns modern society. Global warming and climate change are the biggest challenges the scientific community has faced. The main factor which causes those problems is the high dependence on fossil fuels. Moreover, those resources are naturally limited and will extinct in time.

For all those reasons, during the last decades, there is intense research on finding ways to produce the needed energy in a sustainable fashion. Renewable Energy Sources have a minimal impact on the environment compared to traditional energy sources. Those resources can effectively tackle the problems which arise with fossil fuel usage.

Among all the Renewable Energy Sources, wind energy is the most promising and becomes one of the mainstream power sources in many countries around the world. This happens because wind energy conversions systems have reached a mature stage for wide-scale integration. Type 3 Wind Turbines are those who hold the most significant market share due to their cost-effectiveness and flexibility.

Synchronous Generators, which are dominant in the existing power grid, have the inherent feature to relate system's frequency with load balance due to their characteristics. The most considerable disadvantage of the Renewable Energy Sources and specifically wind energy is that they do not provide that feature since they are inverter-based and lack of inertia. Thus, when their penetration is increased, the system's stability and reliability are endangered. Moreover, during the past years, Renewable Energy Sources were rewarded only for providing Active Power to the grid; thus, they did not participate in voltage regulation. This situation can risk the voltage stability of the system with high renewable penetration.

Current research confronts those problems, by proposing control systems which operate the wind turbine in lower power output than its optimal. By this, a power reserve is kept to be utilized during disturbances. This type of operation is sub-optimal for all the stakeholders (system and wind turbine operators). Regarding voltage support, the existing control systems, for Type 3 wind turbines are not capable of dynamically allocate the reactive power injection between its components. This can overload and damage the power electronic components which are very sensitive to that kind of disturbances. Another drawback of all the previously mentioned controls is that they cannot provide a complete solution since they only act against one disturbance.

To overcome those problems, the presented thesis proposes an enhanced topology for the Type 3 Wind Turbine, by adding an Energy Storage System at the DC Link of its the "Back to Back" converter topology. This storage is controlled with the help of a Bi-Directional DC-DC converter which allows storage charge and discharge to the grid. With this feature, the proposed system can mitigate frequency deviations and store energy, when it is possible, to be used in future disturbances. Moreover, since the extra power is provided from the storage, the wind turbine is capable of operating in its optimal point. Furthermore, appropriate control of the DC-DC converter, which allows the Energy Storage System to support the grid's frequency is suggested.

Moreover, regarding voltage support, the existing Type 3 Wind Turbine controls were expanded to take into consideration system loading when providing reactive power to the grid. With that way, it is ensured that support is provided from the appropriate piece of equipment without any damage risks. Both frequency and voltage controllers are integrated under one controller which is capable of offering both ancillary services.

In order to identify the proposed system's impact on a power grid, the Type 3 Wind Turbine model with its respective controllers is modelled with the help of RSCAD. This model was developed in small-time step, which makes it qualified for Hardware-in-the-Loop simulations. Real time simulations were conducted with the help of Real-Time Digital Simulator (RTDS) platform to investigate the performance of the previously mentioned control systems for different power system disturbances under different scenarios. The results prove that the proposed topology and control strategies can effectively provide ancillary services to the grid and secure its normal operation.

Contents

List of Tables

List of Figures

List of Abbreviations

AVR Automatic Voltage Regulator.

DFIG Doubly-Fed Induction Generator.

ESS Energy Storage System.

FSM Frequency Sensitivity Mode.

GSC Grid Side Converter.

HIL Hardware-in-the-Loop.

LFSM-O Limited Frequency Sensitivity Mode - Over-Frequency.

LFSM-U Limited Frequency Sensitivity Mode - Under-Frequency.

MPPT Maximum Power Point Tracker.

PCC Point of Common Coupling.

PLL Phase Locked Loop.

PWM Pulse Width Modulation.

RES Renewable Energy Sources.

RfG Requirements for Generators.

RoCoF Rate of change of frequency.

RSC Rotor Side Converter.

SG Synchronous Generator.

TSO Transmission System Operator.

VSC Voltage Source Converter.

WF Wind Farm.

WT Wind Turbine.

Dedicated to my family.

1

Introduction

This chapter presents an extensive introduction about the subject and the content of the presented thesis.

First of all, the necessary background about renewable energy and specifically wind energy is shown. Afterwards, the motivation for the research is presented, and the problem that this thesis solves is defined.

Moreover, the research questions and the objectives of the presented thesis are demonstrated.

Finally, the approach chosen in order to answer the research questions and fulfil the objectives is demonstrated, and a summary of each following chapter is presented.

1.1. Background

Nowadays, global warming is becoming a concerning issue for the international community. As it is known, CO_2 emissions are responsible for a high rate of greenhouse gases, one of the main global warming causes. In order to limit this effect, many countries have decided to restrict their emissions in a significant percentage. A drastic measure to deteriorate global warming is the de-carbonization of the energy sector, which is responsible for an important part of the emissions mentioned above [1]. It is clear that fossil fuels are widely used for electric generation, as shown in Figure 1.1. Thus it is critical to limit this rate to reduce electric generation CO_2 footprint.

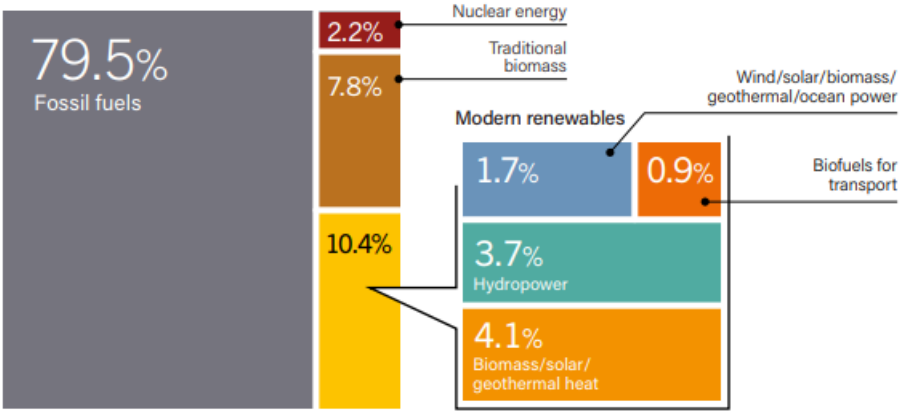

Figure 1.1: Global Energy Consumption mix [2].

To this end, traditional fossil-fuel generators are gradually decommissioned, and Renewable Energy Sources (RES) take their place. Energy is considered as renewable when it can be replenished in a natural way. Examples of renewable energy are geothermal heat, sunlight, wind and tides. Since renewable energy is ”infinite” and produces low amounts of greenhouse gases, it is considered a feasible solution to mitigate the aforementioned global warming problems [3].

Wind Energy becomes one of the most popular power sources among others RES [4]. In fact, Wind Energy is the most used RES (excluding hydro), with its capacity, rapidly increasing globally during the last decades. This happens due to the fact that its energy is "green" and has high reserve. Also, it has almost zero carbon footprint and does not contribute greenhouse emissions [3]. The share between the different RES depicted in Figure 1.2, makes clear that Wind Energy occupies more than half of the RES capacity worldwide.

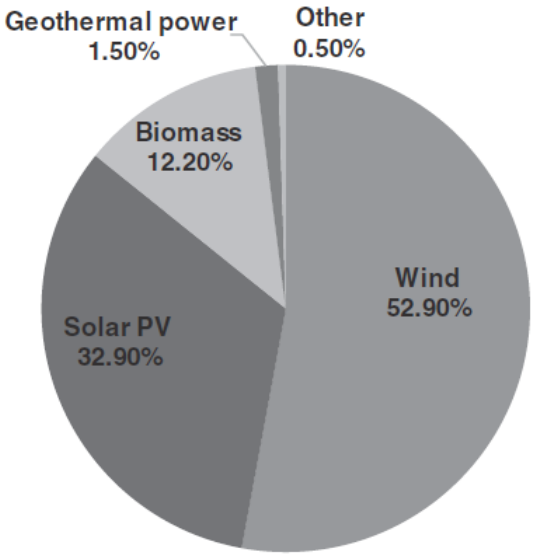

Figure 1.2: Capacity Share of different RES (excluding hydro) [3].

1.2. Motivation

By the aforementioned information, it is clear that renewable sources and especially wind energy is going to hold a key role in the future of power generation. This leads to the need of researching the impact that this penetration is going to have to the existing utility grid and finding ways to make the transition to a RES-based generation system feasible by ensuring grid's stability.

The most important parameters of the grid that define its stability are frequency and voltage, which have to be maintained into specific limits that are defined by each country's grid code. The de-carbonization of the electric energy by increasing renewable penetration can endanger this stability if it is not done in a proper fashion. The substitution of traditional Synchronous Generators (SGs) with power electronic interfaced RES drives to several problems that need to be addressed for a smooth and secure transition.

As it is known, Synchronous Generators, due to their mechanical and electrical characteristics, inherently associate load balance at the power system with frequency. This assumption is not valid for RES which, as mentioned before, are interfaced with the existing utility grid with power electronic devices. This means that RES generators and specifically wind turbines (WTs), which are the subject of the current thesis, cannot inherently support the grid's frequency. This situation, in a future scenario with high wind penetration, is going to make frequency volatile. Except for frequency, rate of change of frequency (RoCoF) is another important index that needs to be taken into responsibility. During the previous years, when generation was provided mostly by SGs with inherent inertia, RoCoF had minor significance, since the inertia as mentioned above inherently limited this rate of change when power imbalance occurred. Although, in a future system with high RES penetration, due to decreased system's inertia, RoCoF values will increase, which endangers the stable operation of the system. Synchronous Generators, due to their inherent mechanical limitations are stressed from high RoCoF values and protection devices can be triggered if high RoCoF happens [5]. It can be perceived that all those reasons become a major drawback when it comes to high levels of RES penetration to the existing grid.

Regarding Voltage stability, Synchronous Generators, which in the existing system are responsible

for providing power to the grid, are equipped with control systems that modify their excitation in order to match their output voltage to the desired one. Those systems are widely known as Automatic Voltage Regulators (AVR). During the past years, most RES power generation units such as WTs, were operated under Unity Power Factor (UPF). This means that they did not provide reactive power to the grid since active power production is the one that was rewarded by the Transmission System Operators (TSOs). As the level of RES penetration increases, more and more TSOs are going to require from WTs operators to be capable of providing reactive power support to the grid, to ensure stable operation [6].

1.3. Problem Definition

It is comprehensible, from section 1.2 that nowadays, SGs are responsible for regulating grid's frequency and voltage. The operations needed, beyond generation and transmission, in order to maintain grid stability and security are widely known as **Ancillary Services**. As mentioned in section 1.2, traditionally, RES did not provide the grid's voltage and frequency stabilization ancillary services to the grid. Although this is not going to be the case in the future power grid, where RES will be dominant.

Currently there are different proposals in literature regarding inertial response and primary frequency control [7, 8, 9, 10, 11, 12, 13]. The drawback of all those techniques that are used in order to provide frequency support to the grid, is that they operate WT in a lower point than their maximum; thus power generation is not optimal. This is not efficient for any of the stakeholders, neither for Wind Farm (WF) operators, who are rewarded by the active power injected to the grid nor for the TSO, since during steady state there is a percentage of "clean" renewable energy that not utilized.

Like frequency, there are also different control strategies in literature regarding WT participation in grid's voltage regulation [6, 14, 15]. The drawback of all those control strategies is that they focus on providing reactive power from a specific WT component, regardless the operational scenario (sub and super-synchronous operation). This may lead to power electronic converter limit overload which can damage the equipment.

Finally, all the aforementioned controllers act separately and manage to cure only one disturbance, frequency or voltage respectively. In a real system those disturbances may happen simultaneously. This means that those controllers are not able to guarantee the stable operation of the grid.

1.4. Thesis Objectives

The main objective of this thesis is to provide an integrated controller which enables Type-3 (Doubly-Fed Induction Generators or DFIG) Wind Turbines to provide frequency and voltage support to the utility grid. Moreover, an enhanced topology is examined, which allows more efficient exploitation of WT by always operating it at its maximum power point, in order to tackle all of the problems mentioned at section 1.3.

To this end, an Energy Storage System (ESS) is implemented at the DC Link of the "Back-to-Back" converter configuration of the DFIG. In order to make it fully controllable and capable of providing its power in order to support the grid's frequency, a DC-DC converter is used as an interface. This converter is Bi-Directional, allowing ESS to inject and also absorb power from the grid when needed. This ESS combined with the DC-DC converter will be capable of providing frequency support when a disturbance is detected.

Moreover, an efficient control strategy is proposed to provide reactive power in a secure manner, to avoid overloading situations and protect the DFIG and its power electronic converter circuits.

Since DFIG utilizes Voltage Source Converters (VSC) it is capable to separately control its active and reactive power output. This feature makes it is possible to combine the aforementioned control systems in order to provide support for both frequency and voltage disturbances.

1.5. Research Questions

Since the thesis objectives were defined, it is possible to define the research questions, that thesis is called to answer. Those questions are summarized below:

- **How the performance of the proposed DFIG combined with ESS configuration is assessed, regarding its frequency and voltage support capabilities?**
  Is the proposed system capable of supporting the system, or a disturbance such as a load change or a generation loss will make the system unstable, which leads to collapse?
  TSOs require from their power generating units to change their active power output in response to a change in system frequency, in such a way that it assists with the recovery to target frequency. The pattern, which the active power has to follow in response to a frequency disturbance is defined in TSO's Grid Code regarding its Requirements for Generators (RfG). Is the proposed system capable of following that pattern to comply with the TSO's RfG? This validation is very important, since TSOs allow grid connection to those generating units which are able to comply with those requirements.
  Regarding voltage stability, TSOs define a specific range, where the system shall be operated. Is the proposed system capable of maintaining the voltage between those voltage levels for a safe steady-state operation?

- **What is the performance of the proposed system for different penetration scenarios?**
  It is mentioned in section 1.2, that increasing RES penetration at a power system, makes it more vulnerable to disturbance events and volatile. Does this also happen with the proposed system and control scheme? In order to identify the performance, comparisons of different system indices, like Rate of Change of Frequency RoCoF, Voltage and Frequency nadir and settling time, between different penetration scenarios are going to be examined. The performance of the system is going to be considered satisfactory since it has similar or enhanced behaviour compared to the system when it is operating only with SGs.

- **How robust is the proposed control scheme, by means of its ability to handle disturbances in power system?**
  Is the proposed system able to mitigate disturbances in the power system, such as load changes or loss of generation by providing the necessary active or reactive power to maintain the system stable? How is the system affected by measurement delays that occur in the control system? What is the influence of the controller gains? Are the controller saturation limit decided in a way that ensures system stability? The proposed system is going to be considered as robust since it can successfully handle the aforementioned disturbances and modify its active and reactive output in an appropriate fashion, which contributes towards grid's voltage and frequency stabilization.

1.6. Methodology

In order to be capable of assessing the impact of a Type-3 WT proposed topology in a power system, a detailed model has to be developed. The software is used for this modelling is RSCAD. Moreover, in order to make the model capable of being used for Hardware-in-the-Loop (HIL) simulations, the DFIG model and its power electronic converter configuration is going to be modelled in "Small Time-Step". This is a feature provided by RSCAD, in order to use the model for that kind of simulations with the help of RTDS hardware.

There is an available DFIG model, with its respective converters. For the sake of this thesis, that model has to be expanded and an ESS has to be connected with the DC Link of the "Back-to-Back" converter configuration via a Bi-Directional DC-DC converter, which needs to be built as a "Small Time-step" model by using the appropriate components.

Finally, the control systems which enable the proposed DFIG topology to provide frequency and voltage ancillary services to the grid have to be implemented, with the help of RSCAD software.

1.7. Thesis Contribution

The key contributions of the presented thesis can be summarized at the following list :

- Design and implementation of a Type-3 (DFIG) WT "Small Time-step" model in RSCAD, equipped with an ESS connected to the DC Link of the "Back-to-Back" AC/DC/AC Converters. For this ESS integration, a Bi-Directional DC-DC Converter is going to be modelled and implemented. This model will be suitable for Hardware-in-the-Loop (HIL) simulations in RTDS hardware.
- Control system development and integration for the Bi-Directional DC-DC Converter, while expanding the existing controllers of the AC/DC/AC converter configuration in order to make them capable of providing ancillary services to the grid.
- Implementation and studies of the proposed DFIG WT with ESS system at a benchmark system for different operational scenarios (like those mentioned at subsection 1.5).
- Comparison and assessment of the system's performance for different operational scenarios.

1.8. Thesis Outline

A summary for each of the next chapters of the presented thesis is presented below:

- Chapter 2: A lower level description of RES and its importance for the future power grid is going to be presented. Since Wind Energy is the subject of this thesis, a review of history and contemporary developments and an explanation of different Wind Farm (WF) applications are shown. After that, the different types of WTs are shown, and their operation is explained. Finally, a literature review of ancillary services and state-of-the-art control strategies that Type-3 WTs are equipped with, in order to provide those ancillary services are discussed, both for frequency and voltage support.
- Chapter 3: In this chapter, mathematical modeling of all the Type-3 WT components is presented. Especially, the system is broken down into simpler components, and their respective mathematical modelling is demonstrated. Moreover, the basic control of DFIG is shown and explained.
- Chapter 4: In this chapter, the proposed topology for the DFIG equipped with an ESS and the respective control systems of the Grid Side Converter (GSC), Rotor Side Converter (RSC) and the Bi-Directional DC-DC Converter which is utilized to control the power injection from ESS to the DC Link of the "Back-to-Back" converter configuration, such as the opposite direction is demonstrated. The integrated proposed control system is capable of mitigating both frequency and voltage disturbances to the grid, with appropriate modification of active and reactive power output.
- Chapter 5: In this chapter, an extensive presentation of simulation results is presented. This includes results for frequency, voltage and combined disturbances, in order to identify the ability of the proposed system and control scheme to mitigate those disturbance events. Results are demonstrated for various scenarios, like different penetration levels, different proportion of WT equipped with ESS and others, mentioned in subsection 1.5 of this chapter. The results are compared, and a brief analysis is provided
- Chapter 6: In this chapter, the results demonstrated in Chapter 5 are furtherly explained, and the performance of the proposed system is evaluated for all different scenarios. The conclusions are demonstrated, and the research questions are thoroughly answered. Finally, the contribution of this thesis is highlighted.

2

Theoretical Background

In this chapter, a review of renewable energy sources and their necessity for the sustainable power system of the future is going to be discussed. Furthermore, a theoretical analysis of wind energy and its conversion to electric power, which is utilized to the grid will be conducted, by also referring to the State-of-the-Art existing technologies. Finally, there will be a description and explanation of ancillary services, the way they maintain system's stable and secure operation is presented and the reason why those services are affected by increased RES penetration changes.

2.1. Importance of Renewable Energy

Nowadays, there is an increasing demand for energy as a consequence of the economic development and growth of the last decades [16]. This increase also applies to electric energy.

Currently, most of the electric power demand is covered by fossil fuels. This leads to CO_2 emissions, which have many side-effects and drawbacks, such as global warming and material emission, which are a hazard for living creatures. Another serious disadvantage of fossil fuels is the fact that they are limited in nature and will diminish in time. The remaining reserves that still exist are in places that is either dangerous or also expensive to look for (i.e. ocean floor) [17] .

Extracting electric power from nuclear plants, which is an alternative, also includes great health, environmental and safety risks. As seen from previous accidents at nuclear plants, a failure in such a plant, which may be caused from a human error or an equipment malfunction, may lead to tremendous disasters for humans and environment, not only after the accident but also in a long term due to the contamination [17].

By the information mentioned above, it is easy to understand why renewable energy sources seem such an appealing and sustainable option for modern societies. First of all, their operation has a minimal footprint on the areas where they are installed, in contrast to the conventional power generation units. Furthermore, the research on renewables and the improvement of infrastructures will lead to a more cost-effective from an economic and environmental perspective, energy. At this moment, European energy policies promote RES, since they can cover electric energy demand. This potential of RES, allow European Union members to strengthen their energy sector in a "green" and sustainable fashion and simultaneously reduce their fossil fuel needs, and as a consequence their dependence from the countries which export them. At this moment, half of the energy consumption is covered with imported fossil fuels, which makes Europe very energy-dependent and insufficient [17].

From what has referred above, it is clear that are able to increase the energy supply, making European countries more independent of fossil fuels. With RES, it is possible to tackle many problems introduced by fossil fuels, such as their price volatility and securing the energy supply. It also has to be stated that, with the proper utilization of RES, the funding of importing conventional energy sources can be reduced significantly, and the difference can be invested in other sectors.

Finally, RES are also capable of allowing governments to reduce CO_2 emissions in order to protect the environment and living creatures. During the last years, there is an emerging trend by European Union countries to reduce greenhouse gases. Their target is, to reduce the aforementioned emissions by 80-95% below 1990 levels, by 2050. Also, as a short-term target, by 2020, EU countries desire to

reduce their emissions by 20% below 1990 levels as a part of the European 2020 strategy, in addition to the Kyoto Protocol agreement.

Carbon dioxide is released mainly due to the fossil fuels that are used for electricity and heat generation, which highly contributes to global warming [17]. The effects of global warming can lead to disastrous consequences for human and environment. To this end, RES which are "green" sources of energy and more Eco-friendly than the conventional sources, are able to help towards the minimization of CO_2 emissions. In comparison with the conventional power plants, RES have a minimum footprint, which is small and localized. Moreover, they can help towards the development of rural areas without electricity in developing countries, by providing cheap and reliable electrification.

2.2. Wind Energy

As seen from section 2.1, renewable energy is going to play an important role during the next years for sustainable economic growth. Among these many renewable resources, wind power is one that offers a mature technique, as well as promising commercial prospects, and is now generally applied in large-scale electricity generation.

2.2.1. Wind Energy History and Development

There are many renewable resources, as previously mentioned, such as solar, tidal, etc. but the wind seems to be the one that is more capable of being applied in a large scale [16]. Extracting power from wind is not a new concept. Societies use wind power for more than 3000 years, and during the last century, humans start to exploit wind energy in order to produce electric power. In Ancient Egypt, windmills were used for water pumping, as well as Chinese farm workers were exploiting wind energy to drain rice fields. At 1887, windmills started to be used for electricity generation [18]. The first horizontal wind turbine was prototyped in 1941 in the US in order to electrify isolated rural areas. Despite that, the following years there was any development, due to oil low, competitive prices [16]. It is noted during the years, that the development of wind power was highly dependent on oil and other fossil fuel cost. After the oil crisis, wind power usage experienced a huge development, and this trend exists until today.

2.2.2. Wind Energy Nowadays

During the last decade, wind energy is used by many countries as an electric power source, as a result of the CO_2 emission targets that were referred at section 2.1. In Figure 2.1, the wind power capacity development during the last decade is depicted. Nowadays, wind power is calculated as 55% of the

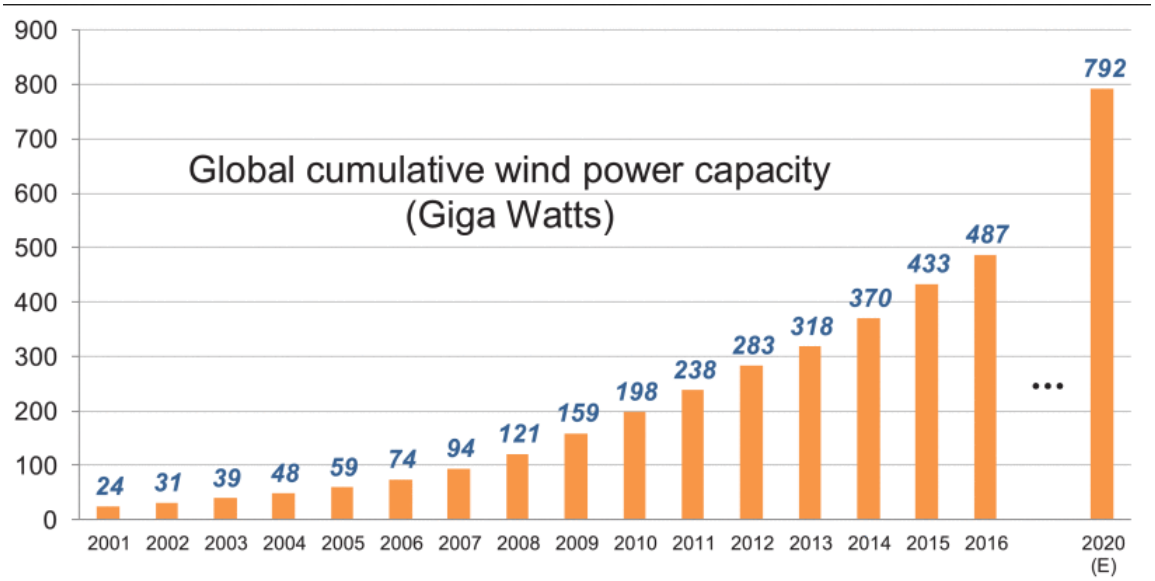

Figure 2.1: Cumulative Wind Power capacity during the last decade [19].

renewable capacity globally, excluding hydro. Wind power covered 3.7% of the global electric power demand during 2015. Especially in Europe, many countries have a high penetration of wind power (i.e. Denmark, Germany, Portugal). Furthermore, it has to be noted that Denmark's power generation from wind quite often exceeds the consumption of the country [19].

This development would be impossible without the evolution of wind turbines. During the previous decades, wind turbine size and power rating have increased as can be seen in Figure 2.2.

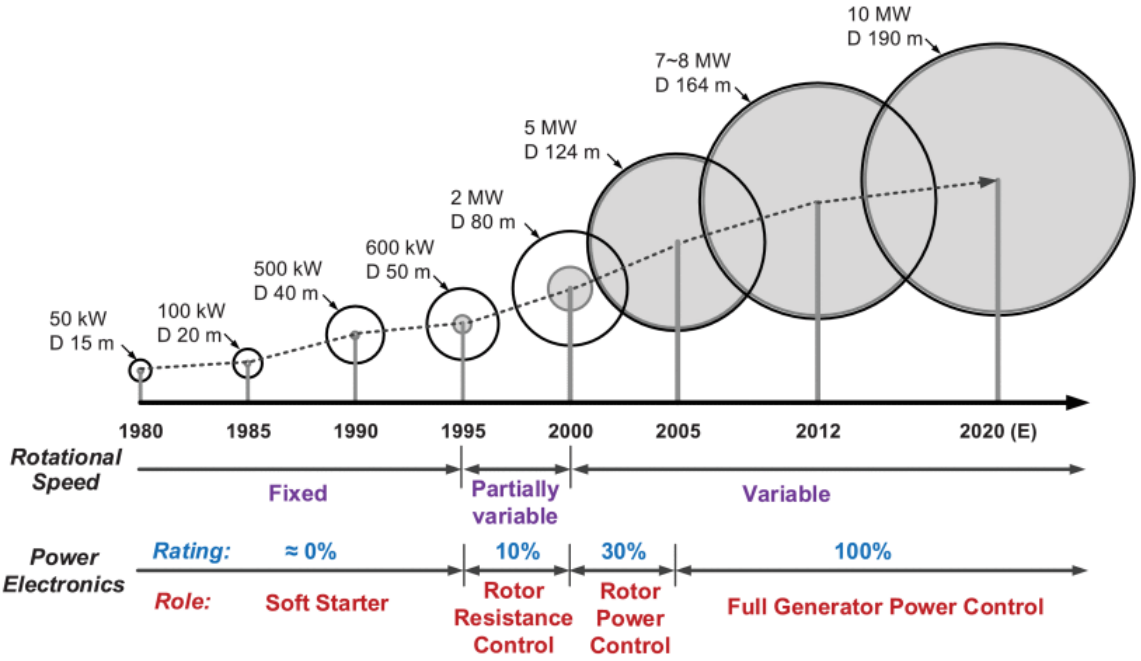

Figure 2.2: Development of WT during the years [19].

It can be noticed by Figure 2.2, that the development of wind turbines, is highly related to the evolution of power electronic devices during these years, which allowed higher power levels and controllability of wind turbines. Nowadays, main WT manufacturers, build their wind turbines in the power range of 4-6 MW and there is an effort to push this range in a higher level, due to the need of electric energy cost reduction.

It is widely known that there are two types of Wind Farm (WF) installations:

Onshore Wind Farms

Onshore wind farms are those farms which lay on the land. Most of the wind farms nowadays belong to this type of wind farms. United States own currently, the largest part of onshore wind farms, in terms of capacity with China coming after. Although Europe has a large number of onshore wind farms, none of them is large enough as a unit, to be compared with the aforementioned infrastructures. Onshore WFs main advantage is that they can be deployed easier than an offshore WF and their connection with the grid is easier to establish. On the other hand, the main disadvantages of the onshore installations are that there is a visual impact on the natural landscape, some animal species like birds may be affected by the rotating blades, and finally, it has been reported that wind turbines contribute to noise pollution [19].

Offshore Wind Farms.

During the last years, there is an emerging trend towards offshore wind farms. This is happening due to the scarcity of available space to install onshore wind farms. As expected, this fact led to extensive research and development of offshore farms, in order to be able to provide power in a secure and consistent manner.

The main advantage of offshore wind farms, is those wind characteristics are better offshore since usually, it is blowing faster and stronger, which means the potential of higher power generation. Furthermore, since they are installed far away from land, their noise can be ignored, and human life is not

affected by their visual impact [16]. On the other hand, their connection with the main utility grid is harder and needs sophisticated equipment, which makes them a more expensive choice.

The increase of offshore wind penetration in Europe can be identified by the following graph shown in Figure 2.3, which depicts the ratio of onshore and offshore wind farm installation. It is clear that during the last years, offshore installations are increasing more rapidly. This fact shows a clear trend toward this kind of infrastructure.

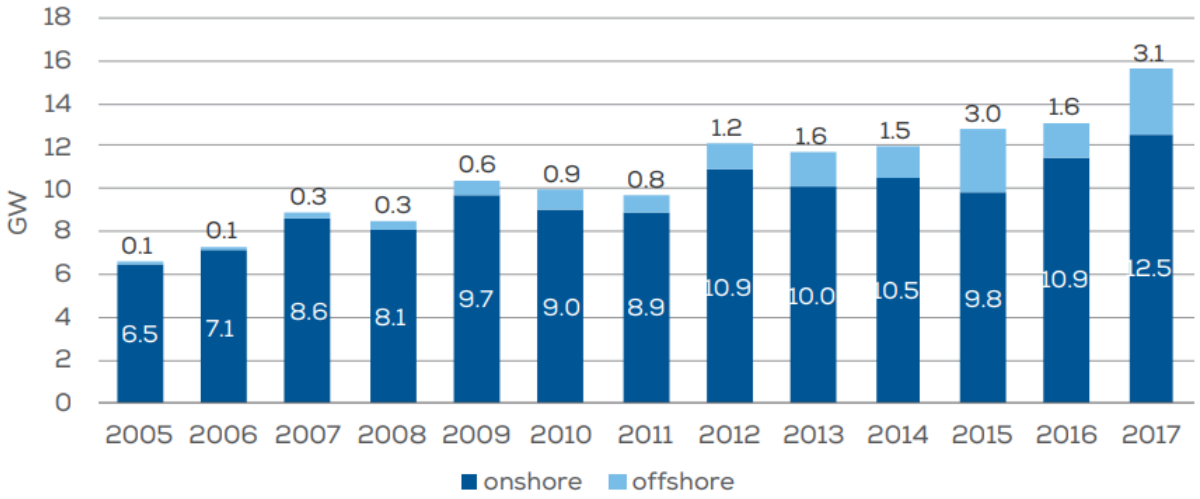

Figure 2.3: Cumulative onshore and offshore Wind installations in Europe [20].

2.2.3. Wind Turbine Types

Wind Turbines (WTs) are those devices, which enable the conversion of wind energy into mechanical energy and finally into electricity. The main parts of a general Wind Turbine are enlisted below [19]:

- A rotor equipped with turbine blades to convert wind energy to mechanical.
- A gearbox (which can be eliminated in fixed-speed wind turbine solutions).
- An electrical generator which converts mechanical power to electrical.
- One (at least) power electronics topology (either converter or soft-starter for fixed-speed wind turbines).
- A transformer to interface the Wind Turbine with the main utility grid.

The process of the wind to electrical power conversion is depicted in Figure 2.4.

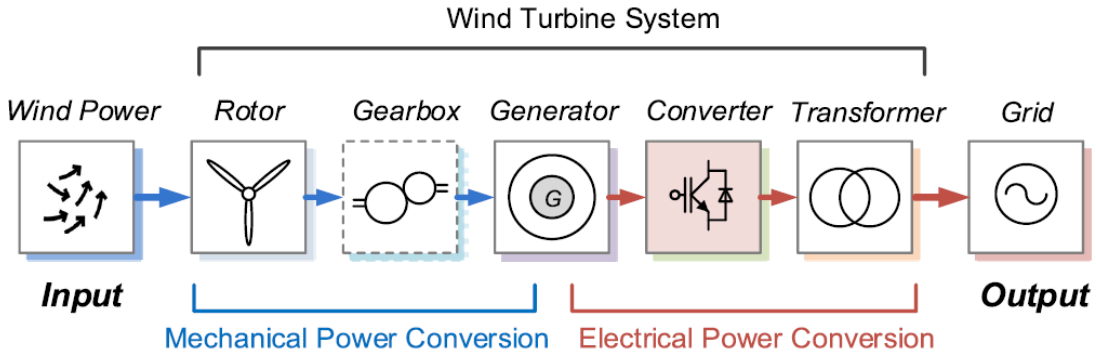

Figure 2.4: Power conversion process in a Wind Turbine System [19].

Despite their common characteristics, wind turbines can be classified into different types, regarding their:

- Type of Generator (Synchronous or Induction Generator)
- Speed Controllability
- Approach to limit aerodynamic power.

This categorization leads to the following main types of Wind Turbines.

Type 1 - Fixed Speed Wind Turbine:
Type 1 WT, is a fixed speed controlled wind turbine, equipped with a squirrel cage induction machine, which is interfaced directly to the grid with the help of a transformer. Moreover, a capacitor bank is applied in this configuration in order to compensate for them, which is drawn from the generator. Furthermore, to achieve a smoother connection with the main utility grid, this wind turbine type also includes a soft-starter. The aforementioned topology is depicted in Figure 2.5.

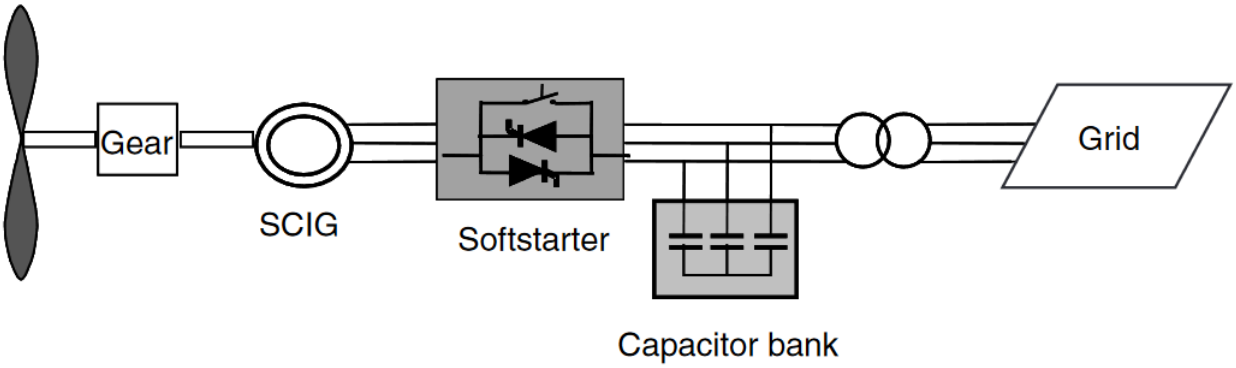

Figure 2.5: Type-1 Wind Turbine Topology [19].

With this type of wind turbine, electric power is dictated from the wind and cannot be controlled. This means that a fluctuation in wind speed will cause a respective fluctuation at the generated electric power. This can cause voltage and frequency deviations at the point of common coupling if the grid is not strong enough to tackle these deviations. Consequently, this kind of WTs is used only in small-scale applications because they do not support any speed control and require a strong grid to connect with. Besides that, their design has to consider high wind speeds, which will be caused by gusts or storms [19].

Type 2 - Variable Speed Wind Turbine with variable rotor resistance:
Type 2 WT, is a limited variable speed controlled turbine, equipped with a wound rotor induction generator. Like Type 1 WT, it is also directly connected with the main utility grid, but the rotor winding of its generator is connected with a controlled resistance. By controlling this resistance, it is able to control the speed of the wind turbine in a range of $\pm$ 10% of its synchronous speed. Similarly to the Type 1 WTs, a capacitor bank is needed, in order to compensate reactive power needs of the generator. Furthermore, the smooth connection with the grid is achieved with the utilization of a soft-starter, just like the previous case [19]. The topology of Type 2 WT is shown in Figure 2.6.

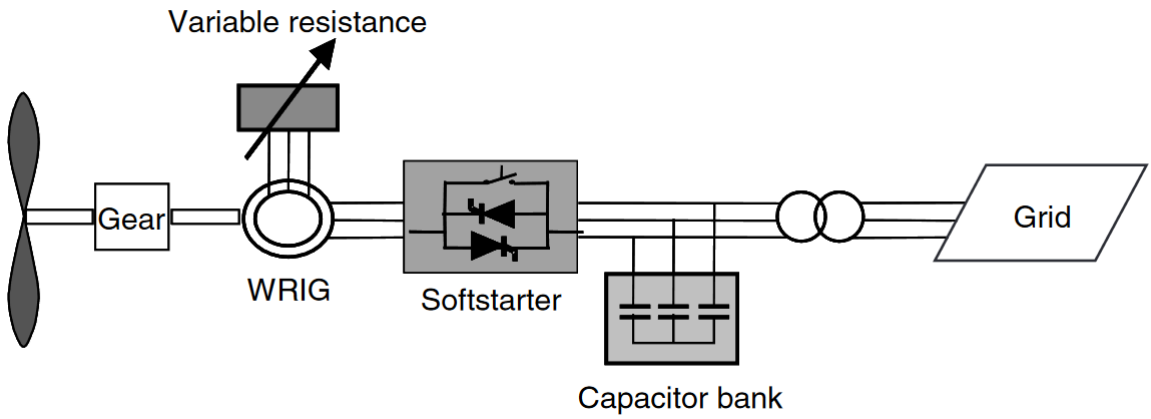

Figure 2.6: Type-2 Wind Turbine Topology [19].

In order to control the variable resistance, an optically controlled converter, which is mounted on the rotor shaft, is utilized. This is a cost-efficient solution since expensive slip rings are avoided. Furthermore, this choice makes the generator more robust since slip rings require maintenance. The drawback of this topology is that there is an energy loss at the variable resistances, which is dissipated in heat loss [19].

Type 3 - Variable Speed Wind Turbine with partially rated frequency converter:
Type 3 WT or Doubly-Fed Induction Generator (DFIG) WT as it is widely known, is a variable speed wind turbine equipped with a wound rotor induction machine. The stator of the DFIG is directly connected to the grid in contrast with the rotor, which is connected to the grid via two, partially rated, "Back to Back" power electronic converters. Those converters, which define the range that speed can be controlled, are usually rated around $\pm 30\%$ of the nominal power output of the stator, which means that they allow operation at 30% slip above and below synchronous speed. Those converters are also able to provide the demanded reactive power and allow a smooth connection with the main utility grid. The topology of this type of WT is shown in Figure 2.7.

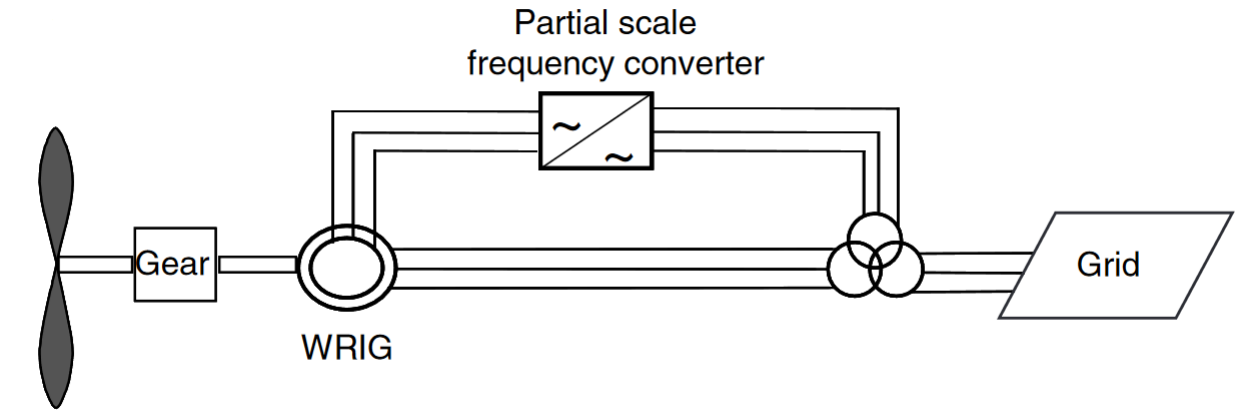

Figure 2.7: Type-3 Wind Turbine Topology [19].

In comparison with Type-2 WT, this WT type is capable of operating in a broader rotor speed range. Furthermore, it is possible to utilize the energy which is produced at the rotor, which does not happen at Type-2 WT, because as mentioned before, this power is dissipated in resistors. From the economic aspect, the partially rated power electronic converters make this concept highly attractive. On the other

hand, the use of slip rings at the machine is a major drawback of this setup since they need regular maintenance. Moreover, it is needed to implement a protection scheme in case of faults [19].

Type 4 - Variable Speed Wind Turbine with fully rated frequency converter:
Type 4 WT, is a variable speed wind turbine equipped with a permanent magnet machine. The machine is fully decoupled from the grid since stator is interfaced with it via fully rated back-to-back power electronic converters. This allows fully controllability of the speed of the wind turbine. The topology of this kind of wind turbines is depicted in Figure 2.8.

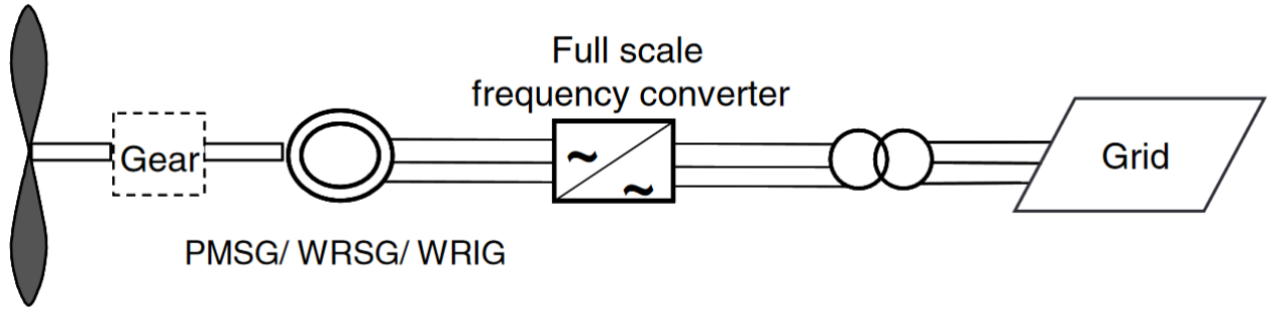

Figure 2.8: Type-4 Wind Turbine Topology [19].

The advantage of this setup, as mentioned above, is that the machine can be operated in the full range of rotor speed. Furthermore, this type is more robust than Type-3, since it does not require slip rings and also can operate without a gearbox. This flexibility, though, comes with an economical cost increase, since the power electronic converters have to be rated to the nominal power output of the WT which leads to a higher cost that Type-3 WTs.

2.3. Ancillary Services

All of the power system services that do not have as a purpose to provide real power to the grid are considered as ancillary services. Those ancillary services can be summarized in three categories, reactive power supply, frequency control and provision of operating reserves. [21].

Reactive power is needed in order to minimize losses in a power system and also maintain voltage levels at the desired level. Reactive power is provided to the system through synchronous generators or by specialized equipment in the power system, such as capacitor banks or Flexible AC Transmission Systems (FACTS) [21].

Frequency control is needed for the system, in order to maintain the frequency in a specific range around its nominal value. The purpose of this control is to balance electric power generation and demand in a power system. Synchronous generators are providing frequency support, by changing their active power output during a power mismatch, which might happen by a load change or by a loss of a generation unit. This output change is achieved, either with manual control or with automatic generation control (AGC, governors, etc.) [21].

Operating reserves are those who assist the power system in order to maintain a constant equilibrium between production and demand for power. Those reserves allow the system to operate during large load changes or drops. Operating reserves are distinguished, based on their availability and the time window they are able to operate. There are 10-minute reserves that can provide their power to the grid within 10 minutes and also scheduling reserves that can provide power within 60 minutes. As a further distinction, ten-minute reserves are separated at spinning and non-spinning reserves. Spinning reserves are generating systems such as heat or hydro units, which can scale up their power output within ten minutes, while non-spinning reserves are quick-start units or non-sensitive loads that can

be interrupted. The spinning reserves that are used to respond immediately to load changes, consist the regulating reserves and they are responsible for the aforementioned voltage control [21].

2.3.1. Frequency Support

During the last years, as mentioned before, there is a huge trend towards the increase of wind power capacity. This increase puts in hazard the security and reliability of power systems. Since the nature of wind is stochastic and intermittent, several challenges arise. This fact leads to the need for more flexible loads that can be operated partially, which causes reduced life cycle and extended costs. It is clear that this situation is not allowing higher penetration of RES and specifically WTs to the existing grid [7].

The variable speed WT, which hold the lion's share in wind turbine market, lack or have highly limited inertial response capability and are not widely used for frequency control. The traditional approach, demanded from Wind Turbines, only to inject their maximum power to the grid, without participating in the ancillary services market. This approach creates serious drawbacks when wind penetration rises [7].

In order to ensure that the power network will operate in a reliable, secure and economical manner, it is required to maintain system's frequency close to the nominal value, within the desired range during its operation. Since wind penetration is gradually increasing and traditional synchronous generators are decommissioned, WT will need to provide frequency regulation capabilities to the grid [8].

It is expected that in close future TSOs will require from WTs to be capable of delivering inertial response and frequency control in order to ensure the grid's normal operation [7]. As referred in section 2.2.3, variable speed WT are interfaced with the grid via power electronic converters. By effectively controlling the switching patterns of those inverters, with different control strategies, it is possible to provide a wide range of ancillary services to the main utility grid. In the following section, the available methods will be reviewed and analyzed.

Inertial Response

In a power system, during steady-state operation, power generation is always equal to power demand, including line losses. During a load or generation change event, the kinetic energy which is stored in the rotating masses of machines that are connected to the system is going to change. This means frequency will fluctuate.
The frequency change is calculated by Equation 2.1 [8]:

$$\frac{dE_{kin}}{dt} \approx J * f_0 * \frac{df}{dt} \approx P_{gen} - P_{demand} \tag{2.1}$$

where :

- E_{kin} : Kinetic energy stored in the generators and motors shaft
- f : System frequency
- f_0 : System's nominal frequency
- J : Total System Inertia

Since generators cannot change their active power output (P_{gen}) instantly, the variation of frequency is mitigated by the system's kinetic energy release from its inertia. That is the inertial response which tries to stabilize the system's frequency after a disturbance. This response is an inherent feature of synchronous generators and happens immediately when there is a disturbance at the grid. Some seconds after the disturbance, primary frequency control, which is explained in the following section, is activated in order to eliminate the remnant frequency deviation.

From the equation 2.1, it is clear that since J is reduced, by decommissioning traditional SGs and increasing the penetration of power, electronic interfaced sources have an impact on the system's inertial response. A system with a high inertia value has a higher frequency nadir during load increases and lower RoCoF.

Natural Inertia Response from WTs :
From subsection 2.3.1.1, it is made clear how the inherent feature of inertia is operating for synchronous generators that are directly coupled to the main grid. On the other hand, for WTs, the rotational speed of the shaft is (partially) decoupled from the frequency when they are interfaced to the grid via power electronics converters. A comparison between the different WT types and their inertial response capability can be seen in the following table.

Table 2.1: Wind Turbine Types Inertial Response capability comparison [7].

WT Type	Inertial Response Capability
SG	++
Type-1	+
Type-2	+
Type-3	-
Type-4	None

The traditional synchronous generators are chosen as a comparison reference for the inertial response capability. It can be identified that fixed speed induction generators have a lower inertial response, due to the slip of the generator, which causes a reduced coupling between rotor speed and system frequency. Furthermore, DFIGs, have restricted inertial response capabilities, by controlling appropriate the Rotor Side Converter (RSC). Finally, Type 4 WTs, which are fully decoupled from the grid with power electronic interface do not inherently provide inertial response, since rotor speed is fully decoupled from frequency due to the power electronic interface.

Nowadays, since variable speed wind turbines are mostly used for wind power conversion, as mentioned before, problems arise regarding the grid's stability, since they are reducing the system's inertial when substituting common SGs. Although, there are appropriate control systems, which allow the exploitation of WT's shaft kinetic energy to emulate inertia response and support the system during disturbances. Those control strategies are summarized below:

- Synthetic Inertia Response: With this type of control, wind generator mimics the behaviour of a SG. This technique is going to be analyzed in the following subsection since it is the one that is enhanced and utilized in the proposed Type 3 WT topology of the presented thesis.
- Temporary Power Surge: With this type of control, there is a power increase during a disturbance, which is not determined by the disturbance itself, but by a pre-defined function. During the event, power output is increased for a period, and after that, a recovery underproduction period follows.

Synthetic Inertia:
As mentioned before, Synthetic Inertia control method tries to mimic the behaviour of a SG. During steady state operation, the power output of the WT is dictated by the Maximum Power Point Tracker (MPPT). During a frequency event, an inertial response K_{in} is added to the MPPT output (P_{MPPT}) value. In order to calculate this value, system frequency has to be measured and filtered with a Low-Pass filter in order to reduce measurement noise. This is mandatory because it is needed to derive the frequency signal in order to obtain RoCoF, and a signal with noise cannot be derivated properly. Moreover, a dead band has to be implemented in order to avoid controller operation during small frequency disturbances. This inertial response extra power output is calculated from Equation 2.2.

$$P_{in} = -K_{in}\frac{df'}{dt} \tag{2.2}$$

Thus, when frequency decreases, P_{in} value becomes positive and it is added to the P_{MPPT} value. This leads to extracting kinetic energy from the rotor shaft and consequently slowing down the turbine. This control strategy is called synthetic inertia due to the fact that, as can be identified with Equation 2.2, WT mimics the behavior of a traditional SG. The kinetic energy is extracted from the rotor can be calculated from Equation 2.3 [8] :

$$P_{in} = \frac{dE_{kin}}{dt} = J\Omega_{syn}\frac{d\Omega_{syn}}{dt} \tag{2.3}$$

where, Ω_{syn} represents the rotational speed of a synchronous generator which corresponds to the frequency of the grid.
In addition to this, another term called P_{droop} which is proportional to frequency deviation from its nominal value (Δf) is added to the MPPT's output (P_{MPPT}). This value is used for two purposes

1. In order to oppose the function of MPPT which will try to operate WT at its optimal power point. If this happened would lead to decreased inertial response during a disturbance.

2. In order to limit frequency deviation (nadir or peak), by modifying the output proportionally to frequency deviation (Δf)

The main disadvantage of this control scheme is that after WT provides the inertial response it should return to the previous steady-state operating point, which leads to a recovery period where power output is less than the WT's optimal operating point.
This thesis, proposes a different approach, by installing an ESS between the DC Link of the "Back to Back" power electronic converters and providing the excess power from that source; thus WT can always operate at its optimal power point.

Primary Frequency Control

In this subsection, different control schemes for primary frequency support by WT are going to be explained and analyzed.

Deloaded Control:

In order to be capable of providing primary frequency response (PFR), variable speed WTs are operated in a lower power point than their optimal. The difference between their optimal and the operational point can be used as an emergency reserve in case of frequency deviation. There are three types of deloaded control in literature [8]:

- "Balanced" control: This control scheme is reserving a constant percentage of WT's rated power as a reserve. The mathematical formulation of this control is described in the Equation 2.4.

$$P_{ref} = \begin{cases} P_{Deloaded} & P_{Deloaded} \leq P_{MPPT} \\ P_{MPPT} & P_{Deloaded} > P_{MPPT} \end{cases} \tag{2.4}$$

$$P_{de} = [0, \dots, P_{rated}]$$

- "Delta" control : This control scheme, is reserving a percentage of WT's maximum active power output. The mathematical formulation of this control is described in the Equation 2.5.

$$P_{ref} = \begin{cases} (1 - K_{Reserve})P_{MPPT} & P_{MPPT} \leq P_{Rated} \\ (1 - K_{Reserve})P_{Rated} & P_{MPPT} > P_{Rated} \end{cases} \tag{2.5}$$

$$K_{Reserve} = [0, \dots, 1]$$

- "Fixed Reserve" control : This control scheme is reserving a fixed amount of active power to provide as a reserve in case of a disturbance. The mathematical formulation of this control is described in the Equation 2.6.

$$P_{ref} = \begin{cases} P_{MPPT} - \Delta P_{Reserve} & P_{MPPT} \leq \Delta P_{Rated} \\ P_{Rated} - \Delta P_{Reserve} & P_{MPPT} > P_{Rated} \end{cases} \tag{2.6}$$

$$\Delta P_{Reserve} = [0, \dots, \Delta P_{max}]$$

A comparison of the power output of a WT for different wind speeds, with the aforementioned control strategies is depicted in Figure 2.9:

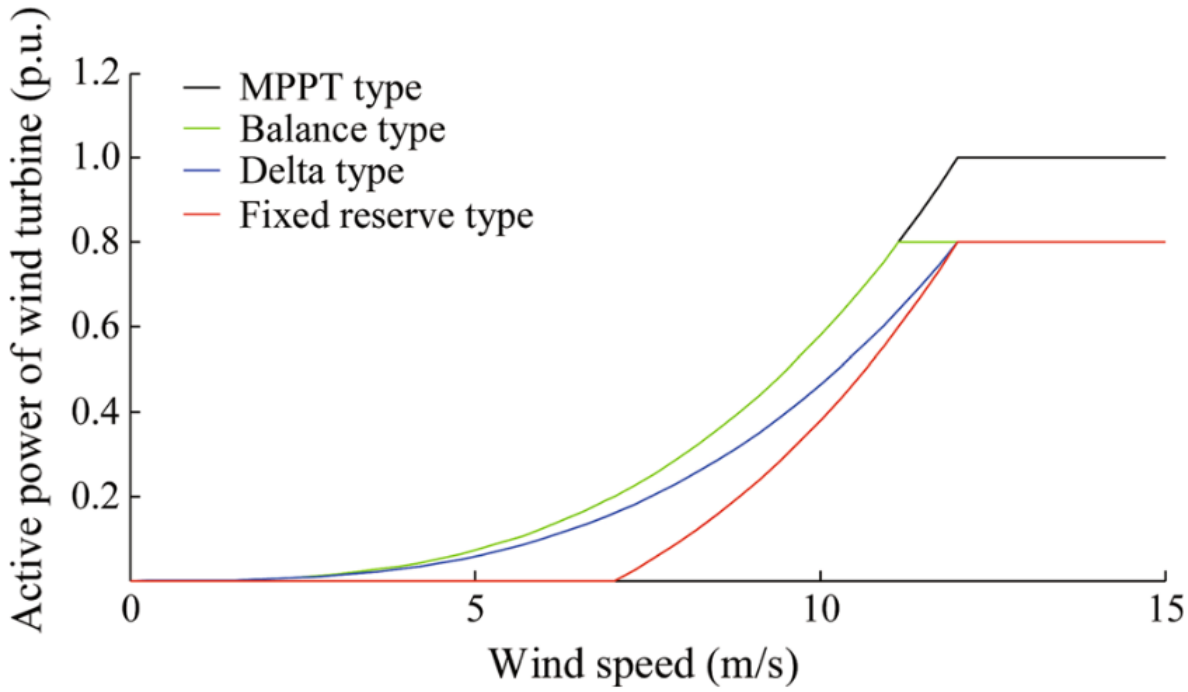

Figure 2.9: Active Power Output for each Primary Frequency Control Strategy [8]

Rotor Speed Control:

It is possible to operate the wind turbine in sub-optimal power level by changing the operating point of the WT, while rotor speed stays below its maximum speed limit.

Thus, the power output of the WT can be adjusted between the desired deloaded value (P_{de}) and its maximal one (P_{max}), by changing the rotor speed between the range of ($\omega r, del$ and ω_{max}). As a consequence, the power reference of the WT can be calculated, as shown in Equation 2.7:

$$P_{ref} = P_{de} + (P_{max} - P_{de})\left(\frac{\omega_{r,de} - \omega_{r,meas}}{\omega_{r,de} - \omega_{r,max}}\right) \tag{2.7}$$

where :

- P_{max}: Maximum Power.
- P_{de}: Deloaded Power.
- $\omega_{r,max}$: Wind Turbine's rotor speed at P_{max}.
- $\omega_{r,de}$: Wind Turbine's rotor speed at P_{de}.
- $\omega_{r,meas}$: Wind Turbine's measured rotor speed.

Pitch Angle Control:

Initially, pitch angle control was used in order to prevent generator and power electronic circuits from overloading and also the rotor from over-speed. In order to support frequency, traditional pitch control needs to be modified according to the wind. The initial pitch angle is used in order to maintain a power back-up in case of a frequency disturbance event. This method is slower than the others because the servo time constant of the pitch controller is slower than the power converter one.

From the details mentioned above, it is clear that, by following these control methods, there is a loss of active power output during steady-state operation of the WT, which is translated to less "green" power injected to the grid and also the sub-optimal operation of WT. This thesis tries to tackle that

issue, by providing this extra power needed for frequency regulation from an ESS which is connected to the DC-Link of the "Back to Back" power electronic converter configuration. With this approach, WT is always able to operate at its optimal power point and provide the maximum available power to the grid, while there is a back-up reserve in order to support grid's frequency when needed.

2.3.2. Voltage Support

As mentioned before, the high penetration of RES dictates the need for new requirements for their interconnection to the existing utility grid. In the previous sections, the importance and the ways to provide frequency support to the grid were thoroughly demonstrated.

Except that, another challenge is to operate WFs in a proper way that they can also provide voltage or reactive power support to the grid when needed. During the previous years, most of the operators preferred to utilize renewable energy sources under Unity Power Factor, since they were rewarded base on the active power contribution to the grid. This is going to change in the future if RES become the dominant generation units.

There are different methods for reactive power control of WT. This thesis will focus on those methods that are used by Type 3 (DFIG) WT, which are listed below [14]:

- Fixed Power Factor Control: In most cases, fixed power factor control is operated under a Unity Power Factor; thus, WT does not contribute reactive power to the grid. Despite that, there is the possibility to use different power factor values (from 0.95, leading to 0.95 lagging, for instance). It is important, not to breach the limits of stator, rotor and power electronic converters when providing reactive power. When a Type 3 WT is operated under Unity Power Factor, magnetizing currents are supplied through the rotor via the appropriate rotor excitation, while stator reactive power remains at zero value. The Rotor Side Converter (RSC) of the "Back to Back" converter configuration of DFIG, is responsible for providing the demanded reactive power to the rotor. This does not affect the grid since its rotor is decoupled via power electronic converters.

  Thus, the rotor side converter, which acts as a Voltage Source Converter (VSC), is capable of fulfilling the reactive power needs of the rotor.

- Voltage Control by Rotor Excitation: With this type of control, stator's reactive power output is modified in order to regulate the voltage at the point of common coupling (PCC) at the desired level. In order to achieve this, the voltage at the PCC is compared with the nominal one and the difference between them is used as an input of a PI controller which gives as an output the stator reactive power reference. This value is provided to the RSC controller, which regulates the reactive power of the stator.

  The main benefit of this control scheme is that machine stator can be overloaded for a short period of time, in contrast to the power electronic components which connect the rotor to the main grid; thus stator can provide a larger reactive power reserve.

- Voltage Control by Grid Side Converter (GSC): With this control type, GSC, which is operated as a VSC, utilizing a proper control scheme is capable of providing the needed reactive power, in order to maintain the voltage at the PCC between pre-defined levels. The drawback of this technique is the possibility that GSC is already loaded with the slip power; thus, the reactive power capacity is lower. This problem arises when the converter is already loaded with the nominal power, which though is not the case for the most time of operation.

- Voltage Control using both RSC and GSC: This control scheme is not so usual, and there is very limited literature about it. There are two types of control that combine RSC and GSC operation:

  - Uncoordinated Control: At this control scheme, each controller tries to regulate the voltage at PCC. With that kind of control, it is possible to cause circulating currents between the GSC and the stator, since both converters trying to regulate the voltage without coordination.
  - Coordinated Control: At this control scheme, there is one controller which defines the reactive power output of GSC and stator with different ways. One possibility is that RSC is the main controller, thus reactive power is provided by the stator, and GSC operates only if needed. Another way is that GSC is the main controller and RSC and stator only participates when GSC reaches its thermal limits. Finally, there is also the possibility to share reactive power between the two converters with a pre-defined ratio.

At this thesis, a combination of the techniques mentioned above is going to be implemented. The reactive power support to the grid is going to be provided either from RSC or from the GSC depending on the rotor's slip. The proposed approach provides the demanded reactive power from the grid side converter when the generator operates at its nominal speed, so grid side converter is not loaded. If the generator is operating with a slip close to its limits (± 0.3), controllers send an appropriate control signal to rotor side converter, so stator provides the demanded reactive power.

3

Mathematical Modeling and Implementation in RSCAD

As mentioned in chapter 2, the Doubly Fed Induction Generator (DFIG) is used by many WT manufacturers for high power (multi-MW) applications. In this chapter, mathematical modelling of this type of generator and its controls are going to be presented, so it is easy to understand how the generator's power output is controlled and to accomplish the model implementation in a simulation software like RSCAD, in order to be used for HIL simulations in RTDS.

3.1. Doubly-Fed Induction Generator (DFIG) steady-state operation

As already stated, DFIG is an induction machine with a wound rotor. In DFIG setup, both rotor and stator are connected to electrical sources, and this is the reason that this type of generator is called as "Doubly-Fed". The rotor is establishing its magnetic field with the help of three-phase currents, which energize rotor windings. The developed rotor magnetic field causes torque development due to the interaction with the stator respective field. The magnitude of the developed magnetic field is a function of the strength of the aforementioned magnetic fields (stator and rotor) and their phase displacement. Thus, mathematically, torque is calculated as the vector product of stator and rotor magnetic fields as it can be validated from Equation 3.1 and Figure 3.1 [22].

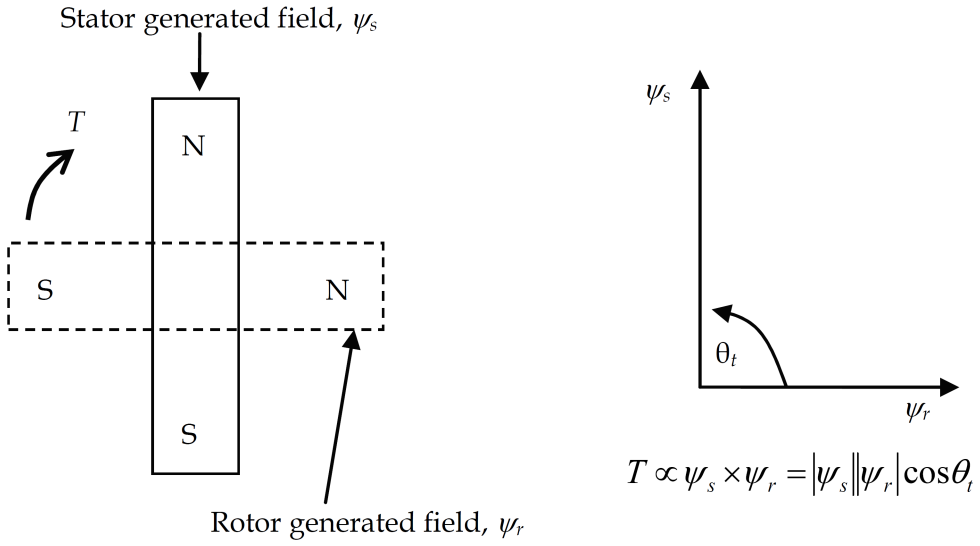

Figure 3.1: Magnetic poles generated by currents in stator and rotor windings [22].

$$T = \psi_s \times \psi_r = |\psi_s||\psi_r|\cos\theta_t \tag{3.1}$$

From 3.1, it is clear that the optimal torque can be achieved when stator and rotor field vectors have $90\,\text{deg}$ phase displacement; thus, they are normal to each other. Since the stator is connected to the main utility grid, which is considered a balanced source, stator flux has a constant magnitude, and its vector rotates with synchronous speed according to grid's frequency [22].

In order to explain the way torque is controlled in the DFIG, the single-phase equivalent circuit of an induction machine is going to be introduced. The aforementioned circuit is depicted in Figure 3.2.

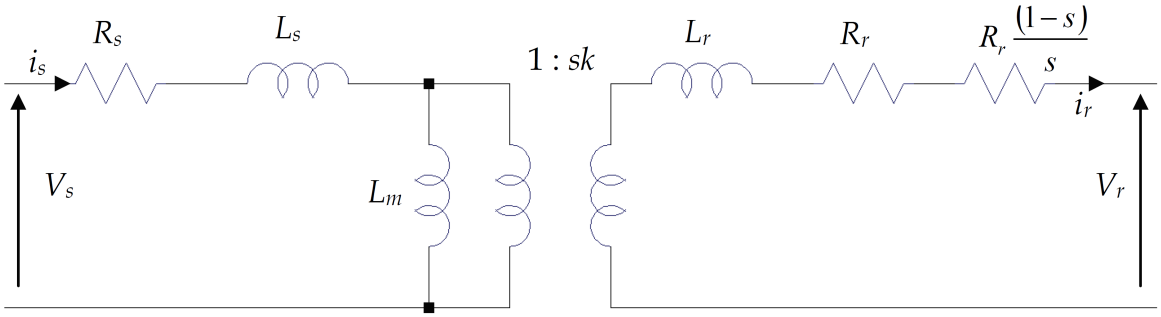

Figure 3.2: Single phase equivalent of an induction machine [22].

The left-hand side part of the circuit is representing the stator, while the other one the rotor of the induction machine.

At the stator side, R_s and L_s are two "parasitic" components which represent the resistance and the leakage inductance of the stator phase winding respectively. The leakage inductance is used to model all the flux which is generated by the stator winding but does not cross the air gap; thus does not participate in torque production. Stator resistance represents the resistance of the conductors, by which stator windings are manufactured.

The L_m inductance represents the generation of the flux which crosses the air gap between the stator and the rotor, which is the flux that is utilized in the machine.

Similarly to the stator, the rotor circuit also includes two "parasitic" elements, R_r which represents the rotor resistance and L_r which represents the rotor's leakage reactance. Moreover, the rotor side includes the representation of the generated mechanical power. To achieve this, an additional resistance $R_r(1-s)/s$ is included.

Rotor and stator are connected via a transformer as can be seen from Fig.3.2. This transformer's turns are dependent on the real turns ratio between stator and rotor and on the slip which the machine is operating.

It is considered necessary to define what slip is in an induction generator. Slip is calculated with the help of Equation 3.2:

$$s = \frac{n_s - n_r}{n_s} \tag{3.2}$$

Where :

- n_s : Synchronous speed.
- n_r : Rotor's mechanical speed.

Synchronous speed is calculated as:

$$n_s = \frac{60 f_e}{p} \quad \text{RPM} \tag{3.3}$$

Where:

- f_e: Electrical Frequency of the voltage which is applied to stator windings (50 or 60 Hz in a grid).
- p : Number of Pole Pairs

For easier understanding, during the following analysis, the DFIG is going to be considered as a conventional induction motor. When the rotor is open-circuited, and rotor shaft is blocked (standstill operation), if the stator is excited, there is a generated voltage at the terminals of the rotor circuit (V_r, as named at Figure 3.2). This voltage will have the same frequency with the voltage of the stator excitation because in this case rotor speed n_r is zero and as a consequence slip s is equal to 1 (by Equation 3.2). As rotor speed increases, the frequency of the output voltage is going to drop. When the rotor reaches the synchronous speed frequency is going to be zero; thus, there is not an induced voltage at the rotor terminals. When the rotor keeps accelerating above the synchronous speed, the voltage will increase again but with opposite phase sequence to the sub-synchronous mode [22]. Rotor frequency can be mathematically formulated, as shown in Equation 3.4:

$$f_r = sf_e \tag{3.4}$$

Since rotor terminals are open-circuited, current does not flow; thus torque is not produced since there is a lack of rotor field (ψ_r) as can be validated from Figure 3.1. When the rotor is short-circuited, rotor currents can flow with a frequency that can be calculated from Equation3.4. This leads to the production of a magnetic field at the rotor (ψ_r). This field rotates with the same speed as stator's magnetic field (psi_s). The interaction between those two fields is capable of produce torque as seen in Figure 3.1.

A critical detail which has to be understood is that rotor and stator magnetic fields are both rotating with synchronous speed, even though rotor might be turning asynchronously.

The mechanical torque output of the generator can be calculated as the power which is consumed or produced by the rotor resistance. This mechanical output can be calculated by Equation 3.5:

$$P_{mech} = 3|i_r|^2\left(\frac{1-s}{s}\right)R_r \tag{3.5}$$

It is possible, for the sake of this analysis to neglect rotor and stator resistances and leakage inductances, so the per-phase equivalent circuit becomes like the own shown in Figure 3.3 :

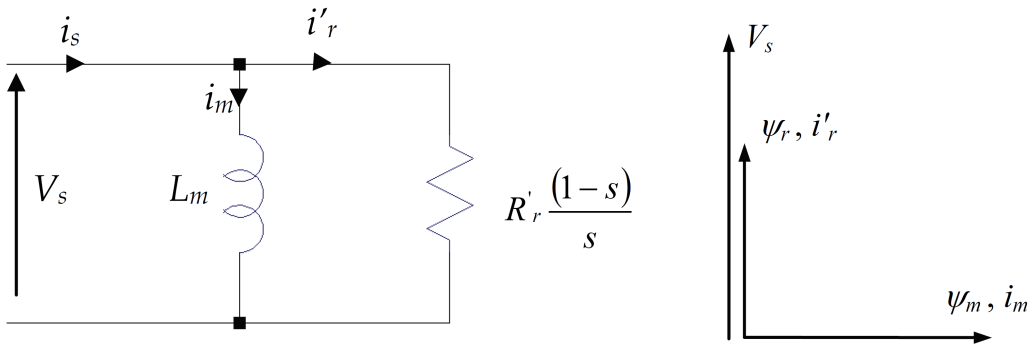

Figure 3.3: Simplified induction machine equivalent circuit and phasor diagram [22].

It is shown from Fig.3.3, the stator flux is normal to the rotor flux component for the optimal torque production. From this circuit, it is possible to derive the produced mechanical torque of the machine as demonstrated in Equation 3.6:

$$T_{mech} = 3|i_r{}'|^2\left(\frac{1-s}{s}\right)\frac{R_r{}'}{\omega_m} \tag{3.6}$$

Since:

$$\omega_m = \frac{(1-s)\omega_s}{p} \quad \text{and} \quad \psi_m = L_m i_m = \frac{V_s}{\omega_s} = \frac{|i_r{}'|R_r{}'}{s\omega_s} \tag{3.7}$$

From Equation 3.7, Equation 3.6 can be written as:

$$T_{mech} = 3|i_r{}'|^2\left(\frac{1-s}{s}\right)\frac{R_r{}'}{\omega_m} = 3p\frac{|i_r{}'|R_r{}'}{s\omega_s}|i_r{}'| = 3p\psi_m|i_r{}'| \tag{3.8}$$

This transformation from Equation 3.6 to Equation 3.8 is performed in order to prove that torque can be controlled in two ways, either by controlling stator flux psi_m or by controlling rotor current magnitude $i_r{}'$, since the vectors remain normal to each other as shown in Figure 3.1.

In an actual DFIG system, the phase and the magnitude of the stator voltage, which are dictated by the grid voltage magnitude, are monitored, and rotor currents are modified in a proper fashion to be normal to the stator flux so that the DFIG can produce optimal torque.

In order to achieve this, most of the DFIGs use a closed-loop control scheme utilizing a Voltage Source Inverter [22]. This Voltage Source Inverter is used as a three-phase voltage source which can change its voltage phase and magnitude instantaneously. This feature makes the Voltage Source Inverter ideal for rotor current regulation [22].

In order to achieve proper rotor current set-point, precise knowledge of the physical rotor position is needed. This can be achieved with the help of a mechanical position sensor. With this equipment, it is possible to modify the rotor current suitably, in order to be normal to the stator flux and achieve optimal torque generation.

3.2. Power Electronic Converters

In the previous section 3.1, the importance of VSC, for the optimal operation of a DFIG was demonstrated. It is known from chapter 2, that in Type 3 WT, the rotor is connected to the grid via a "Back to Back" AC/DC converter setup. This setup can be separated into two different converters, Rotor Side converter (RSC) and Grid Side Converter GSC. Those two converters are coupled via a DC Link, which is established with the help of a capacitor [22]. This capacitor acts as energy storage and keeps voltage fluctuations in the DC Link between the desired range. RSC is responsible for DFIG's torque and speed control. It is also capable of modifying the power factor of the stator output. On the other hand, GSC is responsible for maintaining the voltage at the DC Link between the desired limits, without taking into consideration the rotor's power direction and amplitude. From the aforementioned facts, it is clear that rotor side converter is operated in different frequencies, according to the wind speed in order to maintain torque optimal, while grid side converter is operated at grid's frequency. Nevertheless, GSC can also be operated under leading or lagging power factor in order to absorb or inject reactive power to the grid [22]. A three-phase winding transformer is mostly used, in order to interface stator and GSC to the main utility grid.

This "Back to Back" power electronic converter setup, is mandatory to convert the variable voltage and variable frequency output of the rotor into a fixed voltage and fixed frequency output which can be absorbed by the grid. The DC Link is used as mentioned before as energy storage, which can provide the required energy between the rotor and the grid.

Nowadays, most of the DFIG setups are using the two-level, six switch converter, also known as full bridge converter. This VSC is able to produce two voltage levels (0 and V_{DC}) as an output for each leg of the converter. Each one of the three converter legs consists of two switches; thus, the total number of a three-phase VSC is six. A detailed DFIG arrangement is presented in Figure 3.4:

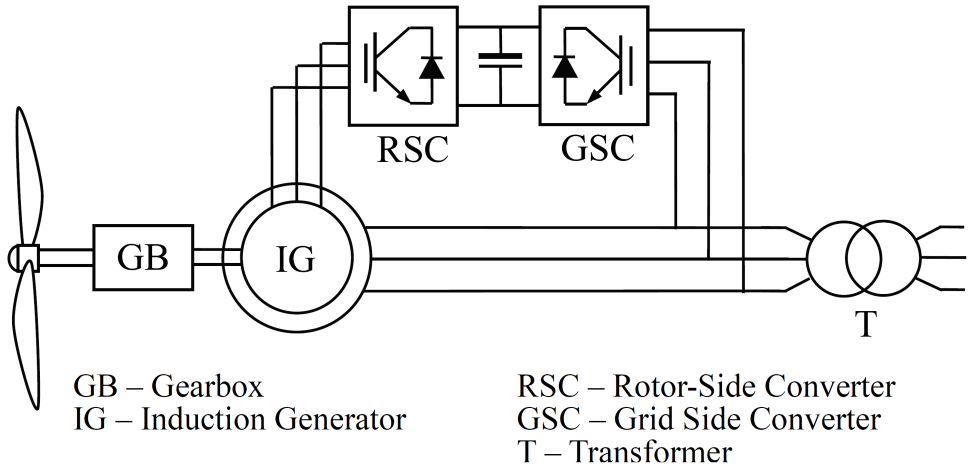

Figure 3.4: Typical DFIG arrangement with back-to-back converters [8].

The full bridge converter mentioned before is capable of providing a three-phase voltage output with variable amplitude, frequency and phase. The output voltage is constrained only by the DC Link voltage level since the peak line voltage is not possible to be higher than V_{DC}. Another important feature of the VSC is that it can modify the output voltage instantaneously, with a short delay which is imposed by switching frequency of the semiconductors. In order to achieve this variation, pulse-width modulation (PWM) is used in order to control the output voltage. In Figure 3.5, a full bridge converter is depicted:

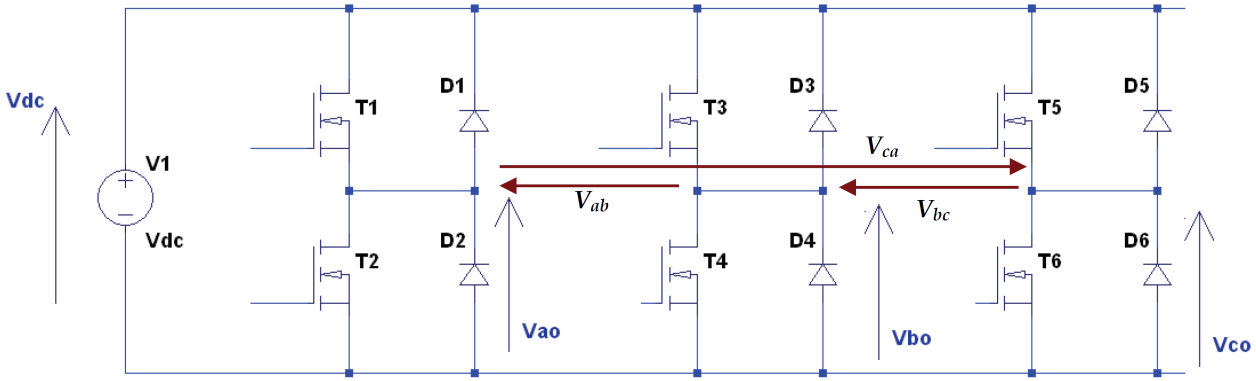

Figure 3.5: Full Bridge Voltage Source Converter circuit [22]

.

In order to explain its operation, only phase A is considered for simplicity purposes. When switch T_1 is on, then V_{a0} is equal to V_{DC}. On the other hand, when switch T_2 is on then V_{a0} becomes zero. It has to be noted that switches T_1 and T_2 are switched in a complementary fashion since it is not allowed to be on at the same time [22]. By switching T_1 and T_2 periodically the average output voltage V_{a0} can be regulated in a range between zero and V_{DC}. For PWM control, switching frequency is kept constant and width is modified in a proper way, in order to achieve the desired voltage output. An example of PWM application is demonstrated in Figure 3.6 :

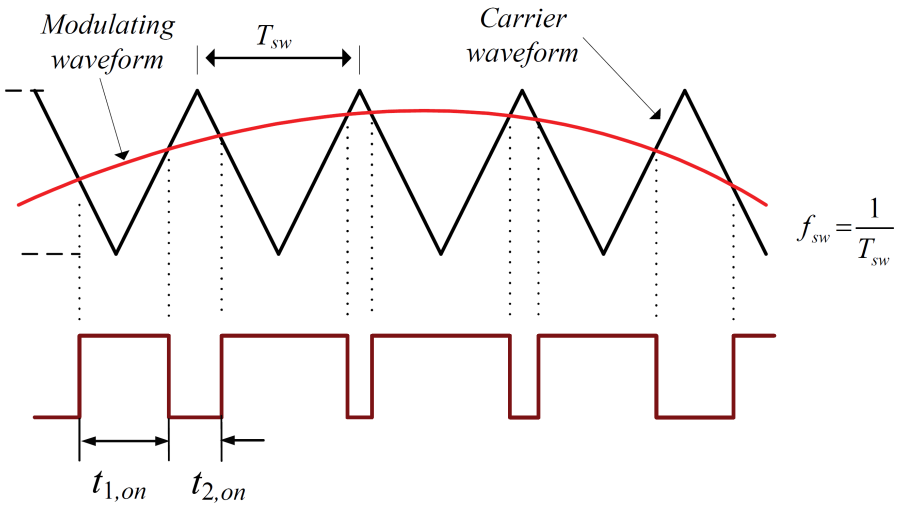

Figure 3.6: Pulse Width Modulation example [22].

From this visualization of PWM, it is clear that, by changing the modulating waveform, it is possible to change the generated pulse waveform. The voltage output can be calculated as:

$$V_{out} = V_{DC}\frac{t_{1,on}}{T_{sw}} \tag{3.9}$$

Where:

- $T_{1,on}$: On time of T_1 switch.
- T_{sw} : Switching period.

For the sake of further analysis, modulation index is calculated as shown in Equation 3.10:

$$m = \frac{t_{1,on}}{T_{sw}} \tag{3.10}$$

This allows to modify Equation 3.9 as:

$$V_{out} = mV_{DC} \tag{3.11}$$

Modulation index is defined in a range from zero (when switch T_2 is continuously on) to one (when switch T_1 is continuously on). By changing the modulation index, it is possible to change output voltage frequency and amplitude.

At a three phase VSC, such as the one depicted in Figure 3.5, three modulation indices are needed, one for each phase. The output voltage of each leg can expressed as a function of modulation index, as shown in Equation 3.12:

$$\begin{cases} V_{a0} = m_a V_{DC} \\ V_{b0} = m_b V_{DC} \\ V_{c0} = m_c V_{DC} \end{cases} \tag{3.12}$$

If the aforementioned modulation indices change sinusoidally, their value can be calculated from Equation 3.13:

$$\begin{cases} m_a = \frac{1}{2} + m\sin(\omega t) \\ m_b = \frac{1}{2} + m\sin(\omega t - \frac{2\pi}{3}) \\ m_c = \frac{1}{2} + m\sin(\omega t + \frac{2\pi}{3}) \end{cases} \tag{3.13}$$

It is easy now to express VSC output line voltage as :

$$\begin{cases} V_{ab} = Va0 - V_{b0} = \sqrt{3} m V_{DC} \sin(\omega t - \frac{\pi}{6}) \\ V_{bc} = Vb0 - V_{c0} = \sqrt{3} m V_{DC} \sin(\omega t - \frac{5\pi}{6}) \\ V_{ca} = Vc0 - V_{a0} = \sqrt{3} m V_{DC} \sin(\omega t - \frac{\pi}{2}) \end{cases} \tag{3.14}$$

From Equation 3.14, it is clear that the created three-phase voltage outputs can be fully controlled since magnitude is controlled by modulation index m, while frequency and phase are regulated by the respective one of the modulation waveform. In a real system, digital signal generators, microcontrollers and computer processors are utilized, in order to generate the demanded modulation waveform and compare it with carrier waveform to send the respective pulses to the switches.
From the previous equations, it is shown that a VSC is able to generate a voltage with any amplitude, frequency and phase, only limited by DC Link voltage and switching frequency. Thus, VSCs can be considered as an ideal voltage source with controlled voltage amplitude, phase and frequency. The capacity of this source is usually higher than the needed one for the excitation that is required [22].

This feature provides the opportunity to control active and reactive power flow from and to the grid according to the needs of the power system. For a lossless DFIG, during steady-state, the mechanical power of the shaft is calculated of the sum of stator and rotor power as $Pm = P_s + P_r$. From this, rotor power can be calculated from the Equation 3.15:

$$P_r = P_m - P_s = T_m \omega_r - T_{em} \omega_s = -T_m \left(\frac{\omega_s - \omega_r}{\omega_s} \right) \omega_s = -s T_m \omega_s = -s P_s \tag{3.15}$$

Since slip can be also calculated as $s = \frac{\omega_s - \omega_r}{\omega_s}$.
This means that, since the maximum slip is limited (± 0.3 is a usual value), the "Back to Back" converters which are loaded with rotor's (slip) power can be partially rated. This is a big advantage of Type 3 WTs against the Type 4 ones, since they use fully rated power electronic converters which are more expensive. In RSCAD's Wind Turbine model, the mechanical power output of the wind turbine is calculated as :

$$P_m = C_p(\lambda, \beta) \frac{\rho A}{2} v_{Wind}^3 \tag{3.16}$$

Where :

- P_m : Mechanical Power Output of the Wind Turbine (kW).
- $C_p(\lambda, \beta)$: Performance coefficient of the turbine as a function of tip speed ratio (λ) and blade pitch angle (β).
- ρ : Air Density (kg/m^2).
- A : Turbine blade area (m^2).
- v_{Wind} : Wind speed (m/sec).

RSCAD model allows the usage of two different performance coefficient functions. The one is used at the presented research is :

$$C_p(\lambda, \beta) = C_1 \left[\frac{C_2}{\lambda_1} - C_3 \beta - C_4 \right] e^{-\frac{C_5}{\lambda_i}} + C_6 \lambda \tag{3.17}$$

Where $\frac{1}{\lambda_i} = \frac{1}{\lambda + 0.08\beta} - \frac{0.0035}{\beta^3 + 1}$.

Furthermore, tip speed ratio is calculated as :

$$\lambda = \frac{\omega_r R}{v_{Wind}} \tag{3.18}$$

Where :

- R : Wind Turbine radius (m).
- ω_r: Turbine rotational speed (rad/sec).
- V_{Wind} : Wind Speed (m/sec).

The power output as a function of turbine speed is depicted in the Figure 3.7:

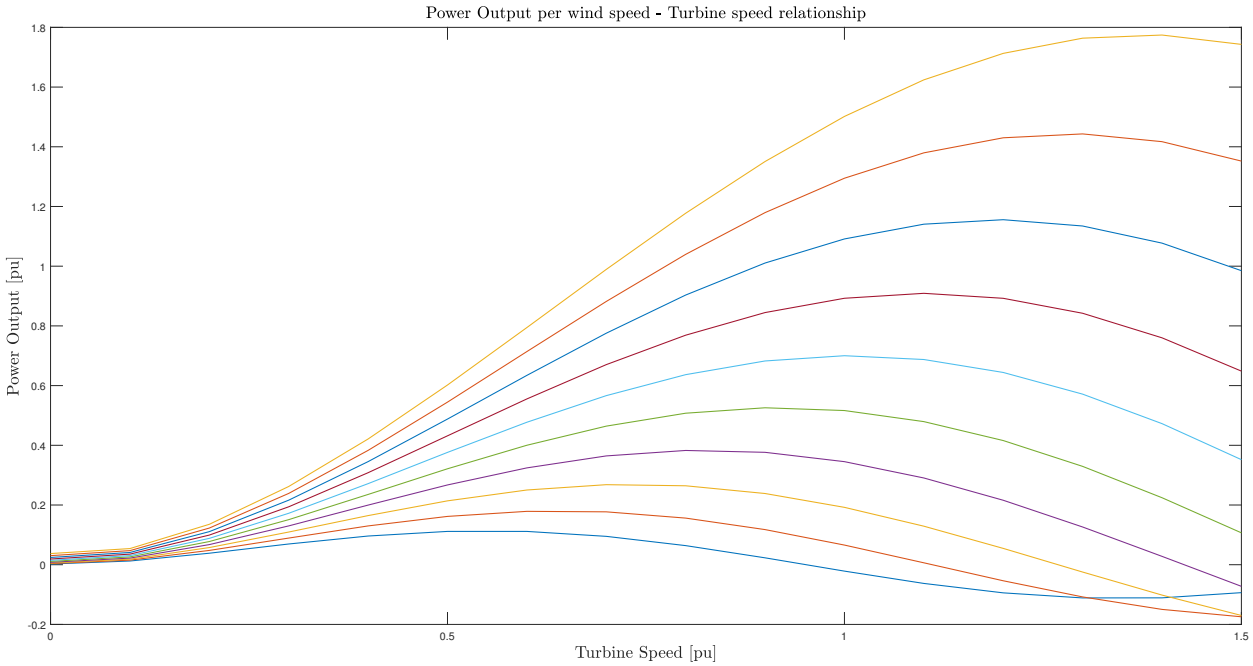

Figure 3.7: Power output as a function of turbine speed.

From the previous figure, it is shown that the extracted power is maximized for a slip equal to -0.2. On the other hand, when turbine speed is synchronous, thus slip is zero, no active power is injected from or to the rotor windings, and consequently, the related converters are not loaded. This characteristic is going to be exploited in a proper manner in order to provide ancillary services to the grid in a fashion that will not add stress to the converters. When speed is higher than the synchronous, the DFIG is operating at supersynchronous mode, and slip is negative. From Equation 3.15, it is realized that there is an active power flow from the rotor to the grid. On the other hand, when DFIG operates at subsynchronous mode, slip is positive, and this causes the rotor to consume reactive power, which is transferred via back-to-back converters.

By this manner, it is achievable to control the extracted from wind turbine power. The proposed control scheme, enables optimal operation of DFIG, since its power output is maximized and also gives flexibility by providing ancillary services to the grid, is thoroughly explained in the following section.

3.3. Doubly-Fed Induction Generator Control System

Before going into detail about the control system of the DFIG, it is important to explain the mathematical transformations needed, in order to achieve vector control. The conventional method that is used to control a quantity in many applications is a PI Controller [22]. In order to simplify the equations it is needed to control, DC quantities are needed as an input of the PI controller. As it is known, the power system operates in three-phase AC such as the DFIG, so there is the need to express the desired values in a DC manner. This is accomplished with the help of the following transformations.

3.3.1. Clark Transformation

Clark or $\alpha\beta$ transformation is used in order to map three-phase instantaneous voltages in ABC frame, into instantaneous voltages on the $\alpha\beta$ stationary frame. Practically, the $\alpha\beta$ reference system is a two-phase system equivalent, where the aforementioned three-phase AC quantities are represented by a

two-phase equivalent with the same space vector. The transformations for voltage and current values are given by the matrix Equation 3.19:

$$\begin{bmatrix} v_\alpha \\ v_\beta \end{bmatrix} = \sqrt{\frac{2}{3}} \begin{bmatrix} 1 & -\frac{1}{2} & -\frac{1}{2} \\ 0 & \frac{\sqrt{3}}{2} & -\frac{\sqrt{3}}{2} \end{bmatrix} \begin{bmatrix} V_a \\ V_b \\ V_c \end{bmatrix} \tag{3.19}$$

$$\begin{bmatrix} i_\alpha \\ i_\beta \end{bmatrix} = \sqrt{\frac{2}{3}} \begin{bmatrix} 1 & -\frac{1}{2} & \frac{1}{2} \\ 0 & \frac{\sqrt{3}}{2} & -\frac{\sqrt{3}}{2} \end{bmatrix} \begin{bmatrix} i_a \\ i_b \\ i_c \end{bmatrix} \tag{3.20}$$

There are also two v_0, i_0 components, which are zero for symmetrical three-phase signals, like those in the examined case, and this is the reason they can be neglected. For better understanding, the transformation is depicted in Figure 3.8:

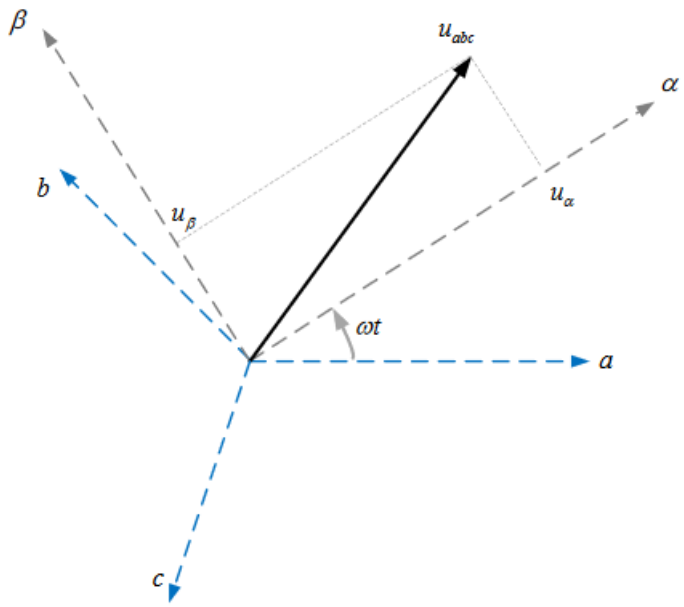

Figure 3.8: Clack Transfromation Diagram [23].

3.3.2. Park Transformation

Clark or $\alpha\beta$ transformation transforms the three-phase signals into a space vector which is still sinusoidal. This means, its magnitude is changing during its rotation. As mentioned before, in order to utilize a PI controller, DC signals are needed as an input; thus, the output of Clark transformation cannot be used to control the system. Despite that, it is a handy tool, since it is used as an input for Park or d-q Transformation. This transformation is using a synchronously rotating reference frame. Its d-axis might be aligned with the voltage vector (SVO) at the PCC or with the stator flux vector (SFO). This way allows any vector expressed in the $\alpha\beta$ stationary frame to be expressed in a rotating reference frame. The transformations for voltage and current values are given by matrix Equation 3.21:

$$\begin{bmatrix} v_d \\ v_q \end{bmatrix} = \frac{2}{3} \begin{bmatrix} cos(\frac{2\pi}{3}) & cos(\frac{2\pi}{3} - \theta) & cos(\frac{2\pi}{3} - \theta) \\ -sin(\frac{2\pi}{3}) & -sin(\frac{2\pi}{3} - \theta) & -sin(\frac{2\pi}{3} - \theta) \end{bmatrix} \begin{bmatrix} V_a \\ V_b \\ V_c \end{bmatrix} = \begin{bmatrix} cos(\theta) & sin(\theta) \\ -sin(\theta) & cos(\theta) \end{bmatrix} \begin{bmatrix} v_\alpha \\ v_\beta \end{bmatrix} \tag{3.21}$$

Where θ is the angle between dq and $\alpha\beta$ reference frames and can be calculated as:

$$\theta(t) = \int_0^t \omega_s(t)dt + \theta_0 \tag{3.22}$$

Where θ_0 is the initial angle.

This method gives as an output two DC signals which can be used as an input for PI controllers at a control system. The new reference frame is shown in the following figure:

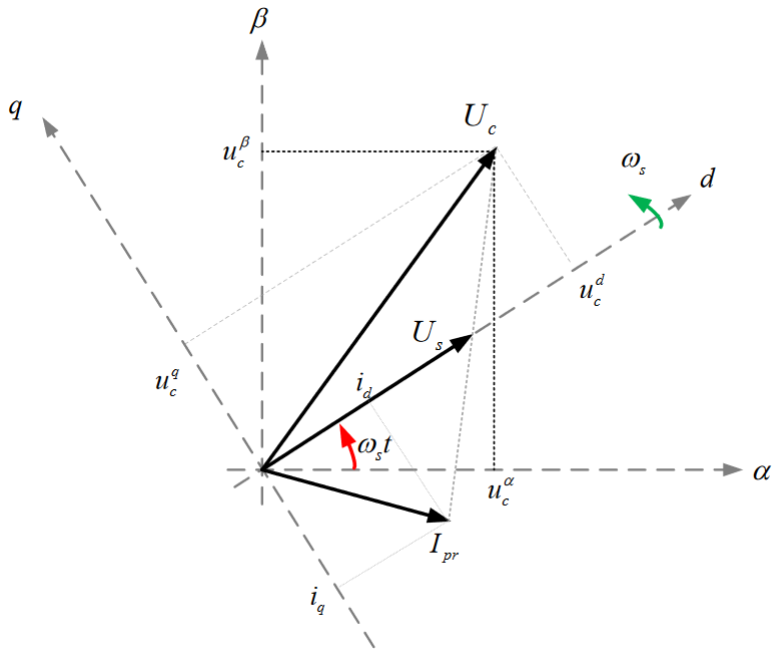

Figure 3.9: Park Transformation Diagram [23].

3.3.3. Rotor Side Converter

As it is already mentioned, RSC is responsible for the rotor windings excitation of the DFIG. RSC is responsibe for controling rotor winding currents in such a way that rotor flux is normal to the stator one, in order to maximize the produced torque that is developed at generator's shaft [22].

For this purpose, RSC utilizes a torque controller to control active and reactive power at stator terminals. The optimal power which is extracted from the wind turbine is calculated from Equation 3.23.

$$P_{opt} = k_{opt}\omega_r^3 \tag{3.23}$$

In RSCAD model, k_{opt} constant is considered as 1. The measured output power is compared to the reference, and a PI Controller is used to mitigate the error. The output of this controller is the rotor q-axis reference current (i_q^{ref}) which has to be injected to the rotor windings to achieve optimal power extraction. Thus, q-axis is used to control electromagnetic torque T_e. On the other hand, the d-axis component is used to control the power factor at stator's terminal by controlling reactive power output.

To describe the aforementioned control strategy more extensively, it is necessary to express it mathematically. In order to do so, general Park's model of an induction machine is used. Using a stator flux oriented (SFO) reference frame, voltage vector can be expressed as shown in Equations 3.24 and 3.25:

$$\vec{v}_s = R_s\vec{i}_s + \frac{d\vec{\psi}_s}{dt} \tag{3.24}$$

$$\vec{v}_r = R_r\vec{i}_r + \frac{d\vec{\psi}_r}{dt} - j\omega\vec{\psi}_r \tag{3.25}$$

Where :

- $\vec{v}_s$: Stator voltage, which is imposed by the grid.
- $\vec{v}_r$: Rotor voltage which is controled by the RSC.

The flux equations can be obtained from Equations 3.26 and 3.27 :

$$\vec{\psi}_s = L_s\vec{i}_s + L_m\vec{i}_r \tag{3.26}$$

$$\vec{\psi}_r = L_m\vec{i}_s + L_r\vec{i}_r \tag{3.27}$$

Where:

- $L_s = Lm + L_{ls}$: Stator Self-Inductance.
- $L_r = Lm + L_{lr}$: Rotor Self-Inductance.

Since, as mentioned before, Stator-Flux Orientation is used, the dq-axis components of stator flux equation are calculated from Equation 3.28:

$$\begin{cases} \psi_{sd} = L_s i_{sd} + L_m i_{rd} = \psi_s = L_m i_{ms} \\ \psi_{sq} = 0 \end{cases} \tag{3.28}$$

The rotor and voltage flux equations are shown below:

$$\begin{cases} v_{rd} = R_r i_{rd} + \sigma L_r \frac{di_{rd}}{dt} - \omega_{slip}\sigma L_r i_{rq} \\ v_{rq} = R_r i_{rq} + \sigma L_r \frac{di_{rq}}{dt} - \omega_{slip}(L_0 i_{ms} + \sigma L_r i_{rd}) \end{cases} \tag{3.29}$$

$$\begin{cases} \psi_{rd} = \frac{L_m^2}{L_s} i_{ms} + \sigma L_r i_{rd} \\ \psi_{rq} = \sigma L i_{rq} \end{cases} \tag{3.30}$$

Where:

- $\sigma = 1 - \frac{L_m^2}{L_s L_r}$: Leakage Factor.
- $L_0 = \frac{L_m^2}{L_s}$: Equivalent inductance.
- $\omega_{slip} = \omega_s - \omega_r$: Slip angular speed.

The stator flux angle which is needed for the dq transformation is calculated from Equation 3.31:

$$\begin{cases} \psi_{s\alpha} = \int (v_{s\alpha} - R_s i_{s\alpha}) dt \\ \psi_{s\beta} = \int (v_{s\beta} - R_s i_{s\beta}) dt \end{cases} \tag{3.31}$$

$$\theta_s = tan^{-1}\left(\frac{\psi_{s\beta}}{\psi_{s\alpha}}\right)$$

From Equation 3.29, Equation 3.32 can be derived:

$$\begin{cases} v'_{rd} = R_r i_{rd} + \sigma L_r \frac{di_{rd}}{dt} \\ v'_{rq} = R_r i_{rq} + \sigma L_r \frac{di_{rq}}{dt} \end{cases} \tag{3.32}$$

Compensation terms are needed to be added to the voltage d-q components, calculated above in order to guarantee proper tracking of currents. So, the d-q axis reference voltage can be calculated as:

$$\begin{cases} v_{cd}^{*} = -v_{cd}^{'} + (\omega_e L_{choke} i_{cq} + v_d) \\ v_{cq}^{*} = -v_{cq}^{'} - (\omega_e L_{choke} i_{cd}) \end{cases} \tag{3.33}$$

Electromagnetic torque can be calculated from Equation :

$$T_e = -\frac{3}{2} p \mathrm{Im}\left\{\overrightarrow{\psi_s} \overrightarrow{i_r^*}\right\} = -\frac{3}{2} p L_0 i_{ms} i_{rq} \tag{3.34}$$

Since Stator-Flux orientation is used, stator flux current i_m can be considered as fixed to the stator voltage [22]. It is possible to control torque via the q-axis component of rotor current. Consequently, the reference current can be derived from Equation 3.35:

$$i_{rq}^{ref} = -2\frac{T_e^{ref}}{3pL_0 i_{ms}} = -2\frac{T_e^{ref}}{3p\psi_s} \tag{3.35}$$

The vector control system for the RSC is depicted in Figure 3.10:

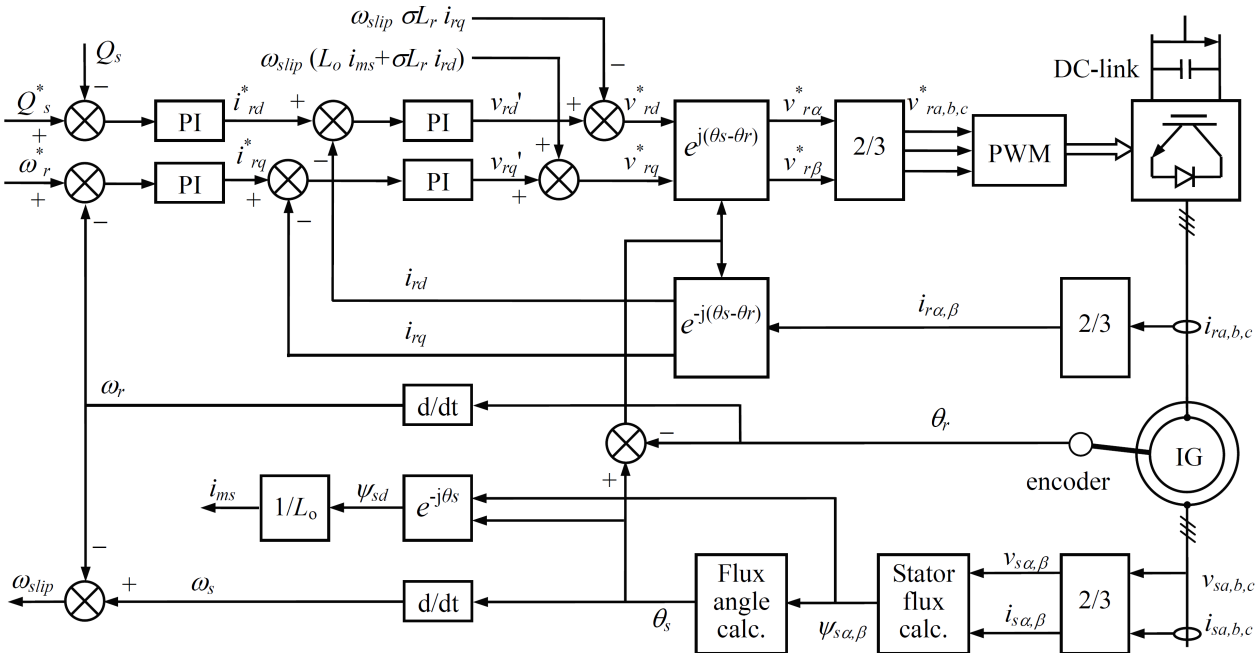

Figure 3.10: Rotor Side Converter vector control system [22].

3.3.4. Grid Side Converter

GSC control strategy targets to maintain the DC Capacitor voltage at the desired level. Moreover, it can also inject or draw active or reactive power from and to the grid. Before going into detail, it is mandatory to explain the way active and reactive power is controlled. In Figure 3.11, the single phase equivalent of the GSC and its phasor diagram are depicted:

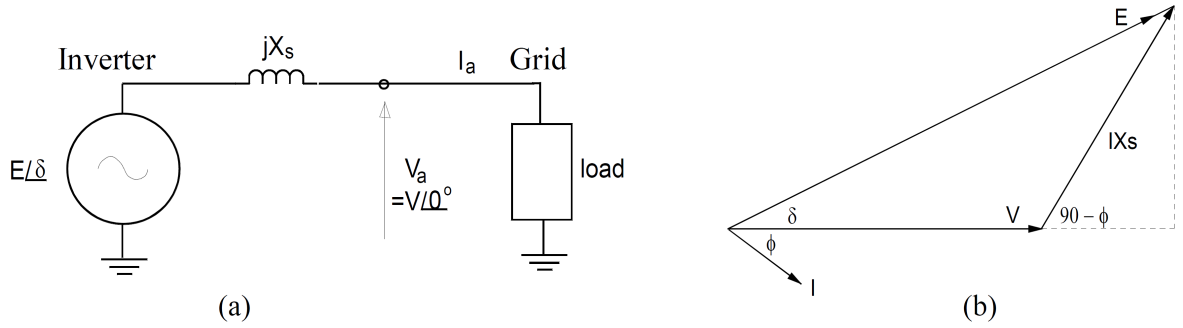

Figure 3.11: (a) GSC single phase equivalent and (b) phasor diagram [22].

As referred in the previous subsections, a VSC is able to produce a voltage with arbitrary amplitude, phase and frequency. This means that voltage E, shown in Fig.3.11 can be fully controlled by the GSC. In order to explain how active and reactive power is controlled, load angle method is going to be utilized, despite the fact that, real-life applications utilize more complex control methods.

Load angle method is imitating the traditional synchronous generator behavior, by using the phase difference δ, depicted in Figure 3.11, in order to control active power. Reactive power, on the other hand, is controlled by changing the amplitude of the voltage generated by the GSC. The steady state equations to calculate active and reactive power are [22, 3]:

$$P = \frac{VE\sin(\delta)}{X_s} \tag{3.36}$$

$$Q = \frac{V^2}{X_s} - \frac{VE}{X_s}\cos(\delta) \tag{3.37}$$

Where X_s is the interface inductance which connects GSC with the main grid. In case that angle δ is small, Equations 3.36 and 3.37 can be simplified as:

$$P = \frac{VE\delta}{X_s} \quad \text{and} \quad Q = \frac{V^2}{X_s} - \frac{VE}{X_s} \tag{3.38}$$

From Equation 3.38, it is clear that active power (P) is controlled by the angle δ and reactive power (Q) is controlled by the voltage magnitude (E). The VSC provides the opportunity to modify those values with the proper control strategy effectively. The active power load of the GSC is dependent on the DC Link Voltage. When DC Link voltage is rising above the desired level, GSC changed angle δ in a way that it injects more power to the grid [22]. On the other hand, if DC Link voltage is decreasing below the limit, GSC reduces the active power injection. The energy stored in the capacitor can be calculated from Equation 3.39 [22]:

$$W_{DC} = \int P_{DC}dt = \frac{1}{2}CV_{DC}^2 \tag{3.39}$$

Where:

- W_{DC} : Capacitor stored energy.
- C : Total capacitance
- V_{DC} : Capacitor voltage.
- P_{DC} : DC link power input.

DC Link voltage and energy changes can be calculated as:

$$\frac{dV_{DC}}{dt} = \frac{P_{DC}}{CV_{DC}} \tag{3.40}$$

$$\frac{dW_{DC}}{dt} = P_{DC} \tag{3.41}$$

Where, P_{DC} is defined as the difference between the power input from RSC and the output from GSC. So, from Equation 3.39 it is clear that V_{DC} remains constant when P_{DC} is zero.
Since the general concept behind GSC control is explained, it is time to demonstrate the vector control method that is used. In this case, reference frame is aligned with the stator voltage vector. Active and reactive power are controlled separately by using d-q reference frame [22].

The voltage equations in d-q axis reference frame can be calculated from Equation 3.42:

$$\begin{cases} v_{cd} = Ri_{cd} + L_{choke}\frac{di_{cd}}{dt} - \omega_e L_{choke} i_{cq} + v_{d1} \\ v_{cq} = Ri_{cq} + L_{choke}\frac{di_{cq}}{dt} + \omega_e L_{choke} i_{cd} + v_{q1} \end{cases} \tag{3.42}$$

The angular position that is needed for the transformation from ABC to d-q reference frame is calculated from Equation 3.43:

$$\theta_e = \int \omega_e dt = tan^{-1}\left(\frac{v_{c\beta}}{v_{c\alpha}}\right) \tag{3.43}$$

Where $V_{c\alpha}, V_{c\beta}$ are the GSC voltages transformed into stationary frame components.

Since grid voltage amplitude is constant, direct axis voltage component V_{cq} is zero and quadrature axis component is constant [22]. By making the assumption that GSC transformer winding has a star connection, power flow can be calculated from Equation 3.44 :

$$\begin{cases} P_c = 3(v_{cd}i_{cd} + v_{cq}i_{cq}) = 3v_{cd}i_{cd} \\ Q_c = 3(v_{cd}i_{cq} + v_{cq}i_{cd}) = 3v_{cd}i_{cq} \end{cases} \tag{3.44}$$

From this equation it is shown that active and reactive power can be controlled from direct and quadrature component of GSC current respectively. As in RSC case, compensation terms for better accuracy are added to the equations as shown in Equation 3.45:

$$\begin{cases} v^*_{cd} = -v'_{cd} + (\omega_e L_{choke} i_{cq} + v_d) \\ v^*_{cq} = -v'_{cq} - (\omega_e L_{choke} i_{cd}) \end{cases} \tag{3.45}$$

Those voltage references are transformed from d-q reference frame to the ABC reference frame, and they are used as a modulating waveform (as shown in section 3.2) for the PWM signal generation.

The vector control system for the GSC is depicted in Figure 3.12

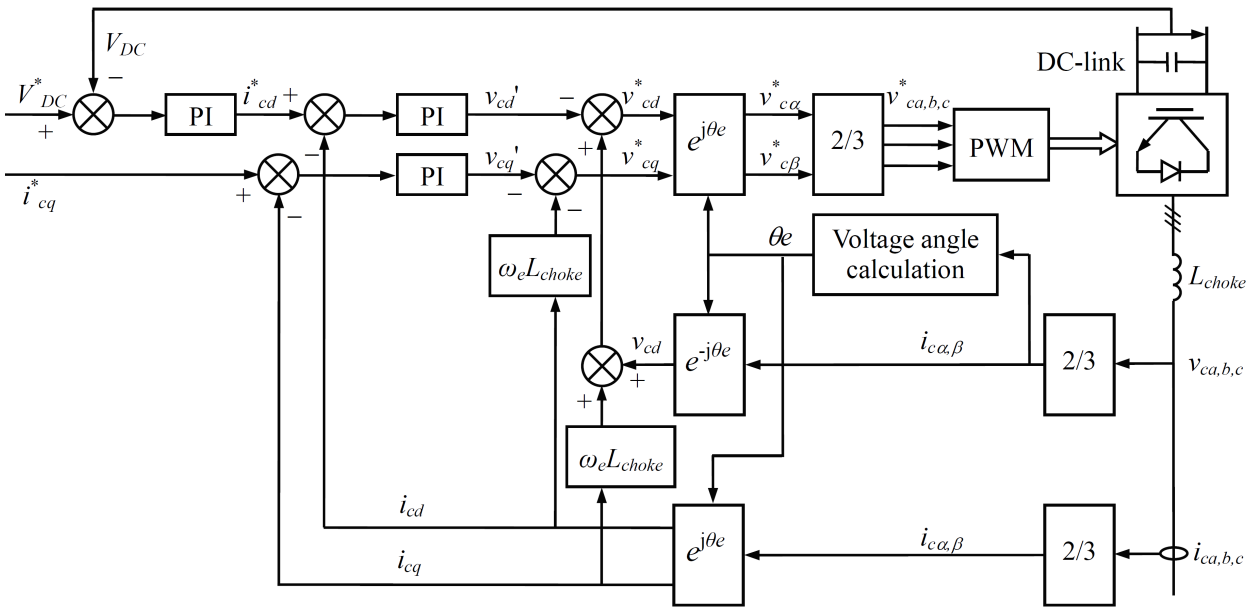

Figure 3.12: Grid Side Converter vector control system [22].

4

Proposed topology and integrated control system for Frequency and Voltage support

In Chapter 2, different existing methodologies for frequency and voltage support were discussed. When it comes to frequency support, all of the existing control schemes in literature have a major drawback. For inertial response, after providing kinetic energy, there is a significant time interval, where wind turbine has to claim back this energy and thus it is providing less power to the grid [8]. For primary frequency response, power loss is even higher, since all the proposed methods suggest to operate WT in lower power output than their optimal one ($10 - 20\%$ lower). This reserve, with proper control, can be used during a disturbance. This leads to a $10 - 20\%$ loss during steady-state operation, which is sub-optimal for both stakeholders since the TSOs have less "green power" injected to their power system and WF operators are earning less since their reward is based on their active power injection to the grid.

In Chapter 3, the basic control strategies for the GSC and the RSC were shown and analyzed. In the following sections, the proposed topology with the new control systems are going to be demonstrated and explained.

4.1. Topology

In order to tackle all the problems, current DFIG control strategies have, this thesis proposes a modified topology. Specifically, a new connection of an Energy Storage System ESS with the DC Link is proposed. The interface between the ESS and the DC Link is achieved with the utilization of a Bidirectional DC-DC Converter. A bidirectional topology is proposed, so ESS can be involved both in under-frequency and over-frequency situations and provide frequency support to the grid.

With this improved proposed topology and the appropriate control system, it is possible to operate the WT in its optimal power output all the time. When frequency support is needed, instead of providing this extra power reserve from turbine's shaft, ESS is activated with the proper control of the interface Bidirectional DC-DC converter and injects the needed extra power. The control system needed to achieve this kind of operation is explained in the following subsection.

The aforementioned topology is depicted in Figure 4.1:

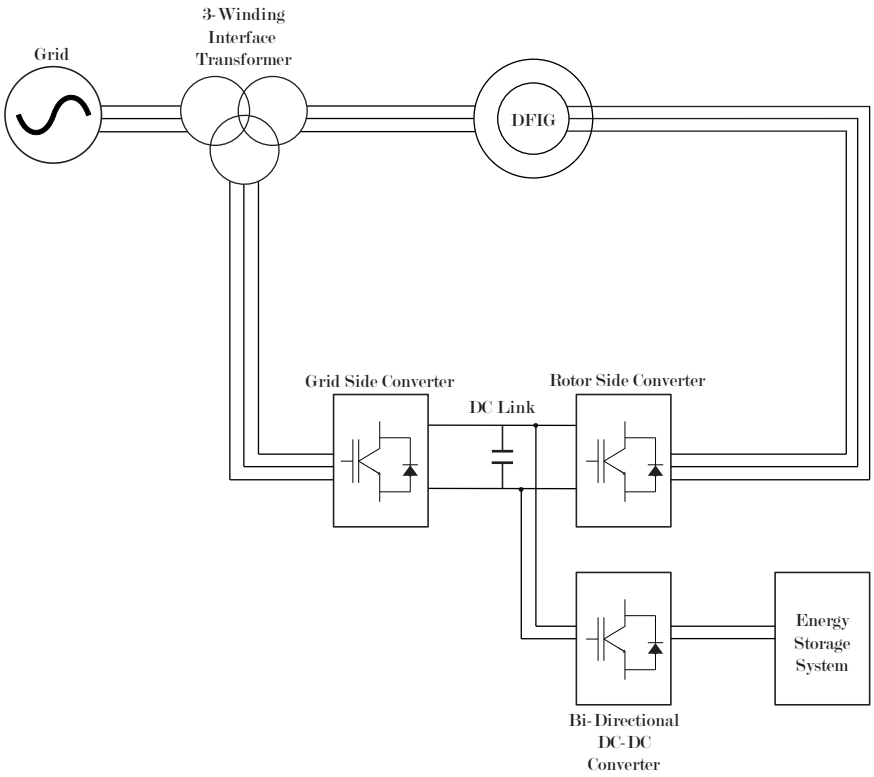

Figure 4.1: Proposed Topology.

With this improved proposed topology and the appropriate control system, it is possible to operate the WT in its optimal power output all the time. When frequency support is needed, instead of providing this extra power reserve from turbine's shaft, ESS is activated with the proper control of the interface Bidirectional DC-DC converter and injects the needed extra power. The control system needed to achieve this kind of operation is explained in the following subsection.

Moreover, since active and reactive power injections are decoupled by utilizing Park Transformation, as shown in section 3.3, it is possible to support the grid's voltage at the PCC and frequency simultaneously. To do so, an expansion of the control schemes, mentioned in section 3.3 for both RSC and GSC is mandatory. The proposed control systems are demonstrated in the following sections.

4.2. ESS and Half - Bridge Bidirectional DC-DC Converter

At Section 3.3.4, the principles of active and reactive power transfer from GSC were explained. From Equations 3.40 and 3.41, it was shown that DC Link voltage is directly related to the power transferred from and to it. In a regular DFIG, this power is calculated as the difference between injected power from RSC and drawn power from GSC plus the system losses. In the proposed topology, this equation has to take into consideration the ESS injection. Equation 4.1 demonstrates the proposed system's behaviour:

$$P_{DC} = P_{RSC} - P_{GSC} + P_{ESS} \tag{4.1}$$

Where P_{ESS} is the power injected from or to the ESS.

This means that during a disturbance, since GSC is controlling d-axis component in order to maintain DC Link Voltage (V_{DC}) at the desired set-point (which means P_{DC} has to be kept zero), power injected from ESS (P_{ESS}), is going to be injected to the grid via GSC. Since ESS is capable of injecting and absorbing the power, a converter which allows bi-directional power flow is needed.

In order to interface ESS with the DC Link in a controlled fashion, a bi-directional converter needs to be utilized.

There are different types of bi-directional DC-DC Converters which can be divided into two categories based on the galvanic isolation between input and output. Those main categories are:

- Non-Isolated Bidirectional DC-DC Converters.
- Isolated Bidirectional DC-DC Converters.

Isolated Bidirectional DC-DC Converters require a high frequency transformer between the two conversion stages. This feature makes that specific type of converters less attractive for this specific application, since the converter with the ESS need to be installed in a limited space. Non isolated DC-DC Converters on the other hand are more compact, which is critical for this type of application, and provide higher efficiency. Between the non isolated DC-DC converter topologies, **Half Bridge Bidirectional DC-DC Converter** is the most common one for this kind of applications due to its simple structure and reliability.

Half-bridge DC-DC converter consists of two switches which are operated separately and not in a complementary fashion like VSC, as described in Chapter's 3 Section 3.2 [24]. Instead of using a triangular carrier waveform, a saw-tooth one is used for the pulse width modulation control of this converter [25]. The aforementioned waveform is scaled from zero to one, and it is compared with the desired duty cycle, which provides the desired power output (P_{ESS}) [25].

In Figure 4.2, the non-isolated Half-Bridge bi-directional Converter topology is demonstrated.

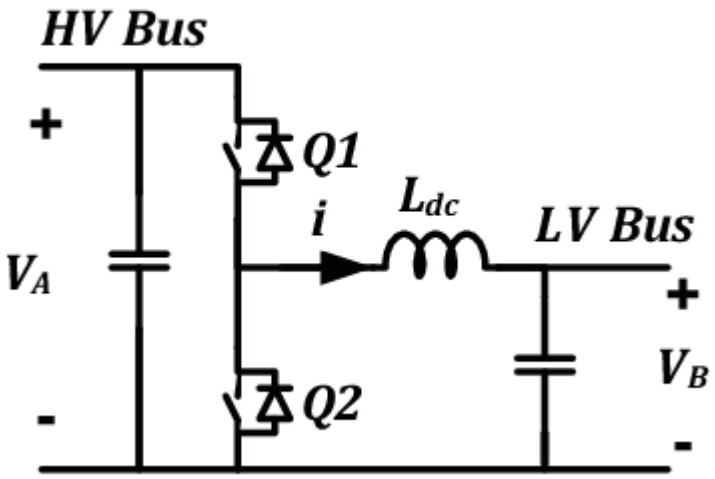

Figure 4.2: Non-Isolated Half-Bridge Bidirectional DC-DC Converter Topology [25].

This topology is chosen because of its simplicity in terms of design and control and also its reduced size and cost, in comparison with similar isolated converters which need a transformer. Comparing with other non-isolated converters, half-bridge bidirectional converter, requires less components has higher efficiency and lower conduction losses.

This converter has two modes of operation:

- Buck mode, where power is transferred from the high voltage side (V_A) to the low voltage side (V_B).
- Boost mode, where power is transferred from the low voltage side (V_B) to the high voltage side (V_A).

Both modes can be utilized with a proper control strategy in order to provide frequency support services to the grid during under and over-frequency situations by injecting or absorbing active power with the help of ESS. Switch Q_1 is used for the buck mode of operation, while switch Q_2 is the one responsible for the boost mode. In the following subsections, each mode will be explained, and the way the duty cycle is controlled will be discussed.

4.2.1. Boost Mode

In this mode of operation, when switch Q_2 is closed, the inductor L_{DC} and the ESS are connected in parallel, causing inductor and ESS voltage to be equal. The rate of change in the inductor voltage is constant; thus current presents a linear increase when the switch is closed. On the other hand, when the switch is open, antiparallel diode of switch Q_1 is conducting and current flows to the high voltage bus.

In order modify ESS power output during boost operation, reference power is compared with the measured power at the dc link. The error is provided to a PI controller which gives Duty Cycle as an output. The block diagram of the aforementioned control system is depicted in Figure 4.3:

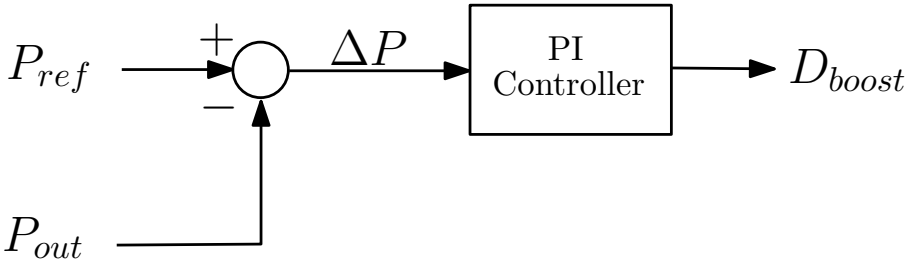

Figure 4.3: Control loop for Boost Mode Duty Cycle.

The aforementioned controller is mathematically expressed as:

$$D_{boost} = (P_{ref} - P_{out}) * (Kp + \frac{K_i}{s}) \tag{4.2}$$

This mode of operation is utilized when an under-frequency is detected and ESS injects power to the grid in order to maintain the frequency between the desired limits.

4.2.2. Buck Mode

For buck mode of operation, a similar process like in the boost mode of operation is applied. In this case, switch Q_1 is switched with a duty cycle dictated by the demanded power output, while switch Q_2 always remains off. It is critical to mention that, like VSC, the two switches cannot be switched on simultaneously because this will cause a short-circuit [25]. Control strategy for buck mode is shown in Figure 4.4:

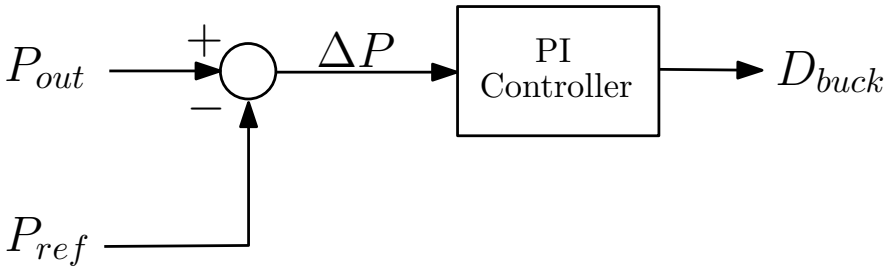

Figure 4.4: Control loop for Boost Mode Duty Cycle.

The aforementioned controller is mathematically expressed as:

$$D_{buck} = (P_{out} - P_{ref}) * (Kp + \frac{K_i}{s} \tag{4.3}$$

This mode of operation is utilized when an over-frequency is detected and ESS absorbs the excess power from the grid in order to maintain the frequency between the desired limits.

From the aforementioned, it is clear that ESS is able to contribute during frequency disturbances, either decline or increase with a proper control strategy applied to the Bi-Directional DC-DC converter, which interfaces it with DFIG's "Back to Back" converters DC Link. This strategy is explained in the following section.

4.3. Integrated frequency and voltage support control system.

It was extensively explained in section 3.3 of Chapter 3, that active and reactive power could be separately controlled with the help of VSC and Park transformation, since they are regulated by a different axis component in each case. This fact provides the flexibility to control active and reactive power output simultaneously and as a result grid's frequency and voltage.

In this section, the proposed control systems for frequency and voltage support are going to be explained.

4.3.1. Inertial Response and Primary Frequency Control proposed approach

The proposed strategy for inertial response and primary frequency control consists of two controls integrated under one system, as shown in Figure 4.5.

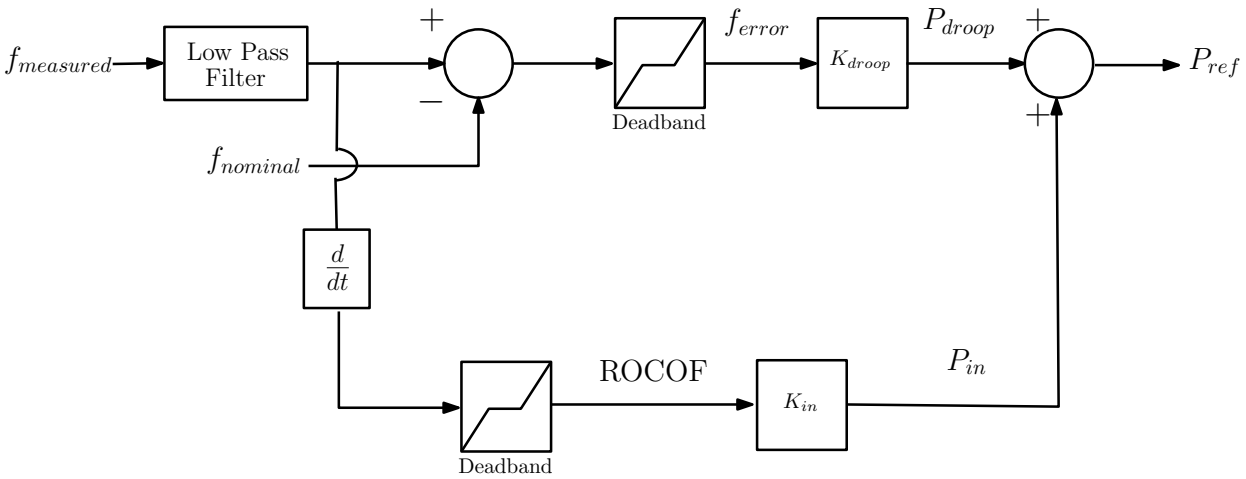

Figure 4.5: Proposed integrated frequency control.

This control scheme can be expressed mathematically with Equation 4.4

$$P_{ref} = (f_{measured} - f_{nominal}) * K_{droop} + \frac{df}{dt} * K_{in} \tag{4.4}$$

The first part, which acts as synthetic inertial response, is a fixed droop control which is adjusting P_{in} value in terms of RoCoF. Thus, controller output tries to restrict the rate of frequency deviation.

The second part, which acts as a primary frequency controller, is a droop controller which changes P_{droop} value according to frequency deviation (Δf) between measured and nominal frequency. This control output enhances frequency nadir (or peak). In contrast with the strategies referred in section 2.3.1 of Chapter 2, this approach allows WT to permanently operate at its maximum power point and does not alternate WT's shaft speed. All the extra power needed to mitigate frequency deviation, which is calculated by the controller (P_{ref}) is provided by the ESS that is paired with the DC Link of the "Back to Back" converter setup of DFIG. The active power set-point is translated to the necessary Duty Cycle for each switch of the Bidirectional DC-DC Converter; thus, the desired power is provided at DC Link and the GSC. This happens due to the fact that, as mentioned at subsection 3.3.4, GSC control uses d-axis current component in order to maintain DC Link voltage stable. As explained before, in order to do so, total active power at the DC Bus has to be zero. Thus, power injected (or absorbed) from the ESS at the DC Link via the converter is also injected to the grid.

4.3.2. Primary Frequency Control for Grid Code Compliance

It was noted in section 1.5, TSOs require from the generating units a specific response pattern during frequency disturbances.

Active Power regulation is divided into **Automatic Frequency Response**, where the active power is automatically adjusted by governors and **Manual Control** where the power output is changed based on the demanded by the TSO set point values.

Requirements for Generators (RfG) define three types of automatic frequency response [26, 27]:

- **Frequency Sensitivity Mode (FSM):**
  This is the operating mode of a power-generating unit in which the active power output changes in response to a change in system frequency, in such a way that it assists with the recovery to target frequency.
- **Limited Frequency Sensitivity Mode for Over-frequencies (LFSM-O):**
  This mode of operation is to be activated, when the system is in an emergency state of over-frequency and all frequency reserves in negative direction have already been deployed.
- **Limited Frequency Sensitivity Mode for Under-frequencies (LFSM-U):**
  This mode of operation is to be activated, when the system is in an emergency state after of under-frequency and all frequency reserves in positive direction have already been deployed.

Those active power control modes details, specified in German Grid Code [28] are shown in Table 4.1:

Table 4.1: Frequency sensitivity modes defined by German Grid Code.

Mode	Description
FSM	0.2 Hz Deadband, 6% droop, 2% of WT capacity
LFSM-U	49.8 Threshold, 2% droop
LFSM-O	50.2 Threshold, 5% droop

A comparison between LFSM-O,LFSM-U and FSM modes is shown in Figure 4.6:

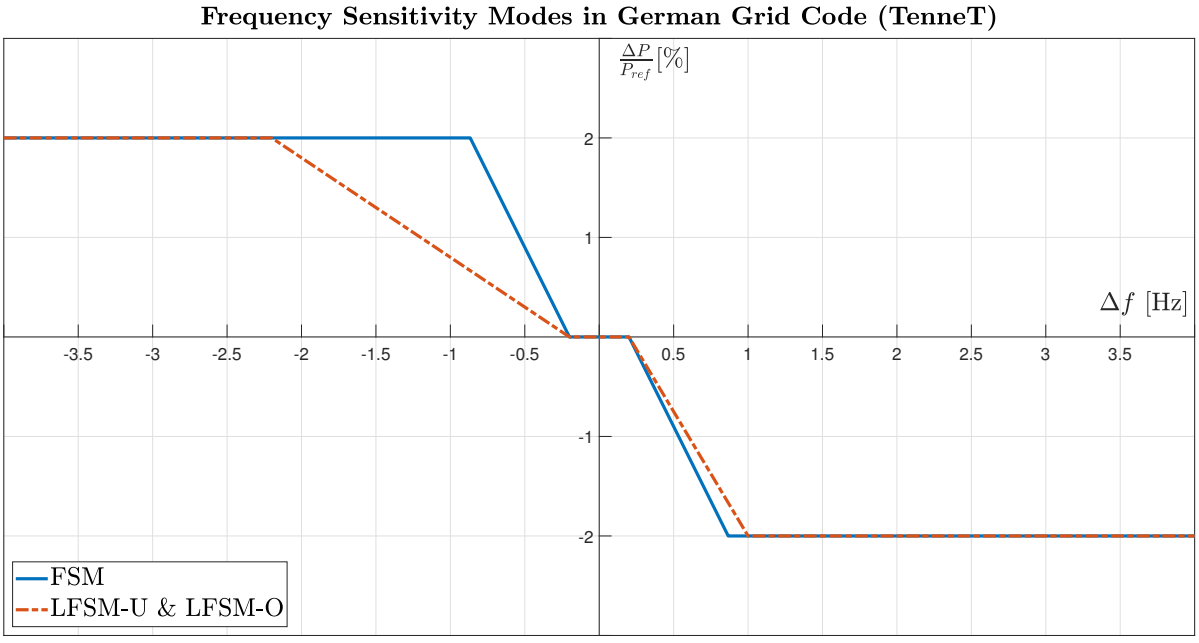

Figure 4.6: Frequency Sensitivity Modes.

A control system for the WT and ESS, in order to comply with the LFSM-O and LFSM-U operation modes is depicted in Figure 4.7:

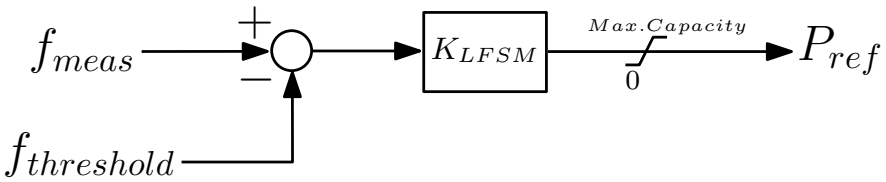

Figure 4.7: ESS Control Strategy for Grid Code Compliance (LFSM-U and LFSM-O).

The mathematical formulation of this controller is shown in Equation 4.5:

$$P_{ref} = (f_{meas} - f_{threshold}) * K_{LFSM} \tag{4.5}$$

Where,

$$K_{LFSM} = \begin{cases} -0.02, & f_{meas} < 49.8Hz \\ 0, & 49.8Hz < f_{meas} < 50.2Hz \\ -0.05, & f_{meas} > 50.2Hz \end{cases}$$

A control system for the WT and ESS, in order to comply with the FSM operation modes is depicted in Figure 4.8:

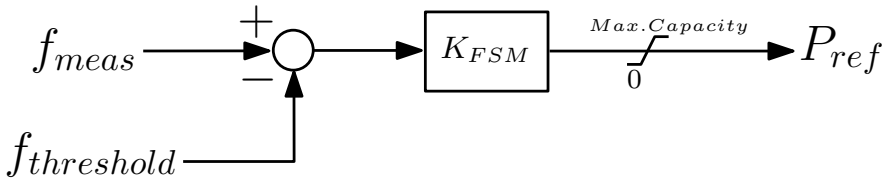

Figure 4.8: ESS Control Strategy for Grid Code Compliance (FSM).

The mathematical formulation of this controller is shown in Equation 4.6:

$$P_{ref} = (f_{meas} - f_{threshold}) * K_{FSM} \tag{4.6}$$

$$K_{FSM} = \begin{cases} -0.06, & f_{meas} < 49.8Hz \\ 0, & 49.8Hz < f_{meas} < 50.2Hz \\ 0.06, & f_{meas} > 50.2Hz \end{cases}$$

With those control systems, the proposed WT topology is capable of complying with the RfG defined specifically by the German Grid Code.

4.3.3. Voltage Support proposed approach

As mentioned in section 3.3, active and reactive power can be separately controlled with the help of VSC topology and Park transformation. This fact provides the capability of controlling active and reactive power output separately in order to regulate the grid's frequency and voltage.

In Chapter 2, different methods for voltage regulations were demonstrated and discussed. The proposed voltage control strategy takes into consideration slip, in order to determine if stator or GSC will provide the needed reactive energy to the grid in order to keep the voltage between the grid code limits for steady-state operation. By doing so, power electronic converters load is taken into consideration, in order to protect them from overloading. At section 3, DFIG's principles of operation were demonstrated. It was realized that, for speeds different than the synchronous one, rotor provides or consumes power, which means that during this state of operation, GSC and RSC are loaded proportionally to the slip. Due to the fact that "Back to Back" converters are partially rated and need to be as small as possible to reduce overall system's cost, it is understood that during high slip values, those converters are not able to participate in voltage regulation.

On the other hand, if slip is close to zero, then GSC is capable of providing reactive power at its full range, which is a feature of DFIG that can be exploited in order to create a flexible control scheme which can always provide the desired reactive power to the grid and utilized all its equipments (stator and power electronic converter topologies).

To begin with, the voltage at the PCC is measured and compared with a reference value, which is the limit for steady-state operation defined by each TSO's grid code. This error is used as an input

of a PI Controller, which provides as an output a current reference i_{ref}. The block diagram of the aforementioned scheme is shown in Figure 4.9:

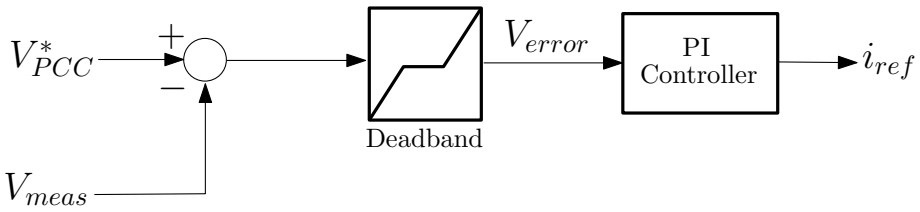

Figure 4.9: Reference current calculation for Voltage Support.

The mathematical formulation of this control scheme is demonstrated in Equation 4.7

$$i_{ref} = (V^*_{PCC} - V_{meas})(K_p + \frac{K_i}{s}) \tag{4.7}$$

After that, current state of operation needs to be determined. For this reason, turbine speed ω_{ref} is measured and compared with the synchronous speed ω_{sync} in order to calculate the slip. It is decided that GSC has to be able to provide (or absorb) a portion of reactive power to (or from) the grid. Thus, a deadband has to be utilized. This deadband defines the amount of reactive power is held as a reserve from GSC. After passing slip through the deadband, this value is compared with zero in order to define which component is going to provide voltage support in case of a disturbance. So, current reference calculated from previous control scheme (Figure 4.9) depending on slip, is provided to the DFIG's converters.

The Equations 4.10, 4.11, 4.8 and 4.9 show the mathematical formulation of the control depicted in Figure 4.10.

$$i^*_{GSC} = i_{ref} * Block_{GSC} \tag{4.8}$$

$$i^*_{RSC} = i_{ref} * Block_{RSC} \tag{4.9}$$

$$Block_{GSC} = \begin{cases} 1, & slip \in [-db, db] \\ 0, & elsewise \end{cases} \tag{4.10}$$

$$Block_{RSC} = \begin{cases} 0, & slip \in [-db, db] \\ 1, & elsewise \end{cases} \tag{4.11}$$

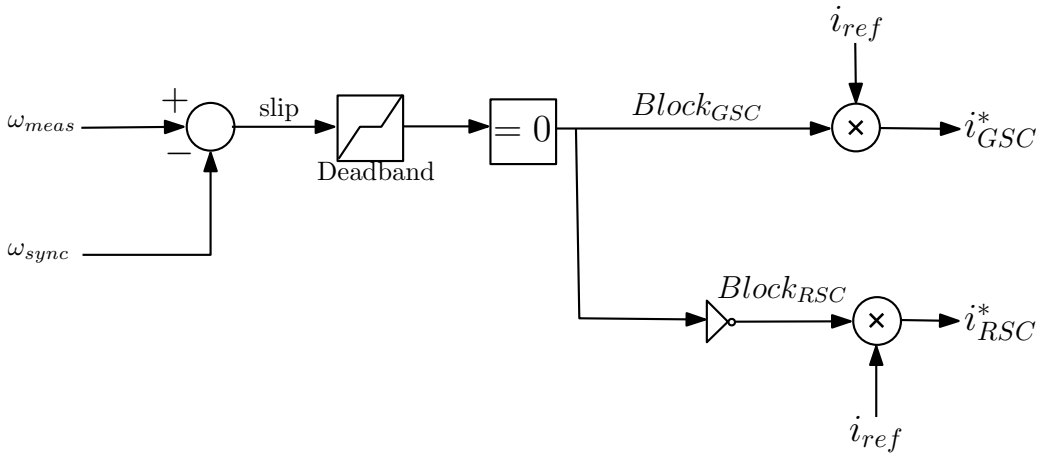

Figure 4.10: Converter participation control logic.

It was demonstrated at section 3.3.4, that q-component of GSC is responsible for controlling its reactive power output. The reference current which is calculated from the aforementioned logic, is compared with the q-axis measured current component. The error is provided as an input to a PI Controller which gives as an output the reference q-axis voltage component. In a following stage, d-component which is defined by DC Link capacitor voltage as referred before and q-component after an inverse Park Transformation are used for PWM control of GSC. Reference voltage control strategy is depicted in Figure 4.11:

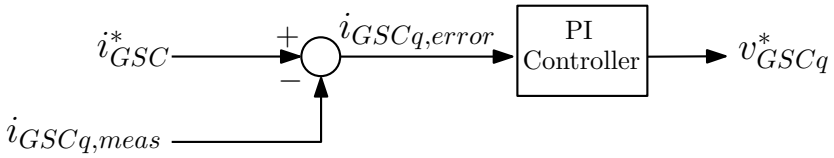

Figure 4.11: Grid Side Converter outer-loop control logic.

This controller can be mathematically expressed as:

$$v^*_{GSC,q} = (i^*_{GSC} - i_{GSCq,meas})(K_p + \frac{K_i}{s}) \tag{4.12}$$

The same logic is applied for RSC control. It is shown above that RSC is able to control stator's reactive power output by properly controlling d-axis component. For this reason, the calculated reference current value is compared with the measured d-axis current component of RSC and the error is provided to a PI Controller. The output of this controller is the d-axis voltage component, which after an inverse Park Transform is utilized for the effective control of RSC with the PWM method. The RSC voltage support control strategy is depicted in Figure 4.12.

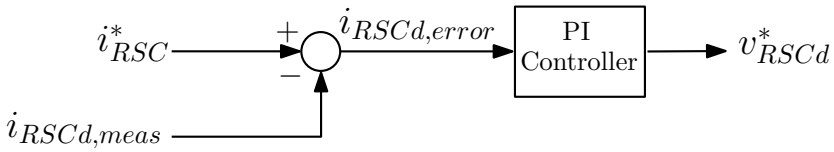

Figure 4.12: Rotor Side Converter outer-loop control logic.

The equation that describe this control is shown below:

$$v^*_{RSC,d} = (i^*_{RSC} - i_{RSCd,meas})(K_p + \frac{K_i}{s}) \tag{4.13}$$

The aforementioned control system is capable of providing voltage support to the grid in each case of operation (sub, synchronous and super-synchronous) by smartly utilizing the converters according to the slip; thus according to their loading and protect them from overcharging. It has to be noted that the system is enabled only when voltage is breaching the allowed operational limits defined by the grid code and maintain it between them. In order to bring the voltage back to its nominal value, TSOs have to proceed to further actions.

5

Simulation and Results

In the previous chapter, the mathematical modelling of each system component was demonstrated. Moreover, the control systems for frequency and voltage support were thoroughly explained and analyzed.

In this section, frequency and voltage behaviour for different operational scenarios is going to be demonstrated, and the impact of the proposed topology and control system is explained. The chapter is divided into three sections. At the first one, frequency behaviour is examined during various situations, such as wind penetration, controller gains, delays and WT percentage equipped with ESS. Furthermore, the comparison between Primary Frequency Response and the proposed integrated controller with Primary Frequency Control and Inertial response is demonstrated.

The second section is examining the voltage support capability of the proposed control system. Two different scenarios are going to be considered. At the first one, demanded reactive power is provided by the GSC and at the other one support is given by the DFIG's stator, by properly controlling rotor's excitation with the help of RSC converter.

Finally, since the proposed controller is integrated and is capable of simultaneously mitigating both frequency and voltage deviations, the third section of the results examines system's frequency and voltage behaviour during parallel active and reactive power load changes at the system.

For all the following simulations, IEEE 14-Bus System was used as a benchmark, since it is suitable for frequency and voltage stability studies. Further information about this system can be found in Appendix A.

5.1. Frequency Support

As mentioned before, the system's frequency behaviour is going to be examined in this section. In order to obtain better insight, frequency nadir (or peak) and RoCoF are presented and compared for the various operational scenarios. As a test system, IEEE 14-Bus benchmark system is used, which is appropriate for frequency and voltage stability studies.

5.1.1. Integrated Control for Inertia Response and Primary Frequency Control

In this subsection, the system's frequency behaviour is examined, and a comparison between traditional primary frequency control with the proposed integrated frequency controller is going to be demonstrated. In order to get a frequency deviation at the grid, a load increase of 10 MW at Bus 9 is introduced at the first second of the simulation. The Wind Penetration at this case is 15% (in terms of active power) and all WTs are equipped with ESS. Frequency and RoCoF responses are shown in the following figures and table:

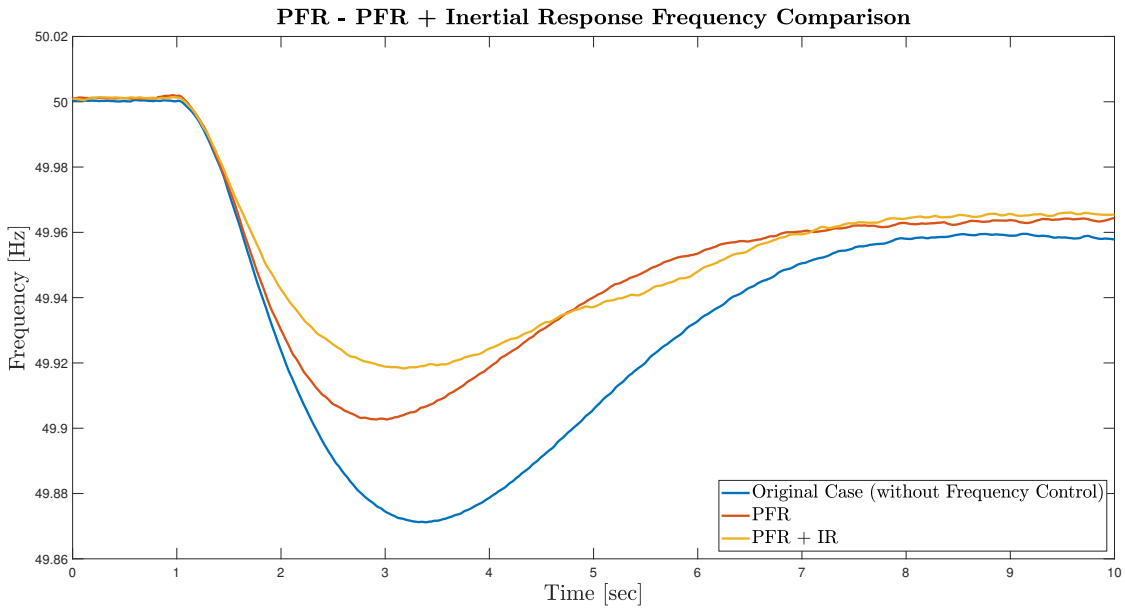

Figure 5.1: Frequency Comparison between PFR and proposed Integrated Control.

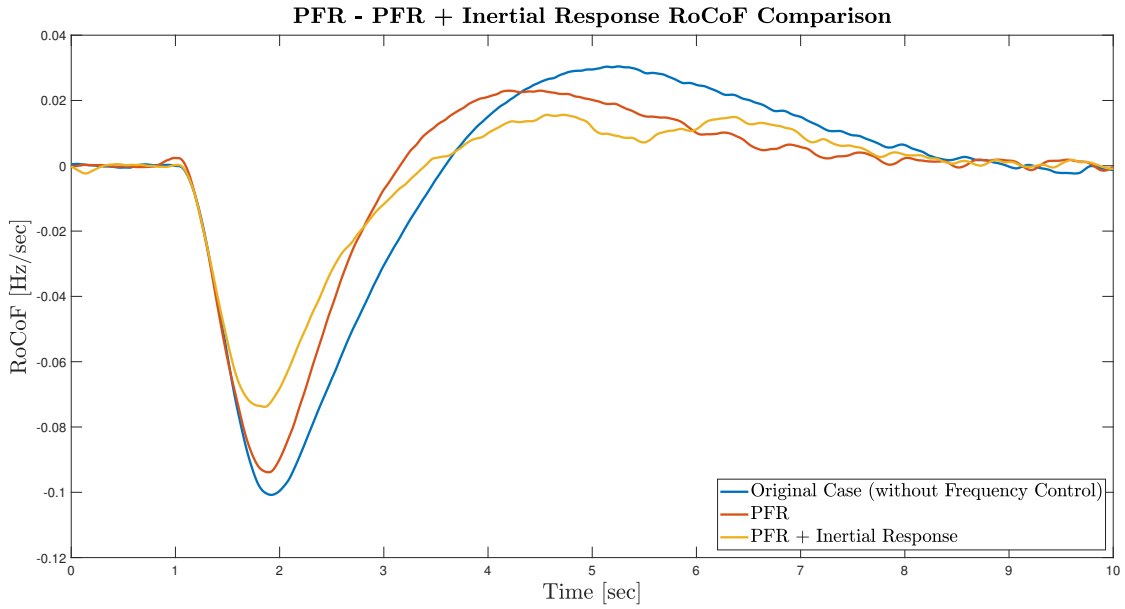

Figure 5.2: RoCoF Comparison between PFR and proposed Integrated Control.

Table 5.1: Frequency and RoCoF Comparison for different Frequency Control strategies.

Frequency Control	Nadir [Hz]	Max.RoCoF [Hz/sec]
No Control	49.8712	-0.1008
PFR	49.9027	-0.0939
Integrated Control	49.9171	-0.0783

From Figures 5.1, 5.2 and Table 5.1 it is clear that Primary Frequency Control has an impact on system's frequency nadir, by increasing it, compared to the base case where WTs do not participate in frequency regulation. Furthermore, it slightly enhances the response of the system by reducing RoCoF immediately after the disturbance. The integrated control strategy, on the other hand, is improving

both primary frequency and inertial response. This can be validated since both Nadir and RoCoF are improved compared to the previous controller.

Since the impact of each controller in frequency and RoCoF was demonstrated above, it is considered necessary to show the participation of the ESS in terms of power and the way this power changes as a function of the indices mentioned above. In the following figures, ESS power injected at the DC Link is shown in the same graphs with the system's frequency and RoCoF:

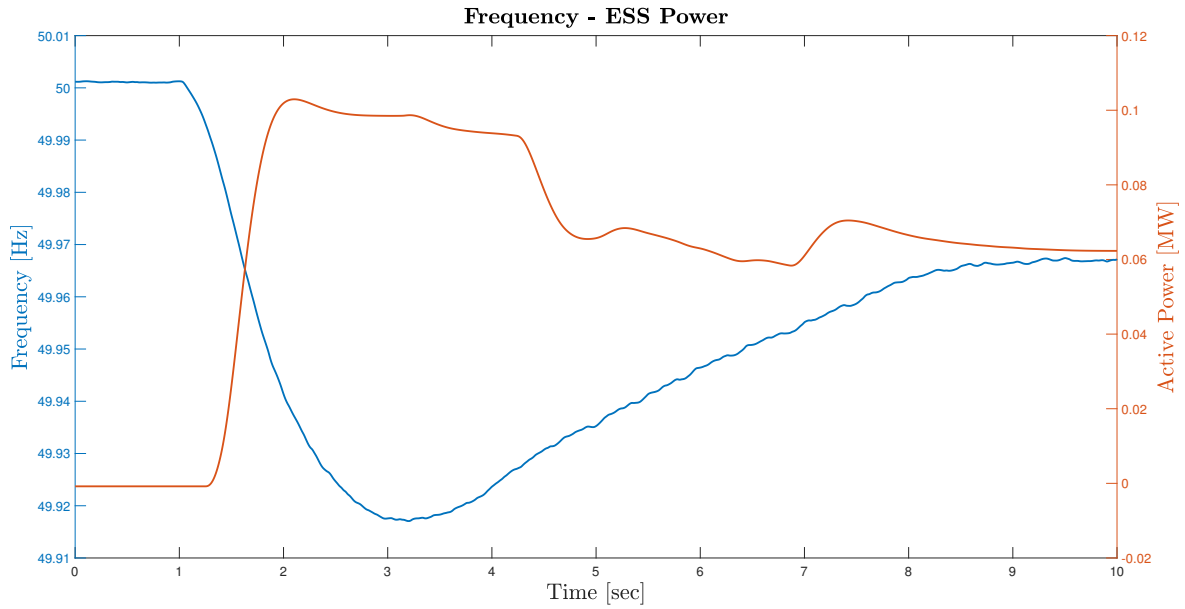

Figure 5.3: ESS Power Output compared with Frequency.

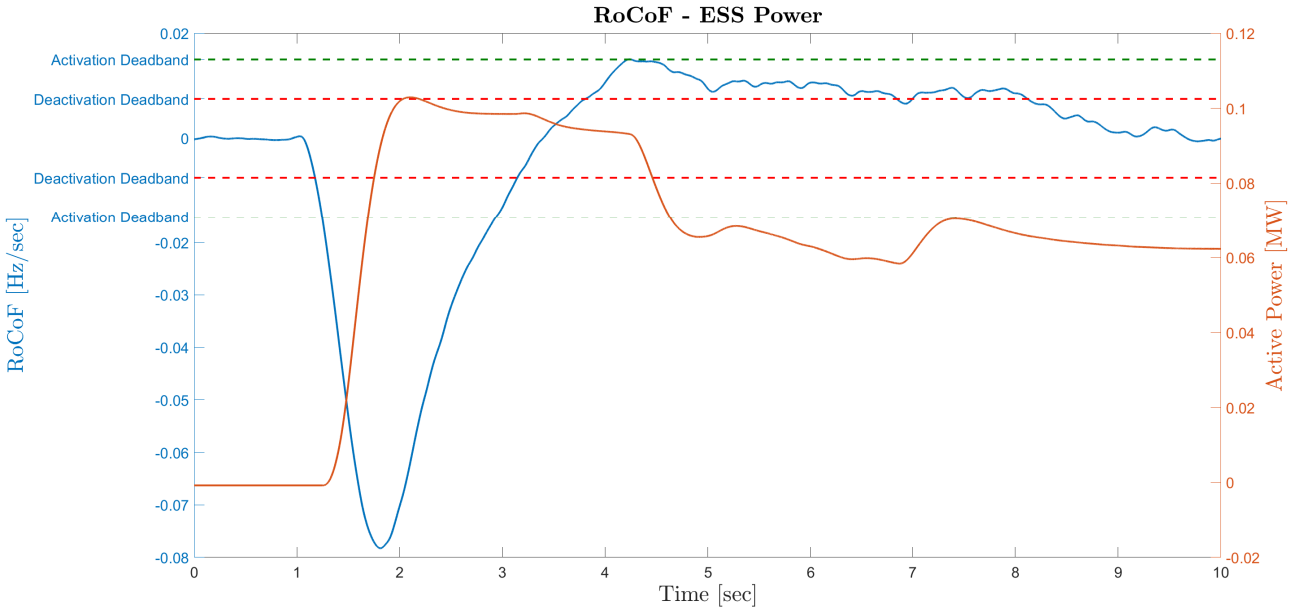

Figure 5.4: ESS Output compared with RoCoF.

It is clear that after the disturbance, almost immediately ESS starts injecting power to the DC Link in order to mitigate the frequency deviation, mimicing the response of a SG. The short delay is a consequence of control system's deadbands. When deadband becomes positive and higher than the activation deadband, injected power is reduced in order to mitigate this increasing RoCoF. The active

power which is still injected after RoCoF is diminished is due to the Primary Frequency control.

In Figure 5.3 and 5.4, ESS power injection at DC Link is depicted. It is also important to demonstrate that this injected power is also transferred and injected properly at the PCC, since TSOs are interested on this injection and not for the "internal" operation of the DFIG. This is shown in Figure 5.5, where ESS, WT and total power at the PCC are depicted:

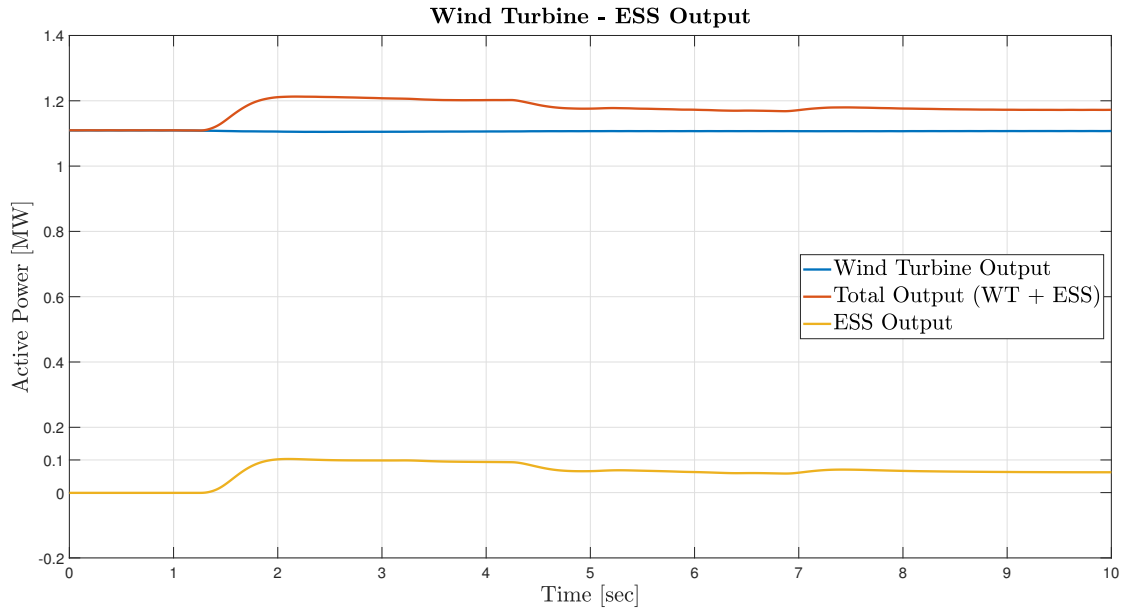

Figure 5.5: Active Power from ESS to the PCC correlation.

It is obvious, that the injected power from the ESS at the DC Link of the "Back to Back" converter configuration of DFIG, is translated to an equal active power increase at the PCC. This means that GSC is capable of providing this extra power to the PCC without any further control actions (as also demonstrated in Equation 4.1).

In order to assess the contribution of the proposed control strategy to system's stability, a comparison between the eigenvalues, obtained with the help of Prony analysis on SG's output power signal is demonstrated in Figure 5.6:

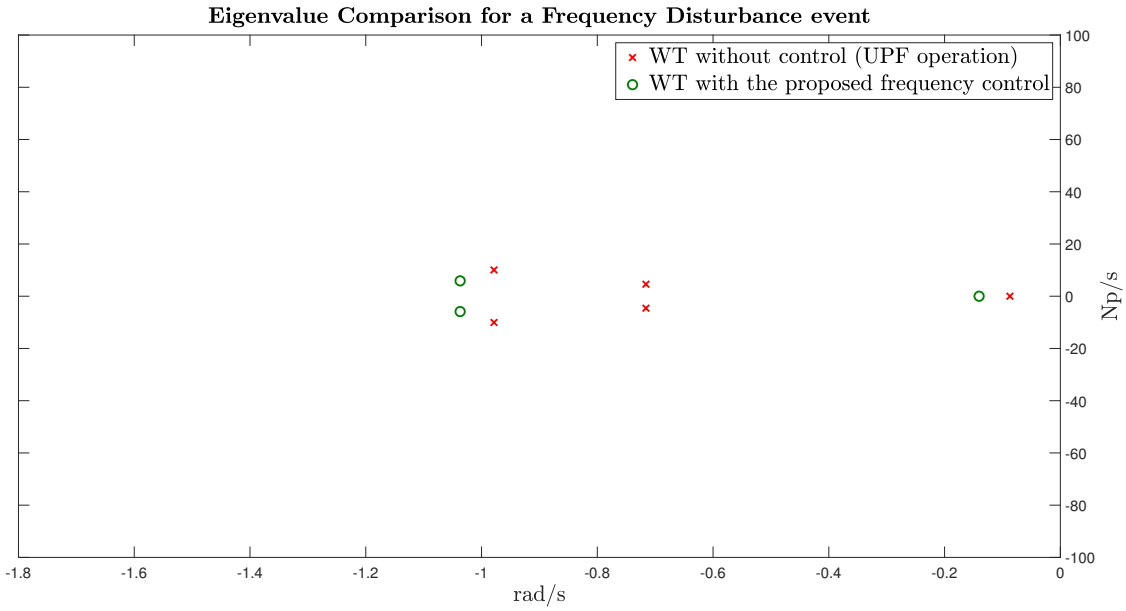

Figure 5.6: Active Power from ESS to the PCC correlation.

It is clear, that oscillations are damped faster with the implementation of the proposed control system, since damping ratio of the derived modes is higher than those, when the WTs are operated under UPF mode. In Figure 5.7, ESS' State-of-Charge is presented.

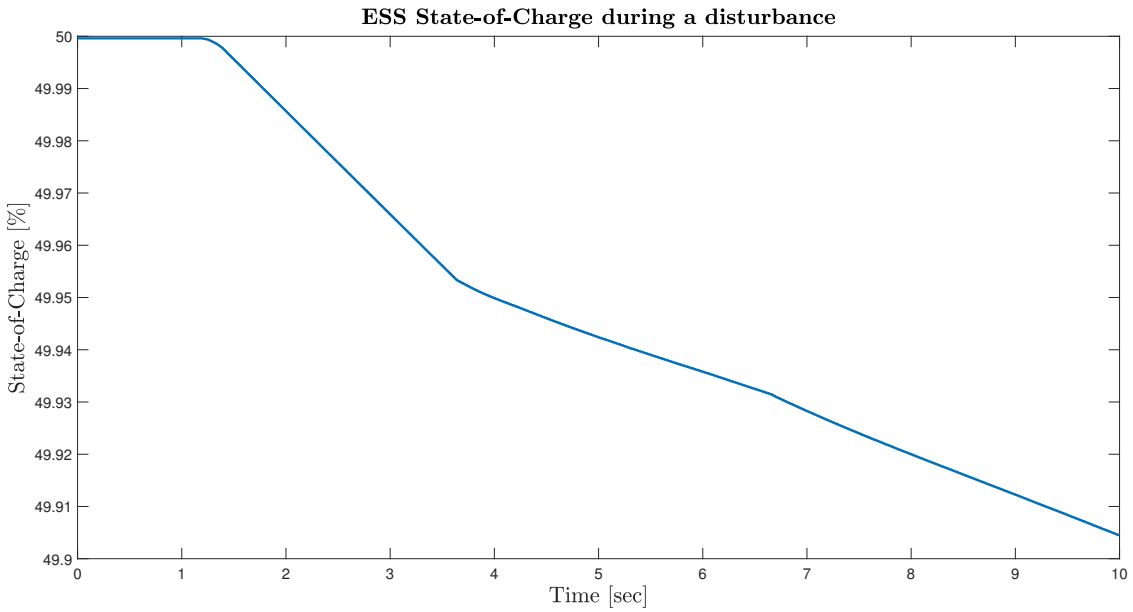

Figure 5.7: ESS State-of-Charge during an under-frequency event.

It is clear that the ESS is discharging after the disturbance and the slope is varying according to the power that is pushed to the grid.

5.1.2. Frequency Comparison for different proportion of WTs equipped with ESS

In this section, a comparative frequency behaviour study for different percentage of WTs equipped with ESS and the proposed control strategy is going to be demonstrated. This study is capable of highlighting proposed topology's impact and its ability to mitigate frequency fluctuations even if it is partially implemented. For the following simulation, Wind Penetration of 15% is considered.

Furthermore, this analysis can provide information about the reserve power needed from ESS in order to achieve an operation similar to the synchronous system's (without any RES, only with SGs). The following figures and table, show the frequency and RoCoF behaviour and indexes of the system for a 10MW load increase at Bus 9 :

Table 5.2: Frequency and RoCoF comparison for different percentage of WTs equipped with ESS.

% ESS	Nadir [Hz]	Max.RoCoF [Hz/sec]
Base Case (Only SG)	49.8853	-0.0906
0 %	49.8691	-0.1000
25 %	49.8812	-0.0931
50 %	49.8941	-0.0878
75 %	49.9064	-0.0820
100 %	49.9171	-0.0783

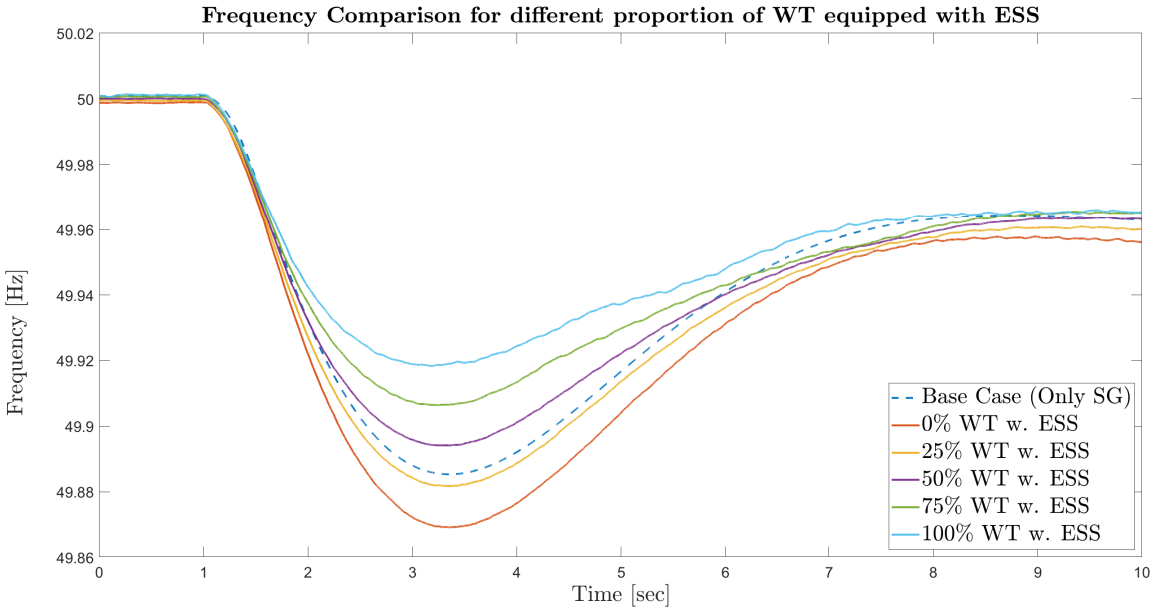

Figure 5.8: Frequency Comparison for different percentage of WT equipped with ESS.

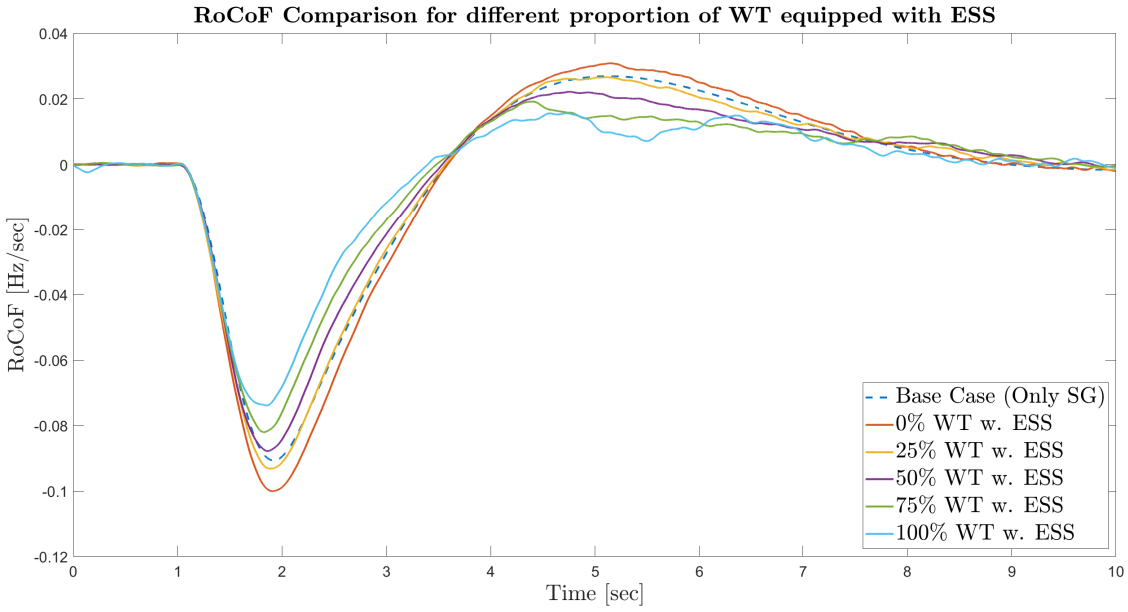

Figure 5.9: RoCoF Comparison for different percentage of WT equipped with ESS.

From Figures 5.8, 5.9 and Table 5.2, it can be observed that, when 50% of farm's WTs are equipped with ESS and the proposed control scheme, frequency's nadir and maximum rate of change are similar to those of the base case, when system operates only with SGs. For a higher rate of the proposed system implementation, frequency becomes more stable than the synchronous system, since power reserve from ESS increases. This is an important feature of the enhanced system, which can be exploited in order to achieve better performance and simultaneously reduce WTs costs.

5.1.3. Frequency Comparison for different Wind Penetration Levels

As mentioned in Chapter 1 (especially in section 1.2) and 2, a serious drawback of RES penetration is that system's inertia decreases; thus the grid is more vulnerable to large frequency deviations. This leads to lower frequency nadirs and higher RoCoF, which stresses the existing synchronous generators and endangers the normal operation. At this subsection, the system's frequency response to a load increase of 20MW at Bus 3, for different penetration levels (in terms of active power) is examined. It has to be noted that, for each level, all WTs are considered to be equipped with ESS and the proposed integrated control system. The findings of those simulations are shown in Figures 5.10,5.11 and Table 5.3:

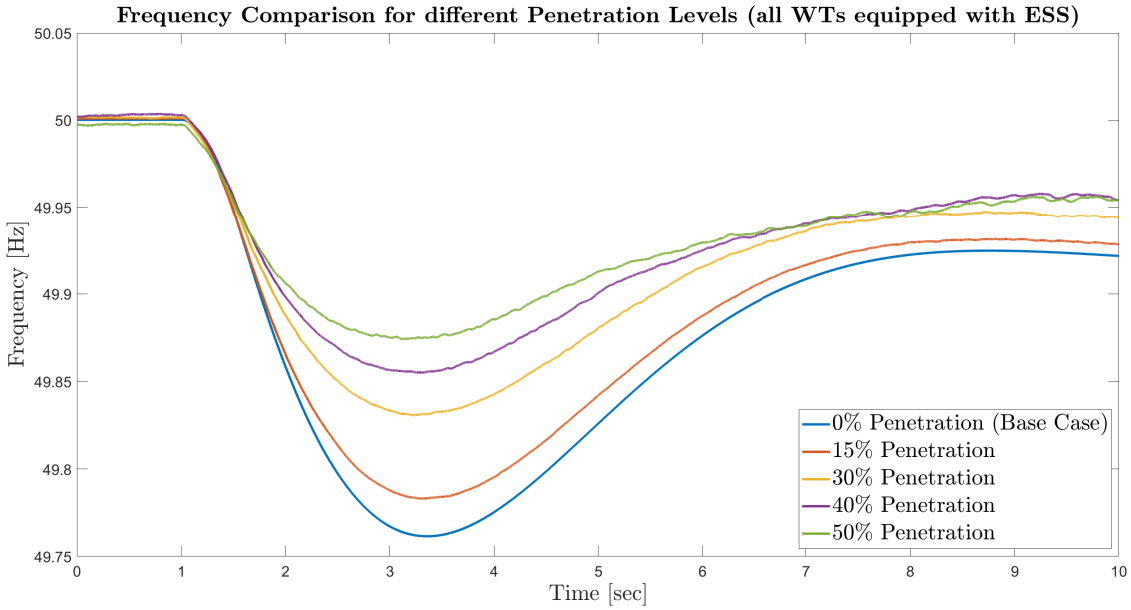

Figure 5.10: Frequency Comparison for different levels of Wind Penetration.

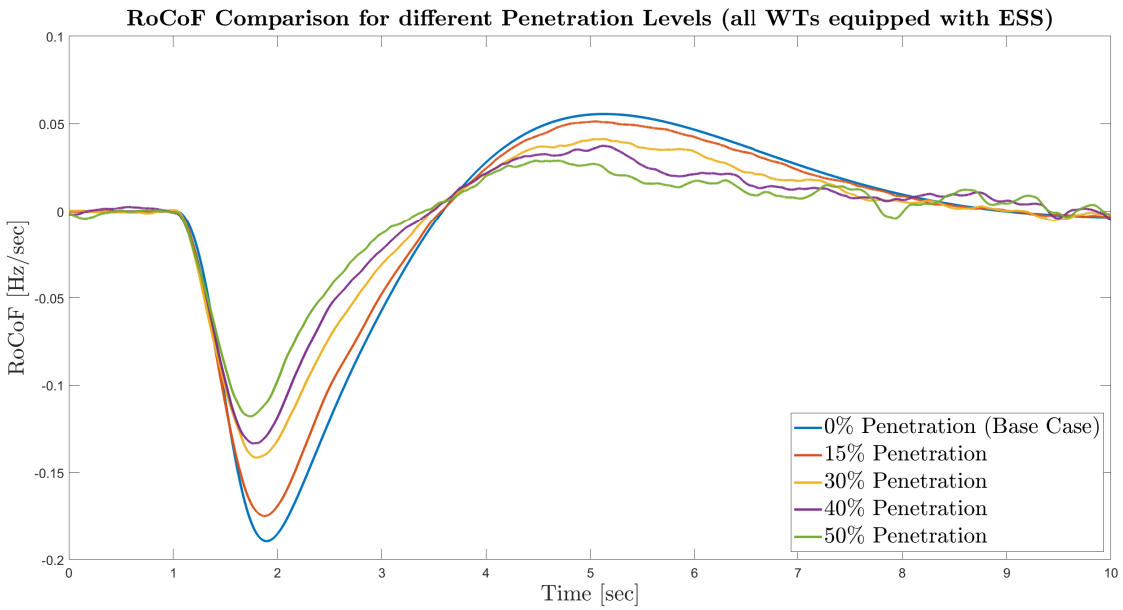

Figure 5.11: RoCoF Comparison for different levels of Wind Penetration.

Table 5.3: Frequency and RoCoF comparison for different Wind Penetration Levels.

Wind Penetration Level	Nadir [Hz]	Max.RoCoF [Hz/sec]
Base Case (Only SG)	49.7615	-0.1895
15 %	49.7830	-0.1751
30 %	49.8308	-0.1416
40 %	49.8551	-0.1334
50 %	49.8742	-0.1180

From the results, it is notable that, while penetration increases, frequency has enhanced performance, since nadir is increased and maximum RoCoF decreases. This is contrary to the system's behaviour when WTs are integrated without control to the grid. Figures 5.10, 5.11 clearly show that frequency nadir and maximum RoCoF are significantly improving as penetration increases. This is a consequence of adding a small ESS (in this case, 5% of DFIG's output). This reserve can be immediately injected to the grid when a frequency disturbance is detected. Furthermore, ESS implementation allows WT to operate at its maximum power point and always provide optimal during its operation.

5.1.4. Frequency Comparison for different Controller Delays

During the previous simulations, it was considered that all of the measurements and controller outputs were obtained in real time. Although this is not the case in an actual power system. In the real world, there is a period of time needed, in order to transmit the data from the measurement location to the control centre and to provide these data from the control centre to the individual controllers [29]. This time period is commonly referred to as communication delay. Those delays shall be implemented in the simulation in order to identify if they cause oscillations and instability. In Figures 5.12, 5.13 and Table 5.4, frequency and RoCoF behaviour, for different delay values that exist in literature [29] are examined. It has to be noted that for the following simulations, Wind Penetration of 15% is considered.

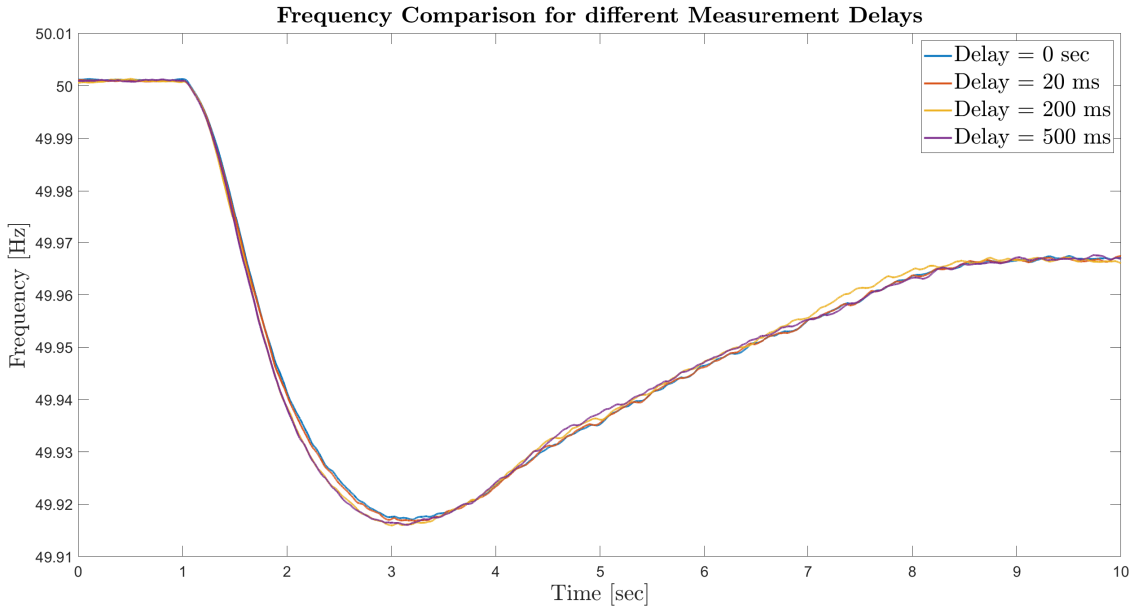

Figure 5.12: Frequency Comparison for different measurement delays at the control system.

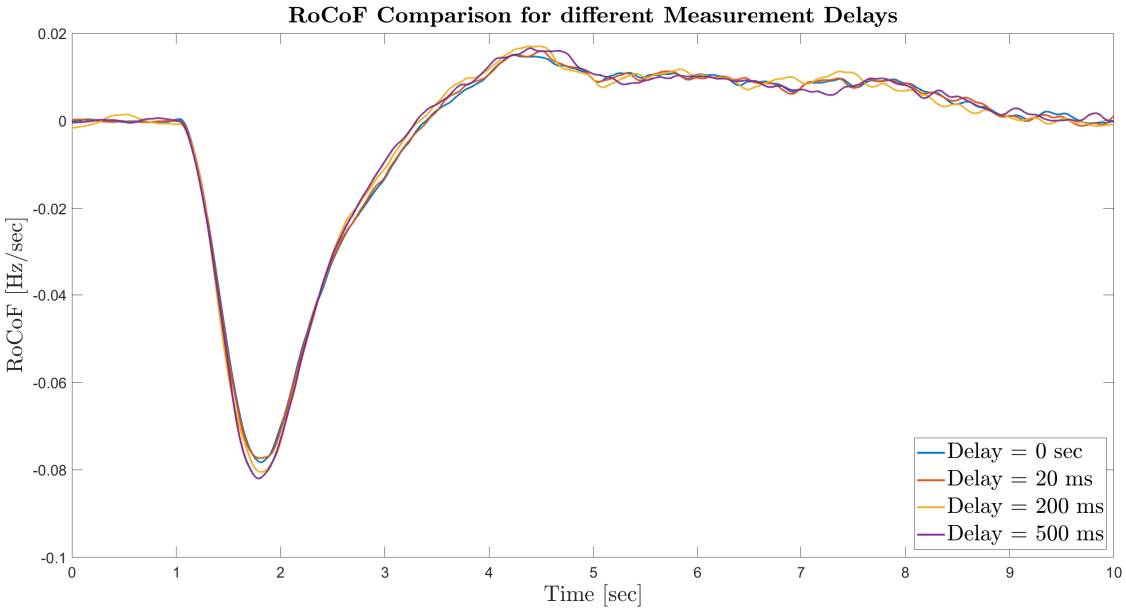

Figure 5.13: RoCoF Comparison for different measurement delays at the control system.

Table 5.4: Frequency and RoCoF comparison for different measurement delay values.

Measurement Delay [ms]	Nadir [Hz]	Max.RoCoF [Hz/sec]
0	49.9171	-0.0783
20	49.9171	-0.0784
200	49.9072	-0.0805
500	49.9071	-0.0820

From those results, it can be observed that measurement and communication delays have a minor impact on frequency's nadir and rate of change. While delay increases, frequency indices go into decline, with RoCoF being more influenced than frequency nadir. Although the impact is not so critical since the difference is insignificant, despite that, those simulations show that delay can be a factor which is capable of limiting and deteriorate the controller if their value is high enough.

5.1.5. Frequency Comparison for different Controller Gains

As shown in section 4.3.1 of chapter 3, integrated control for inertial response and primary frequency control utilize two droop controllers with different gain values. In this section, the sensitivity of the system as a function of those gains is going to be examined. For the following simulations, Wind Penetration of 15% is considered.

Primary Frequency Control Gain Variation

First of all, frequency and RoCoF response during a 10MW load increase at Bus 9 are compared for different K_{droop} values. The results are demonstrated in Table 5.5 and Figures 5.14 and 5.15:

Table 5.5: Frequency and RoCoF comparison for different primary frequency controller gain (K_{droop}) values.

K_{droop}	Nadir [Hz]	Max.RoCoF [Hz/sec]
0	49.9019	-0.0784
1	49.9141	-0.0788
3	49.9173	-0.0746
9	49.9173	-0.0760

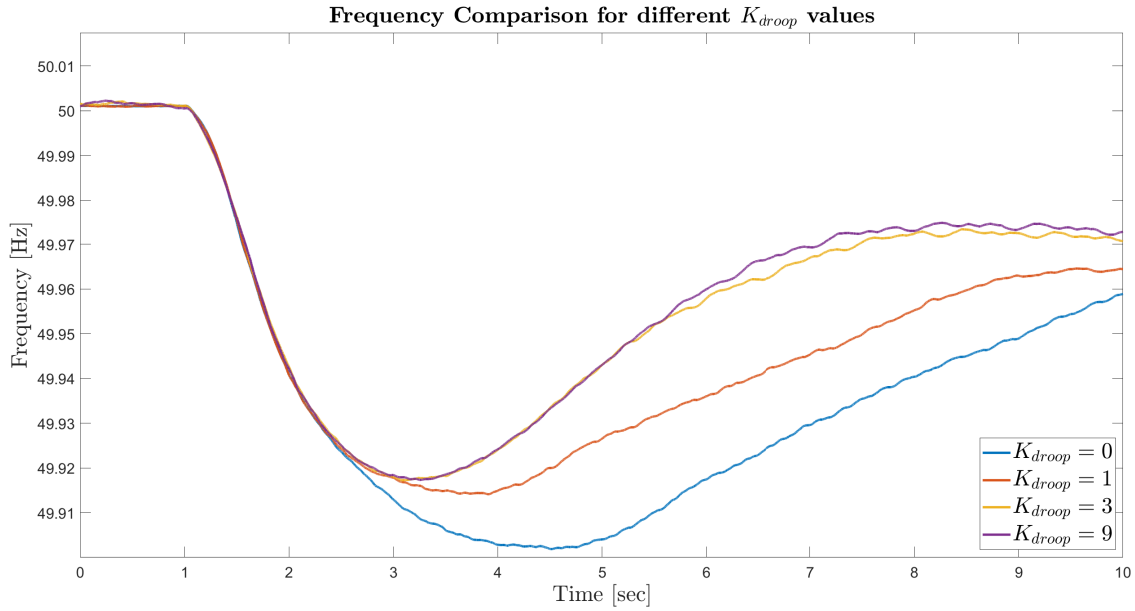

Figure 5.14: Frequency Comparison for different primary frequency controller gain (K_{droop}) controller.

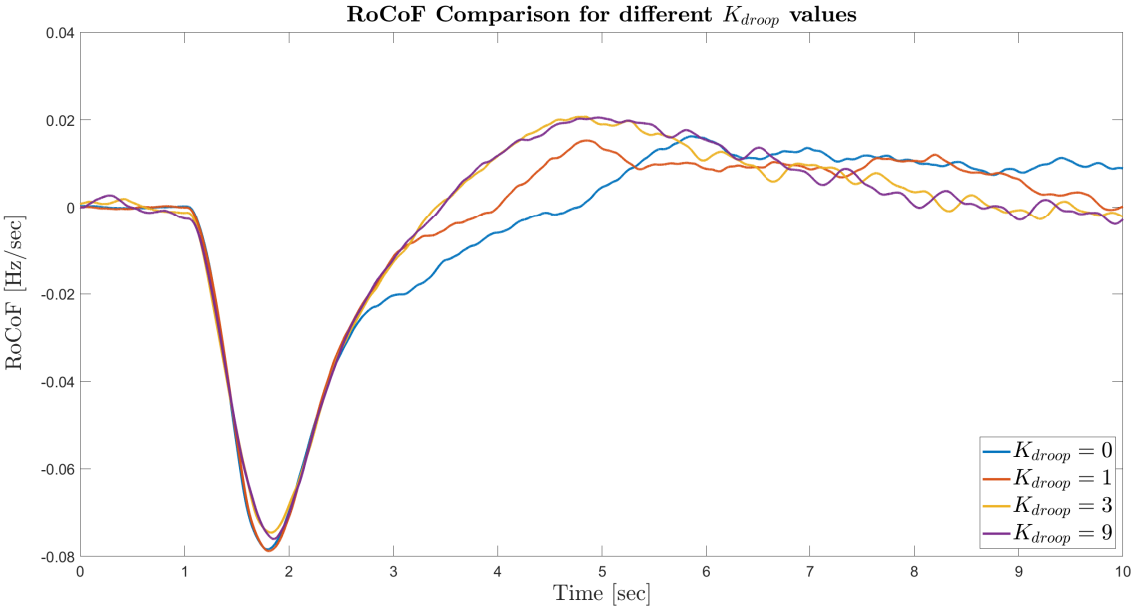

Figure 5.15: RoCoF Comparison for different primary frequency controller gain (K_{droop}) values.

It is noticed from the results, that RoCoF is slightly improved by the droop change. It is expected that this gain variation would have minimum impact on RoCoF since as it was explained in section 4.3.1, K_{droop} acts against frequency deviation and not against RoCoF. On the other hand, it is clear that by changing K_{droop} value, frequency nadir is changing. Specifically, when droop increases, nadir is improved. This trend is not noticed for high gains due to the limits on the duty cycle of the DC-DC converter, which does not allow higher active power injection to the DC Link and as a consequence to the grid.

Inertial Response Gain Variation

It is also considered necessary to identify system's response for different values of the K_{in} gain which is responsible for deteriorating RoCoF by providing inertial response. The frequency and RoCoF behavior for a a 10MW load increase at Bus 9, with different K_{in} gain values are depicted in Figures 5.16, 5.17 and Table 5.6:

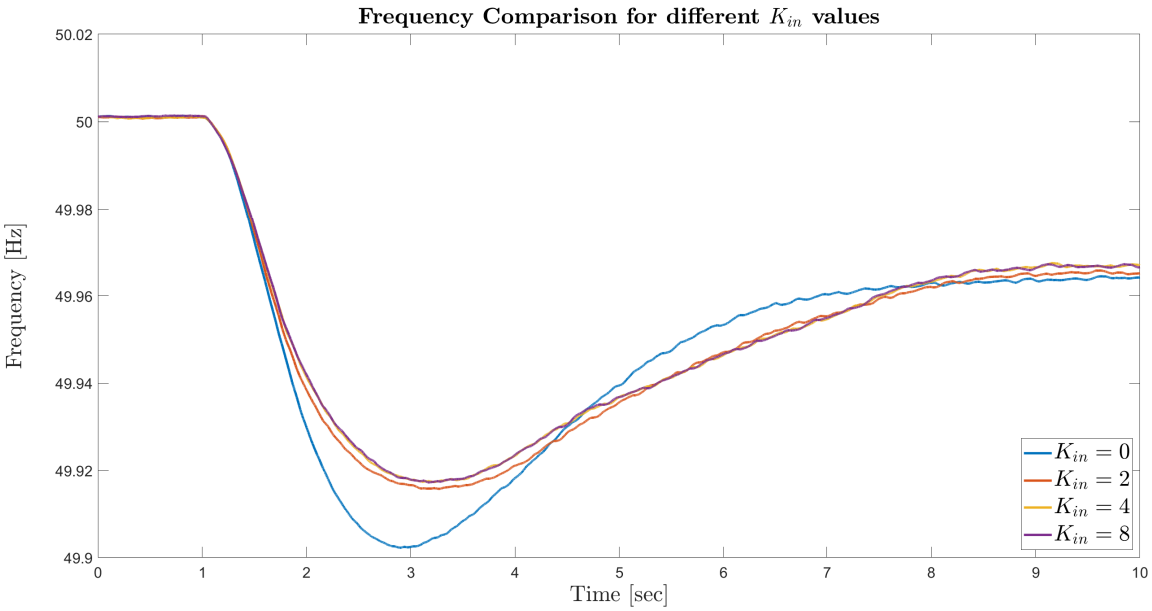

Figure 5.16: Frequency Comparison for different inertial response controller gain (K_{in}) values.

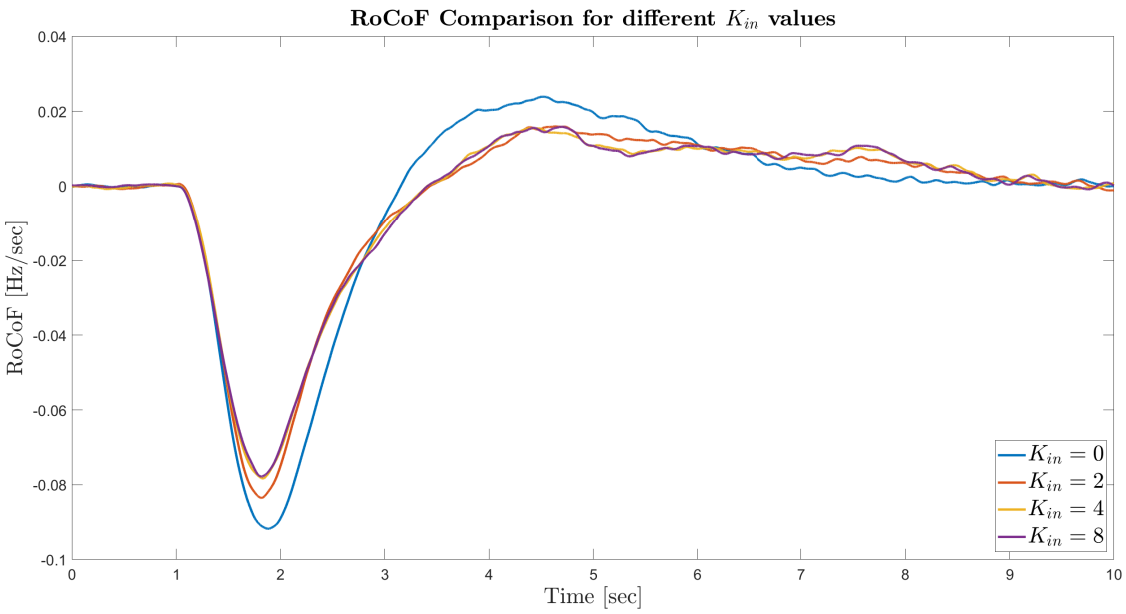

Figure 5.17: RoCoF Comparison for different inertial response controller gain (K_{in}) values.

Table 5.6: Frequency and RoCoF comparison for different inertia response controller gain (K_{in}) values.

K_{in}	Nadir [Hz]	Max.RoCoF [Hz/sec]
0	49.9022	-0.0918
2	49.9158	-0.0835
4	49.9173	-0.0783
8	49.9173	-0.0778

From the results, it is noted that, as explained in section 4.3.1, there is no significant impact of K_{in} gain variation at the system's frequency nadir, since this gain acts against RoCoF. In contrast, while K_{in} gain increases, it is observed that maximum RoCoF is limited. Such as the previous case, after a value, further increase of the gain is not translated into improved RoCoF performance. This happens due to the limitations of the duty cycle of the DC-DC converter.
At this section, it was made clear how each gain affects the behaviour of the system, and the limits of the controller contribution to the system's frequency were demonstrated.

5.1.6. System response during Over-Frequency situations

Most of the frequency disturbances in a transmission system happen for two main reasons, either generation loss, which means that production is decreasing, or load connection to the grid, which is translated to demand increase. Both of the changes mentioned above cause frequency decline since demand is higher than the generation. For that reason, under-frequency disturbances were examined at the previous subsections.

With the development of the existing power system, isolated areas that were previously autonomous and operated with the help of small generators and RES are now connected to the main utility grid with long overhead lines. If for any reason, this connection is lost during steady-state operation, there will be an excess of active power in the isolating grid, which causes over-frequency [30].

In order to tackle this problem, the proposed control scheme is capable of absorbing the excess of active power with the help of ESS and the appropriate control of the interface Bi-Directional DC-DC converter. Figures 5.18 and 5.19 demonstrate frequency and RoCoF comparison during a 15 MW load decrease at Bus 9. It is mentioned that for this simulation, Wind Penetration of 15% is considered.

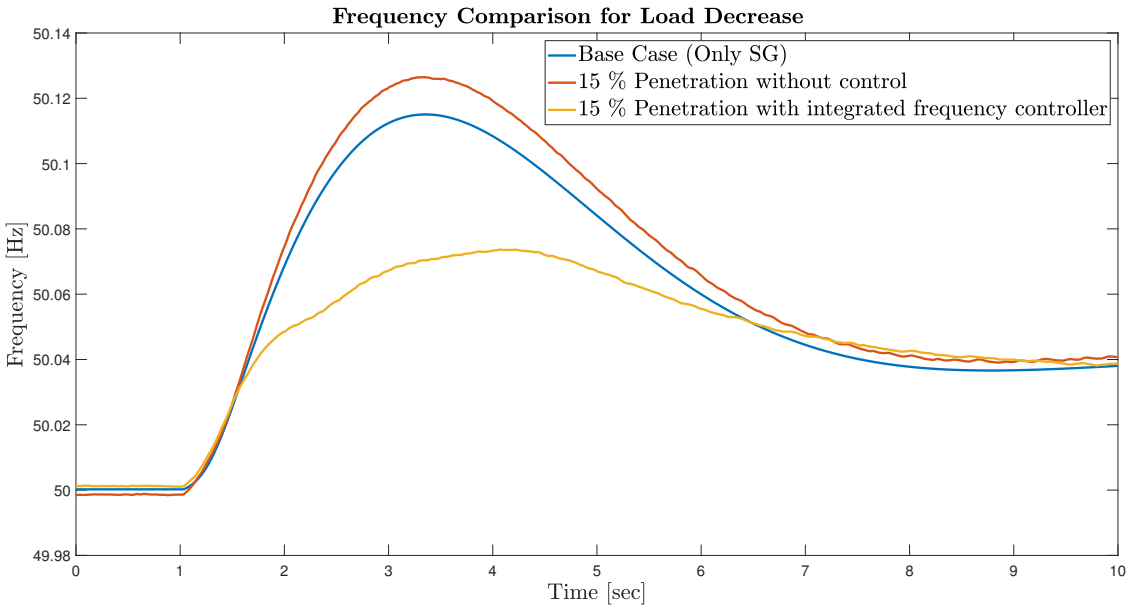

Figure 5.18: Frequency Comparison for over-frequency disturbance.

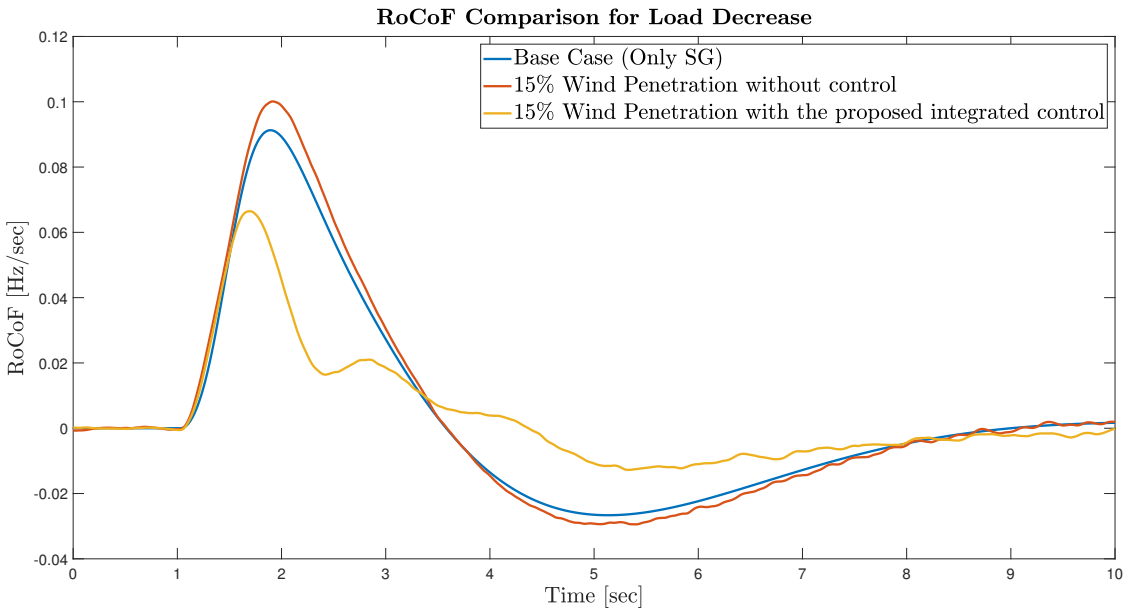

Figure 5.19: RoCoF Comparison for over-frequency disturbance.

A comparison between frequency performance indices for those different operational scenarios is shown in Table 5.7 :

Table 5.7: Frequency and RoCoF comparison for over-frequency disturbances.

Operational Scenario	Peak [Hz]	Max.RoCoF [Hz/sec]
Base Case	50.1151	0.0913
15% Wind Penetration without control	50.1265	0.1001
15% Wind Penetration with the proposed integrated control	50.0737	0.0665

From the results, it can be clearly seen that the proposed controller is capable of effectively mitigating over-frequency disturbances at the grid. In fact, at the specific penetration level (15% in terms of active Power) and proportion of WTs equipped with ESS (100% for this simulation), systems performance is even better than the one when system is running exclusively on SGs.

Specifically, frequency peak is notably decreasing when the proposed control system is implemented. The same behavior is also observed for maximum RoCoF, which is drastically diminished, reducing the stress on the remaining SGs. Moreover, as a consequence of Primary Frequency Control, when the proposed control strategy is deployed, frequency returns to a steady state value which is closer to the nominal one (50 Hz).

Another benefit of the proposed topology and control strategy is that the system is capable of capturing the excess power during imbalances, store it, and uses it when it is needed to provide frequency support in the future. In Figure 5.20, ESS's State of Charge is demonstrated. It can be seen that, when the disturbance happens, at the first second of the simulation, DC-DC converter operates in buck mode and charges the ESS. Until Secondary Frequency Control takes action, which is responsible for active power re-dispatch in order to bring frequency back to the nominal value, ESS is going to absorb power which will be utilized at a later frequency dip. State of charge is shown in Figure 5.20:

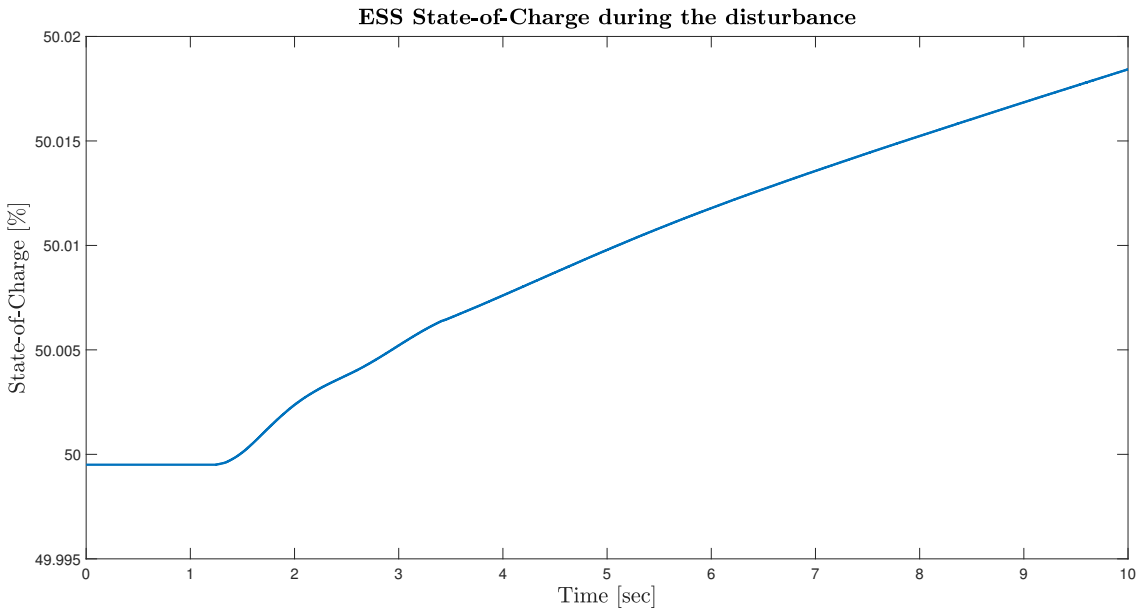

Figure 5.20: ESS State-of-Charge during an under-frequency event.

5.1.7. Grid Code Compliance

In this subsection, system's capability of complying with the Requirements for Generators (RfG) is going to be examined for both under and over-frequency disturbances. Moreover, all three modes explained in Chapter 4 are going to be examined and demonstrated.

Frequency Sensitive Mode (FSM)

This paragraph examines active power output of the WT for different frequency disturbances, when WT is operated under Frequency Sensitive Mode (FSM). As stated in section 4.3.2, WT shall change its output with 0.06 droop while deadband is set at 0.2 HZ. Figures 5.21,5.22,5.23 show WT's response to under-frequency disturbances, while Figures 5.24,5.25 and 5.26 depict the response to over-frequency events. Moreover, Table 5.8 shows the results for over and under frequency events.

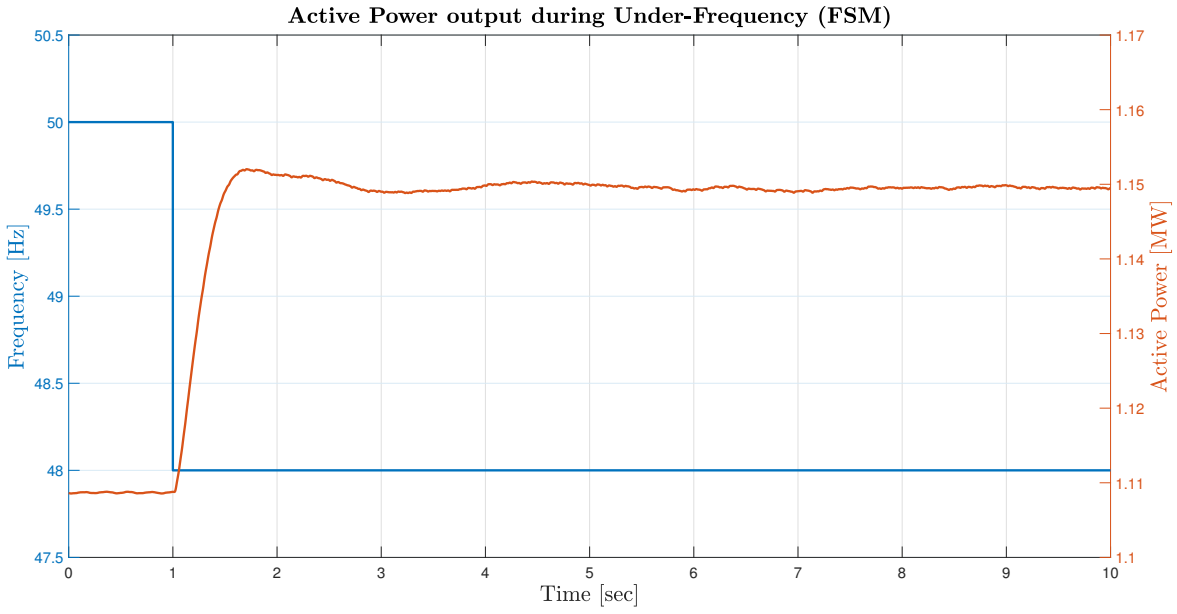

Figure 5.21: Wind Turbine response during under-frequency event (FSM operation, 2 Hz disturbance).

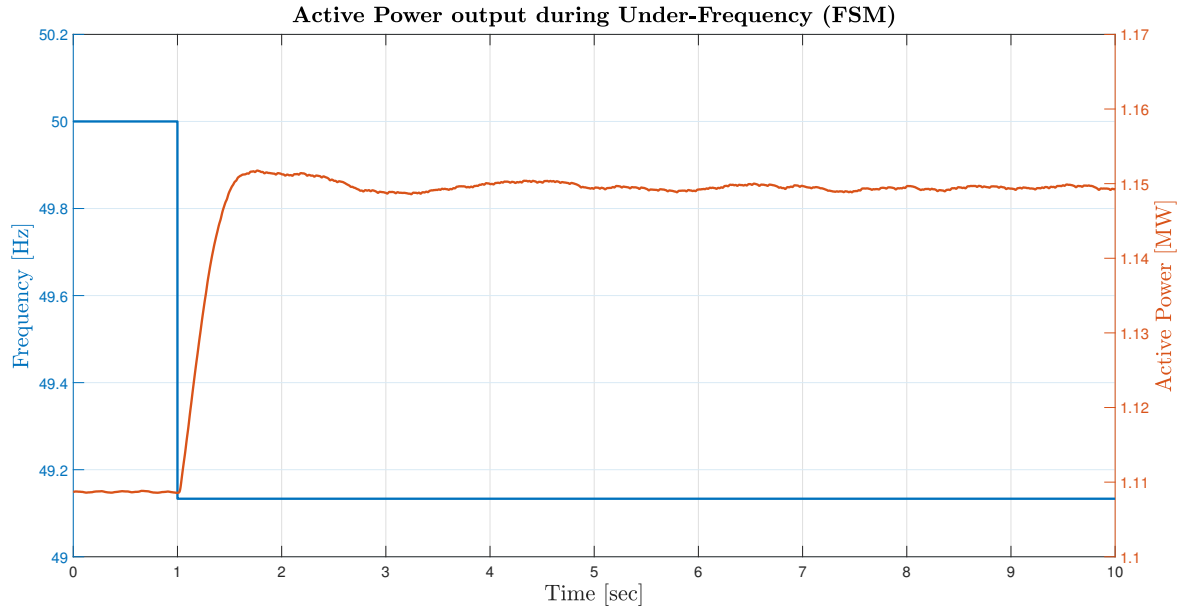

Figure 5.22: Wind Turbine response during under-frequency event (FSM operation, 0.87 Hz disturbance).

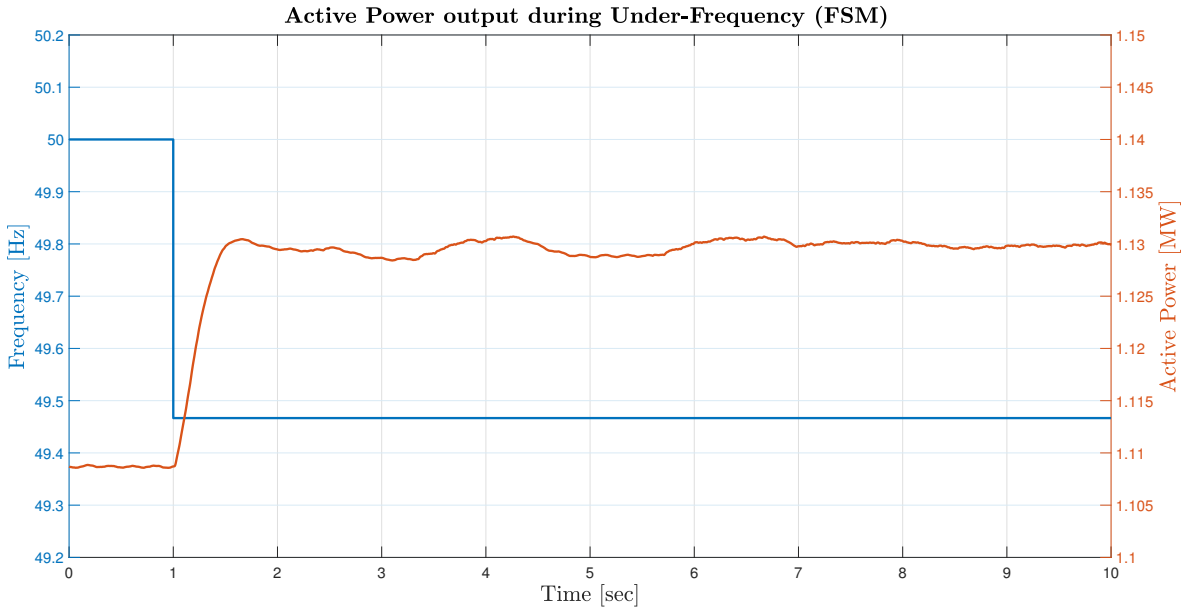

Figure 5.23: Wind Turbine response during under-frequency event (FSM operation, 0.54 Hz disturbance).

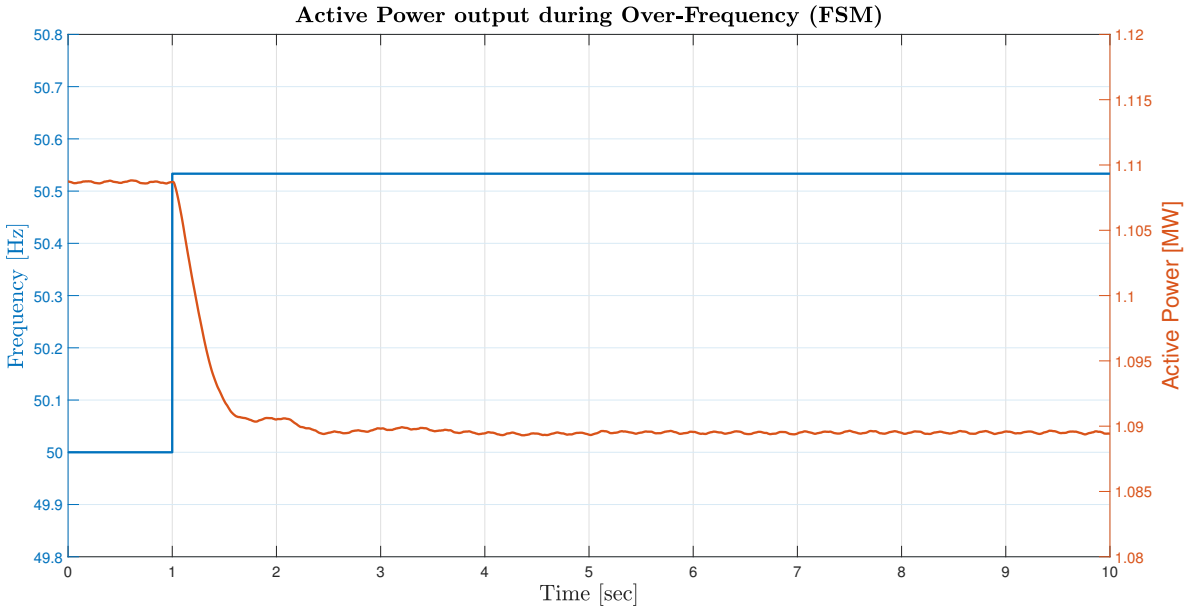

Figure 5.24: Wind Turbine response during over-frequency event (FSM operation, 0.54 Hz disturbance).

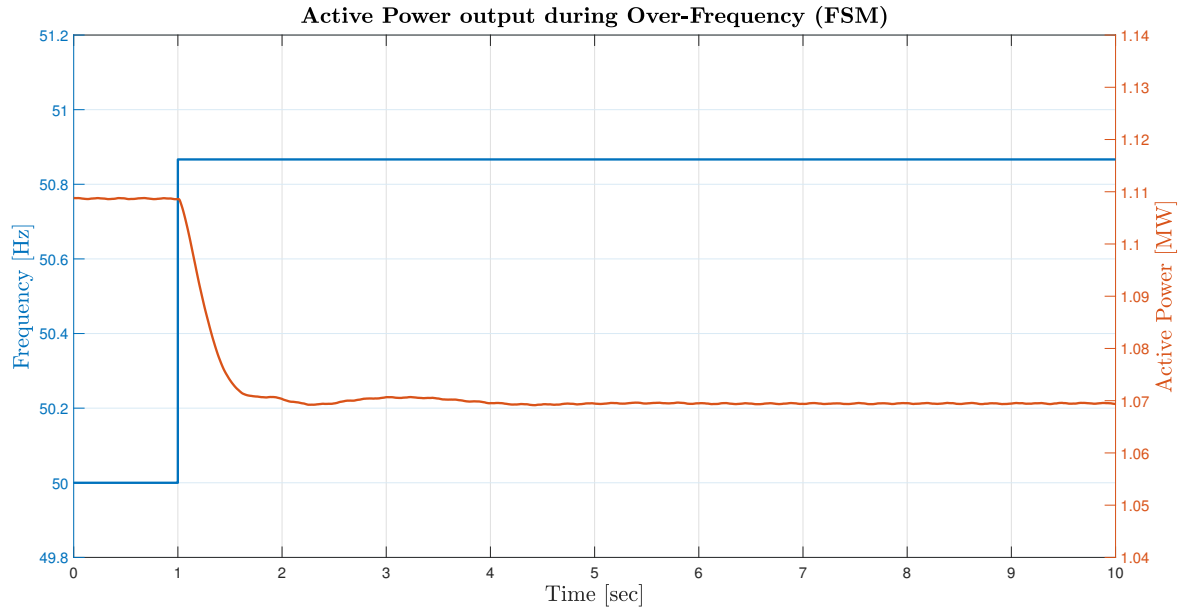

Figure 5.25: Wind Turbine response during under-frequency event (FSM operation, 0.84 Hz disturbance).

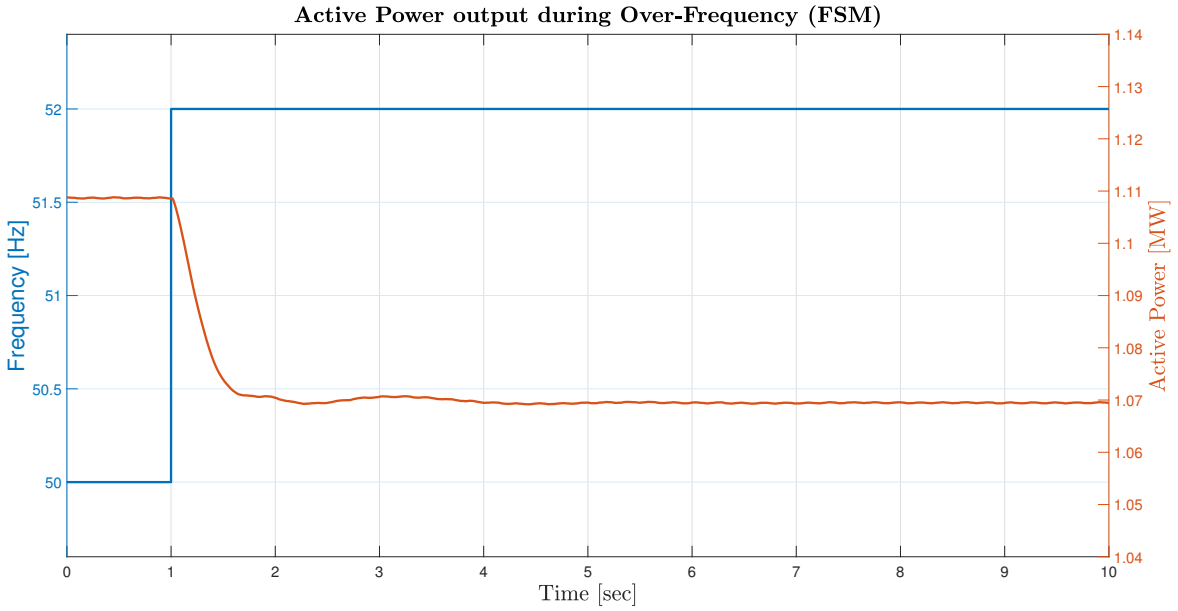

Figure 5.26: Wind Turbine response during over-frequency event (FSM operation, 2 Hz disturbance).

Table 5.8: WT response during FSM operation.

ΔF [Hz]	P_{pre} [MW]	P_{post} [MW]	ΔP [MW]	$\frac{\Delta P}{P_{ref}}$ [%]
-2	1.11	1.15	0.04	2
-0.87	1.11	1.15	0.04	2
-0.54	1.11	1.13	0.02	1
0.54	1.11	1.09	-0.02	-1
0.87	1.11	1.07	-0.04	-2
2	1.11	1.07	-0.04	-2

It is clear that immediately after the disturbance, active power injection at the PCC is modified, according to the frequency deviation. This is happening since ESS is providing frequency support to the grid according to the controller. The proposed system is capable of complying with the Frequency Sensitive Mode, as stated in Germany's grid code.

Limited Frequency Sensitivity Mode - Under-Frequency (LFSM-U)

In this paragraph active power output of the WT for different frequency disturbances, when WT is operated under Limited Frequency Sensitivity Mode for Under-Frequency (LFSM-U). As discussed in section 4.3.2, WT shall change its output with 0.02 droop while deadband is set at 0.2 HZ. Figures 5.28,5.27,5.29 show WT's response to under-frequency disturbances. Moreover, Table 5.9 shows the results for over and under frequency events.

Table 5.9: WT response during LFSM-U operation.

ΔF [Hz]	P_{pre} [MW]	P_{post} [MW]	ΔP [MW]	$\frac{\Delta P}{P_{ref}}$ [%]
-1.2	1.91	1.93	0.02	1
-2.2	1.91	1.94	0.04	2
-2.33	1.91	1.94	0.04	2

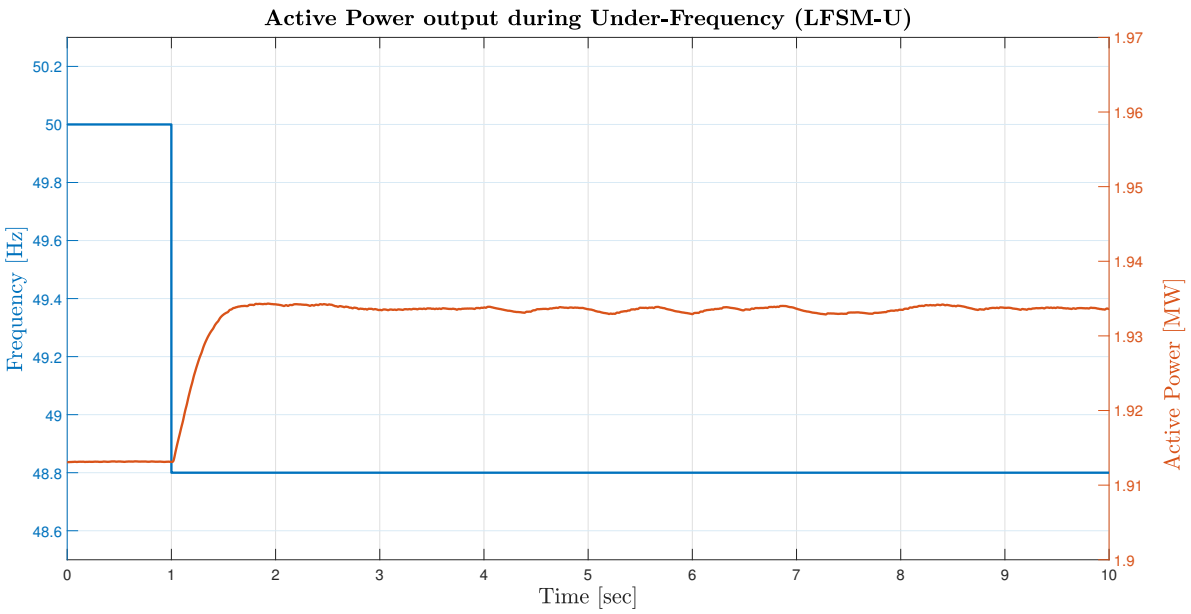

Figure 5.27: Wind Turbine response during under-frequency event (LFSM-U operation, 1.2 Hz disturbance).

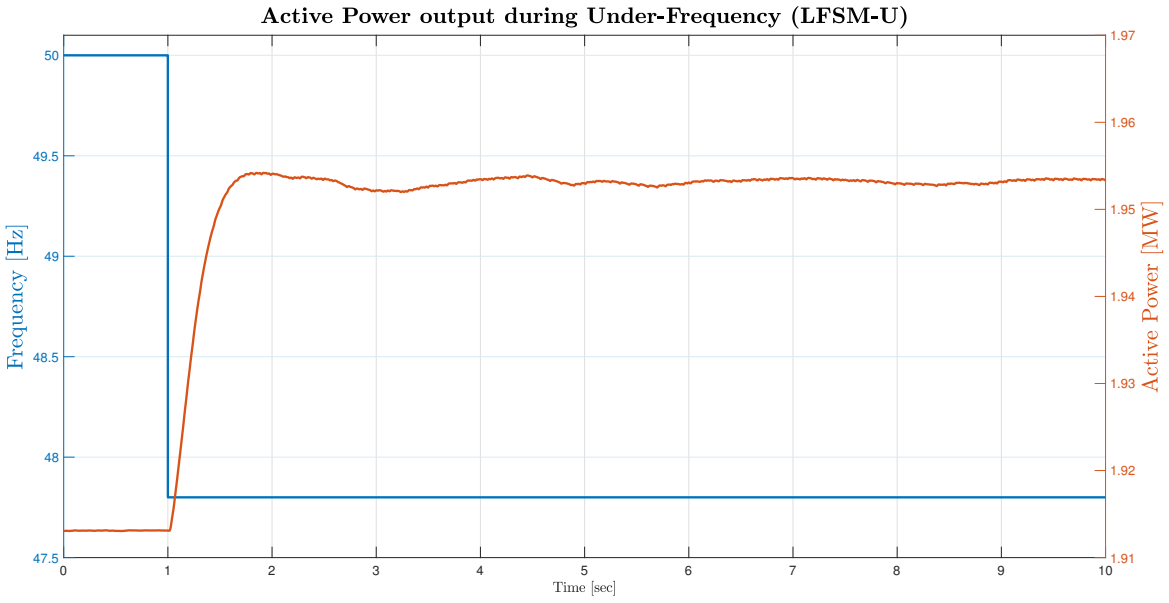

Figure 5.28: Wind Turbine response during under-frequency event (LFSM-U operation, 2.2 Hz disturbance).

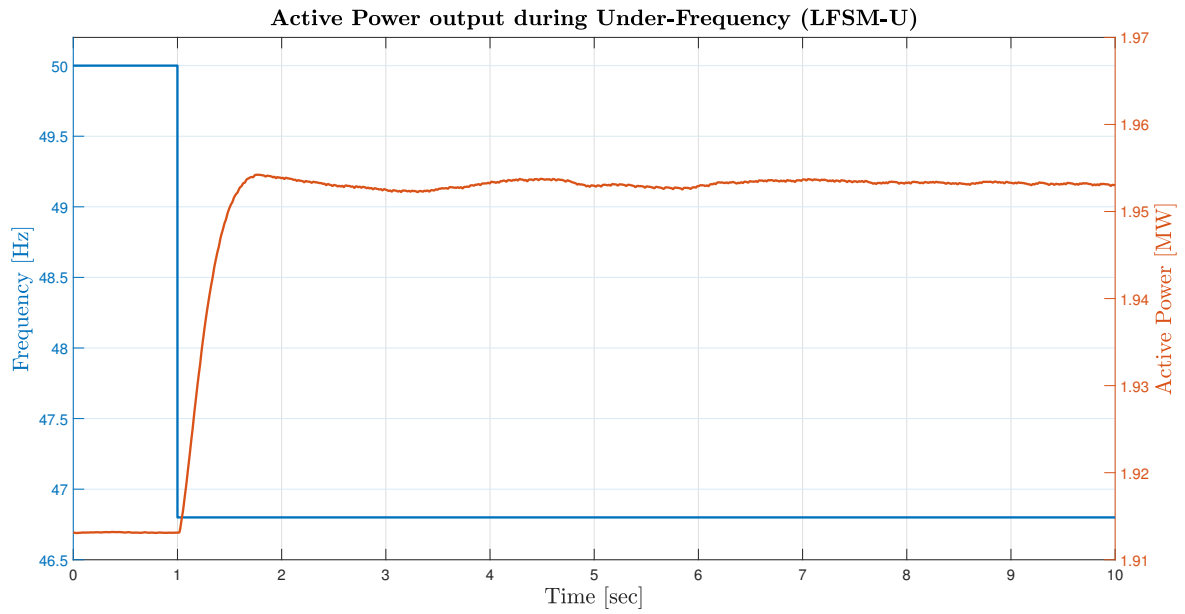

Figure 5.29: Wind Turbine response during under-frequency event (LFSM-U operation, 2.33 Hz disturbance).

When the frequency disturbance occurs, active power injection at the PCC is increasing, according to the frequency deviation. This is happening since ESS is providing frequency support to the grid according to the controller. The proposed system is capable of complying with the Limited Frequency Sensitivity Mode - Under-Frequency, as stated in Germany's grid code.

Limited Frequency Sensitivity Mode - Over-Frequency (LFSM-O)

In this paragraph active power output of the WT for different frequency disturbances, when WT is operated under Limited Frequency Sensitivity Mode for Over-Frequency (LFSM-O). As discussed in section 4.3.2, WT shall change its output with 0.05 droop according to frequency deviation while deadband is set at 0.2 HZ. Figures 5.30,5.31 and 5.32 depict the response of the WT to over-frequency events. Moreover, Table 5.10 shows the results for over and under frequency events.

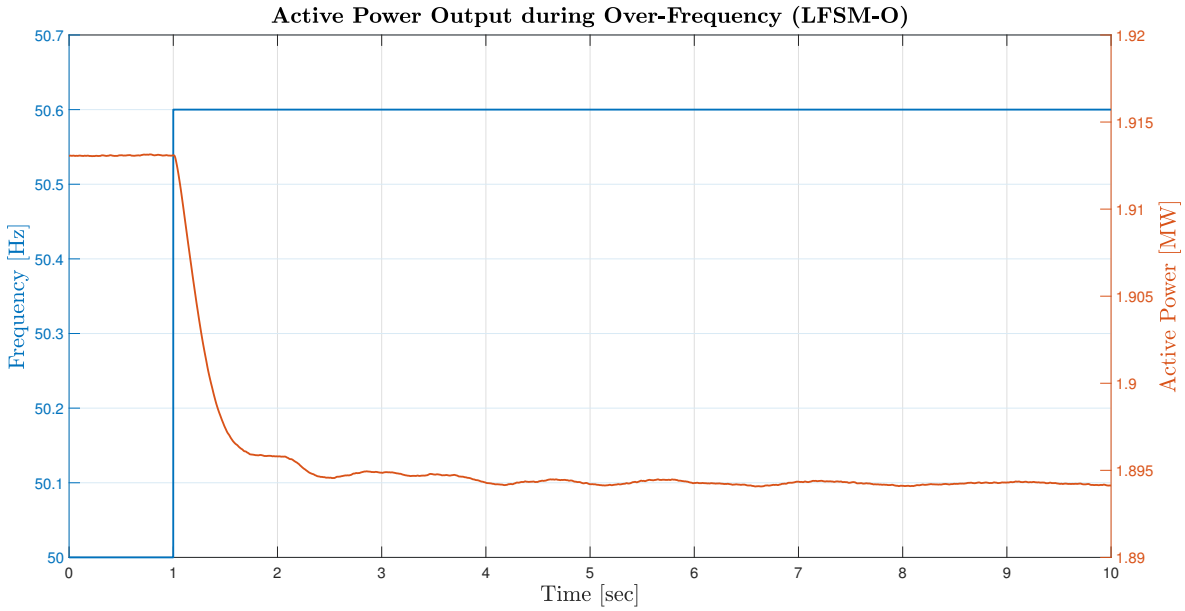

Figure 5.30: Wind Turbine response during over-frequency event (LFSM-O operation, 0.6 Hz disturbance)

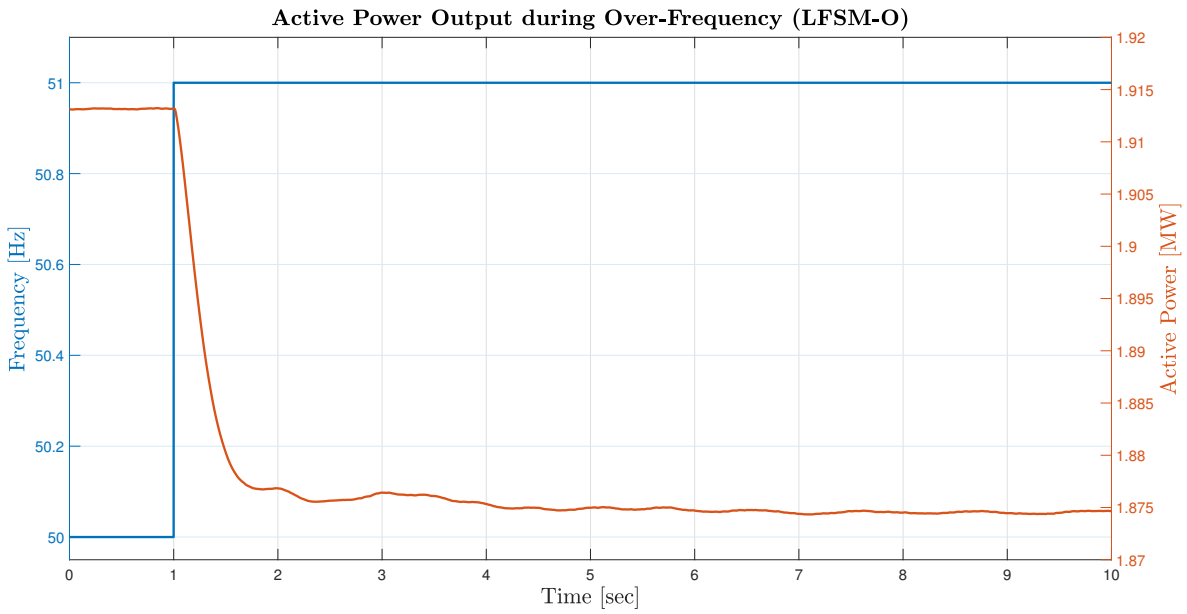

Figure 5.31: Wind Turbine response during under-frequency event (LFSM-O operation, 1 Hz disturbance)

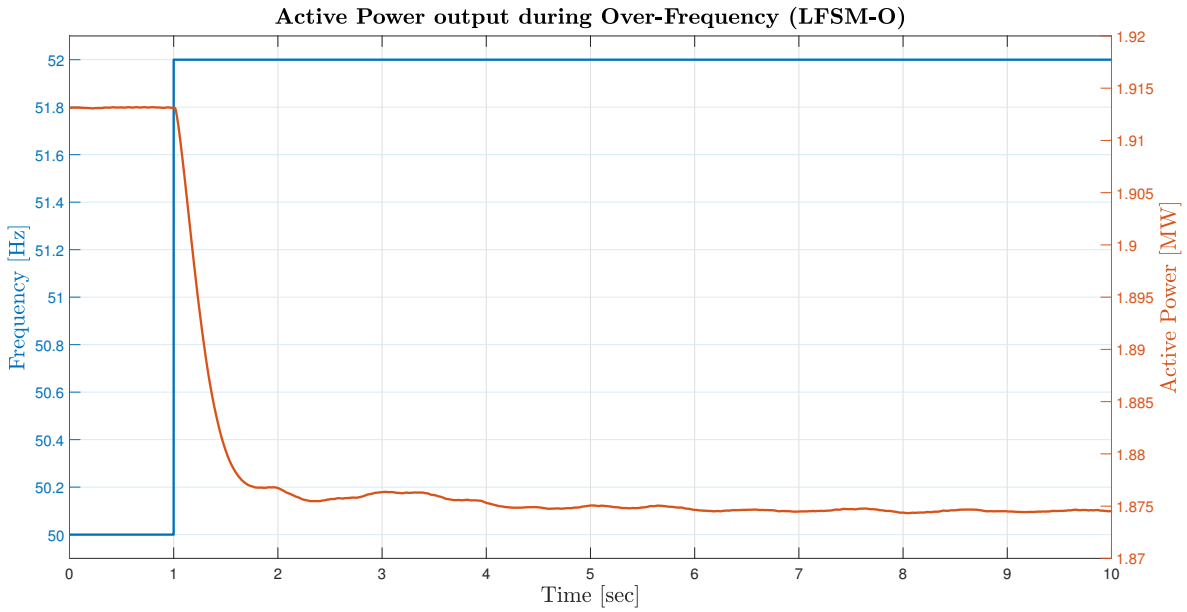

Figure 5.32: Wind Turbine response during under-frequency event (LFSM-O operation, 2 Hz disturbance)

Table 5.10: WT response during LFSM-O operation.

ΔF [Hz]	P_{pre} [MW]	P_{post} [MW]	ΔP [MW]	$\frac{\Delta P}{P_{ref}}$ [%]
0.6	1.91	1.89	-0.02	-1
1	1.91	1.87	0.04	-2
2	1.91	1.87	0.04	-2

5.2. Voltage Support

In the previous section, controller performance for frequency disturbances was demonstrated. As stated at Chapters 1 and 2, keeping the system's voltage into a specific range is also important for the normal operation of the grid. Till today, most of the WT were operated under Unity Power Factor (UPF), which means they do not provide reactive power to the grid. The proposed controller is capable of mitigating fluctuations and maintaining voltage into the limits, decided by the TSO, by providing reactive power support.

Every TSO has its own grid code which defines voltage limits for normal operation. From ENTSO-E documentation [31], it is noted that Hungarian grid code is the stricter one, regarding voltage limits ($0.95p.u. < V < 1.05p.u.$). Those limits are going to be taken into consideration during the following simulations, in order to assess the system's voltage behaviour. As a consequence, if the controller can maintain voltage stability in terms of this grid code, then it is capable of complying with all European Grid Codes.

In order to create a voltage drop, a load of 50 MVAR is connected to the grid at Bus 2 at the first second of the simulation. For the next simulations, Wind Penetration is considered as 15%, in terms of active power.

The results part is divided into two subsections. The first one presents simulation results and voltage behaviour of the system when slip is in that range, where voltage support is provided by the GSC since it is not fully utilized. The second part, on the other hand, presents the results of the simulations, where reactive power support is provided from DFIG's stator, by appropriate controlling rotor excitation currents with the help of RSC.

5.2.1. Reactive Power support from GSC

When controller was explained at Chapter 3 (see section 4.3.3 and Figure 4.10), it was made clear that the reactive power support can be provided by GSC or DFIG's stator with the help of RSC according to generator's slip. It was also shown that, while slip increases, the load of the "Back to Back" inverter configuration also increases. For those reasons, in order to protect the converters from overloading, it was decided that the controller should provide reactive power from the GSC when slip is lower than 0.1.

In this simulation, generator speed is considered as 1p.u., thus slip is zero. This means that the reactive power support is provided by the GSC, as mentioned above. A comparison of voltage behaviour, when WT is operated under Unity Power Factor and when the proposed control is deployed, is demonstrated in Figure 5.33:

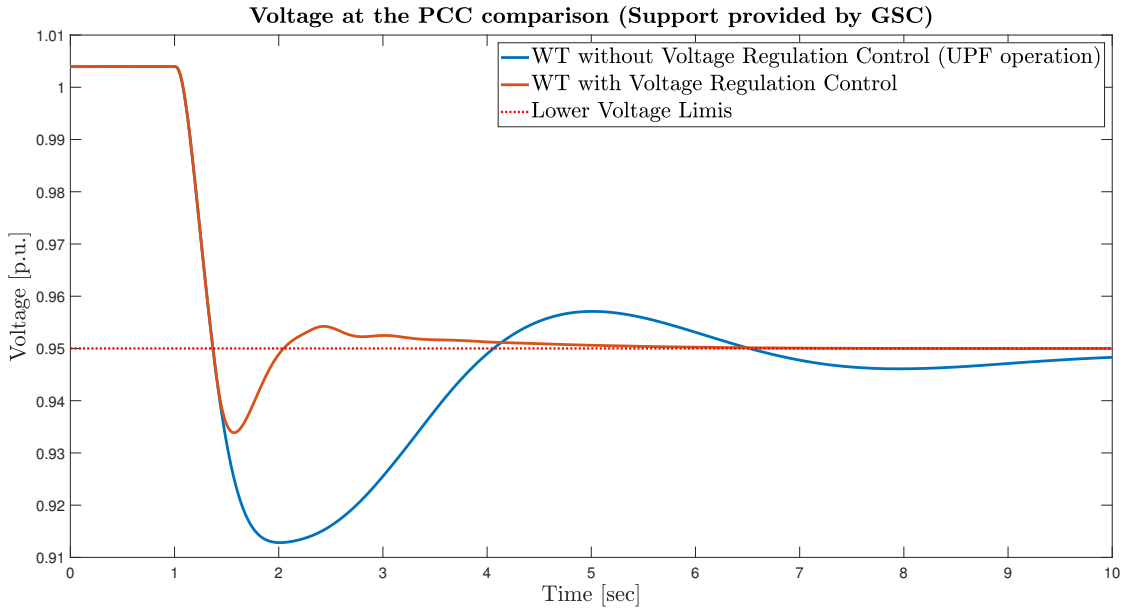

Figure 5.33: Voltage Comparison at the PCC (voltage support provided by GSC).

It is clear that when the WT are operated under Unity Power Factor, voltage drops under the lower voltage limit defined by the grid code (Red Line at the diagram) for over than 3 seconds and after that it is settled in a point below than the lower limited one. On the other hand, when the proposed control system is deployed, when voltage drops under the lower limit, the controller is activated and compensates the demanded reactive power in order to stabilize the voltage. The settling point of the voltage is above the lower limit, opposite to the previous result.

In order to examine the operation of the controller in depth, it is considered necessary to show the reactive power output of the GSC, compared to the voltage deviation. This response is shown in Figure 5.34.

It can be realized that, during steady state operation, GSC is not injecting reactive power to the grid. When the load change happens and voltage begins to decline, GSC does not provide reactive power support to the grid, until the point that voltage falls beyond the Grid Code limits. When this happens, GSC increases its Reactive Power output in order to bring voltage back to the desired levels, which is successfully achieved after a short time period.

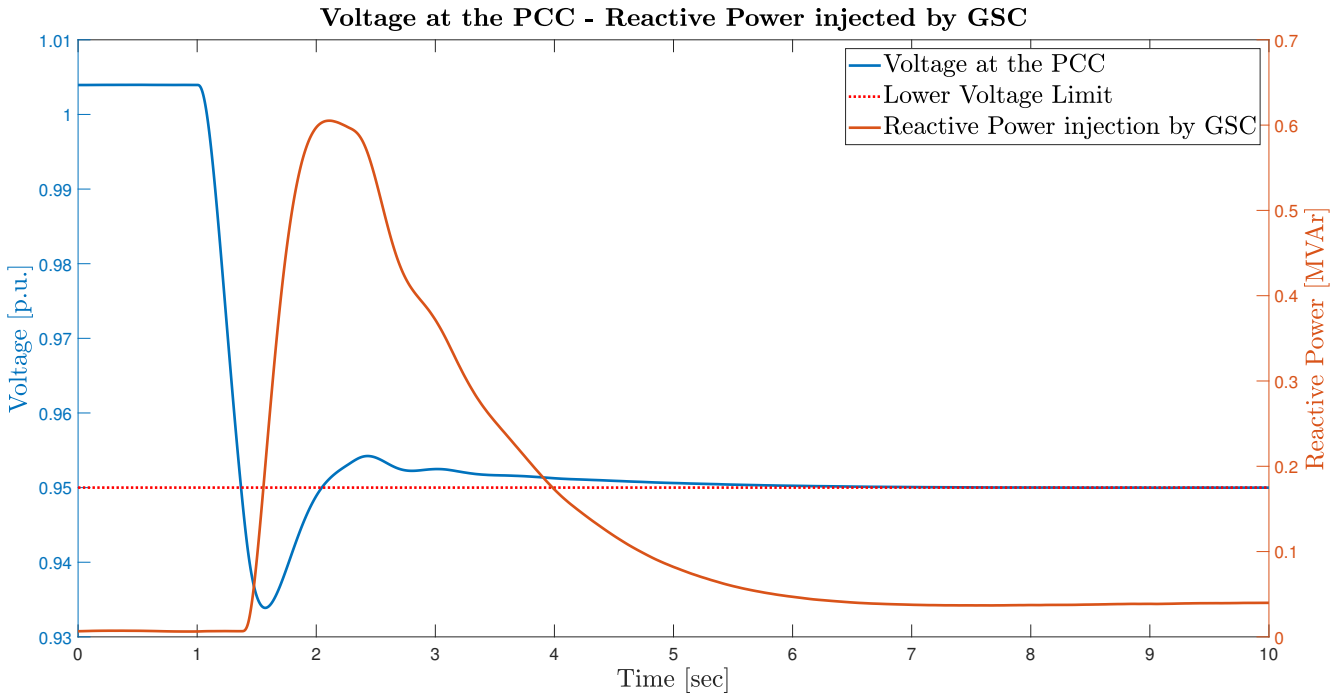

Figure 5.34: Voltage at PCC and Reactive Power injection from GSC correlation.

As mentioned in section 5.1.1, TSOs are interested for the injection at the PCC and not what for the separate WT component outputs. For this reason, it is needed to also show the injection at the PCC, which is depicted in Figure 5.35:

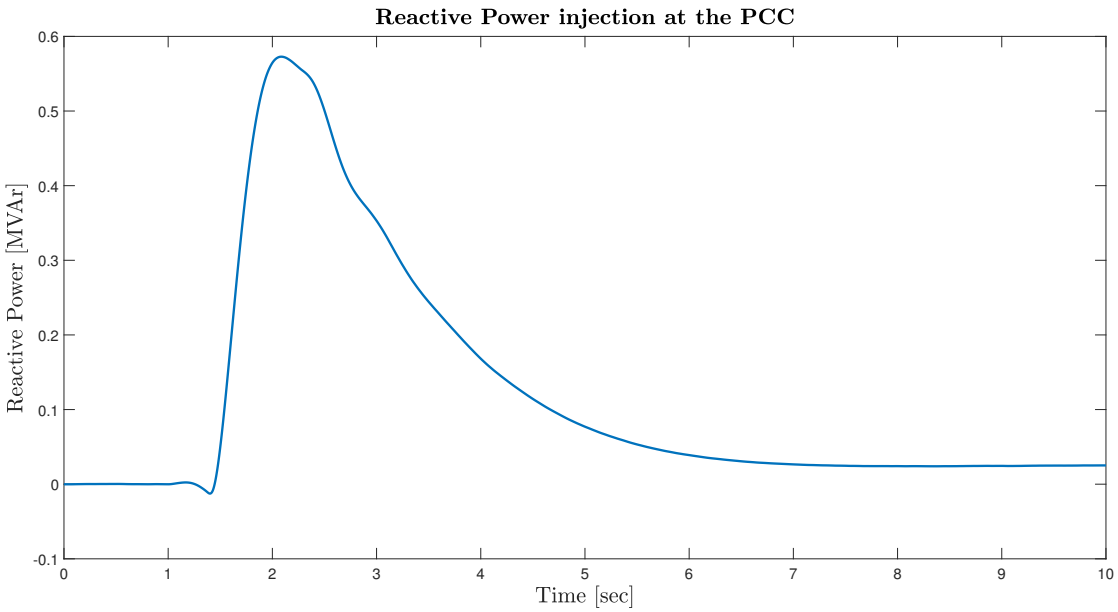

Figure 5.35: Reactive Power injection at the PCC (voltage support provided by GSC).

It is obvious that reactive power injection at the PCC, follows the same pattern of the GSC reactive power output. This means that GSC's injection is translated to an equal reactive power injection at the PCC.

5.2.2. Reactive Power support from Stator

This sections demonstrates the reactive power support of DFIG WTs, when stator is providing this ancillary service to the gird. For this simulation, turbine speed is considered as 1.2p.u., thus slip is equal to 0.2. This means that the "Back to Back" configuration is already loaded close to it's limits, since it is transferring active power to the grid, and cannot provide further support.

For this reason, controller provides the support via DFIG's stator by appropriately controlling rotor excitation currents. Voltage at the PCC, compared with the respective one when WTs are operated under Unity Power Factor is demonstrated in Figure 5.36:

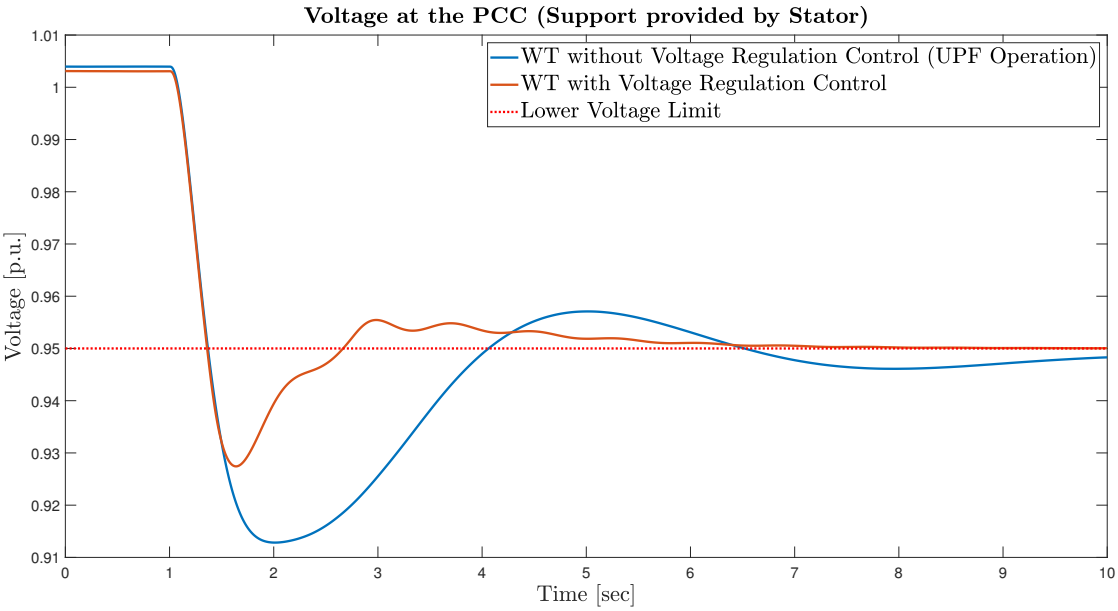

Figure 5.36: Voltage Comparison at the PCC (voltage support provided by DFIG's stator).

Voltage response is similar to the one was observed when support was provided by GSC (see Figure 5.33). For this mode of operation, voltage is again successfully maintained above lower limit, in contrast to the case when WT is operated under Unity Power Factor. Figure 5.37 demonstrates the reactive power output of the stator, compared to the voltage at the PCC :

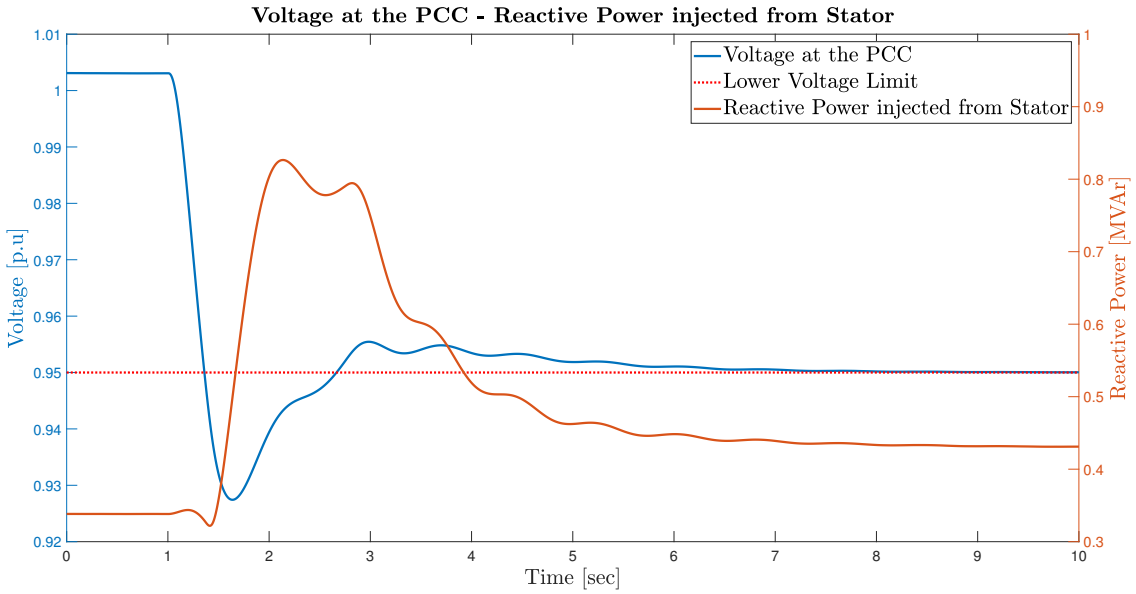

Figure 5.37: Voltage at PCC and Reactive Power injection from DFIG's stator correlation.

In this mode of operation, the reactive power follows the same pattern with the one, when it is provided by the GSC (see Figure 5.34). Initially, during steady-state, where DFIG is operated under Unity Power Factor, stator provides an amount of reactive power, in order to compensate the needs of the rotor and "Back to Back" converter configuration; thus only active power in PCC is provided. When voltage breaches the lower limit, reactive power provided by stator is rapidly increasing in order to support voltage at the grid. The total injected reactive power of the WT at the PCC is shown in Figure 5.38:

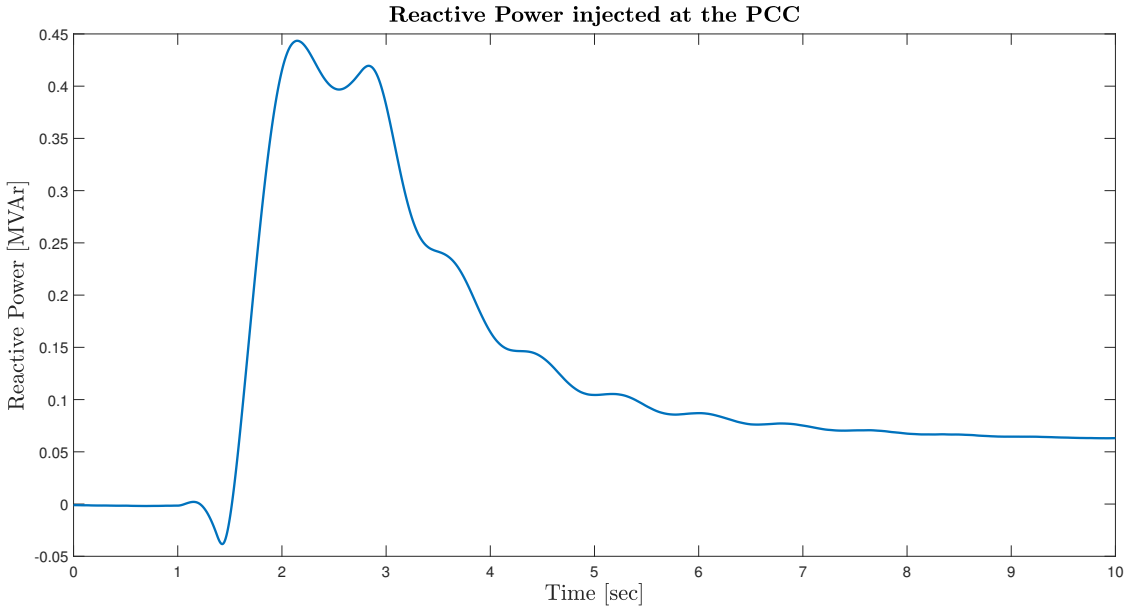

Figure 5.38: Reactive Power injection at the PCC (voltage support provided by DFIG's stator).

It is shown that during steady-state operation, there is an insignificant amount of reactive power

which is injected to the grid. After the disturbance, reactive power output is scaling up in order to compensate system needs and support system's voltage, which is a result of controller actions to counteract the voltage dip.

5.3. Integrated Control for Frequency and Voltage support

During previous sections, frequency and voltage behavior of the system with the proposed topology and controls were demonstrated. As mentioned in thesis introduction, those kind of events can happen simultaneously during the operation of a power system and threaten its stable operation. For this reason, it is necessary to integrate the aforementioned controls under a system and implement it at the DFIG WT in order to enable it to mitigate both frequency and voltage disturbances simultaneously.

In order to investigate the controller's response, a simultaneous active and reactive power step load increase is considered. Specifically, a 10MW + 50MVAr load increase occurs at Bus 2. Moreover, the Wind Penetration is considered as 15% (in terms of Active Power).The section is again divided in two subsections. The first one shows the results when voltage support is provided by GSC and the other one when support is responsibility of DFIG's stator.

5.3.1. Voltage Support from GSC

As in section 5.3.1, generator speed is considered at 1p.u., so controller will provide reactive power, when needed, from the non utilized GSC. Frequency and RoCoF results for DFIG Unity Power Factor operation compared to those with the proposed controller implemented are shown Table 5.11:

Table 5.11: Frequency RoCoF comparison for simultaneous frequency and voltage disturbance (voltage support provided by GSC).

Control System	Nadir [Hz]	Max.RoCoF [Hz/sec]
Without Control	49.7925	-0.1905
With Integrated Control	49.8878	-0.1299

For better understanding of system's behavior, Frequency and RoCoF after the disturbance in comparison with the scenario where WTs are operated under Unity Power Factor are depicted in Figures 5.39 and 5.40. Those figures help to visualize frequency and RoCoF fluctuations and spot the differences between the operational scenarios.

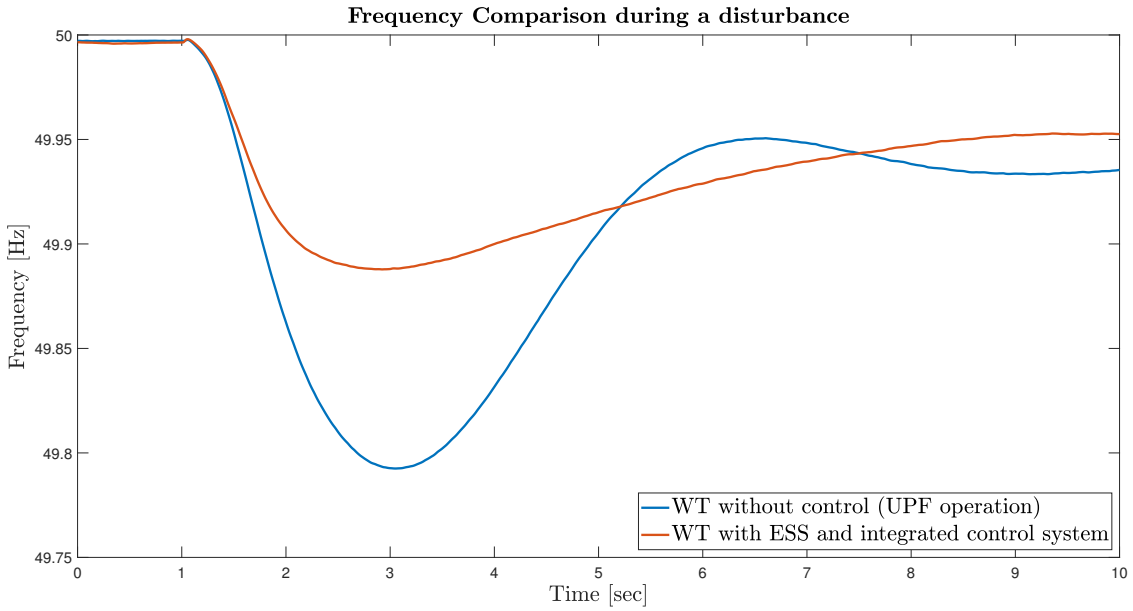

Figure 5.39: Frequency comparison for simultaneous frequency and voltage disturbance (voltage support provided by GSC).

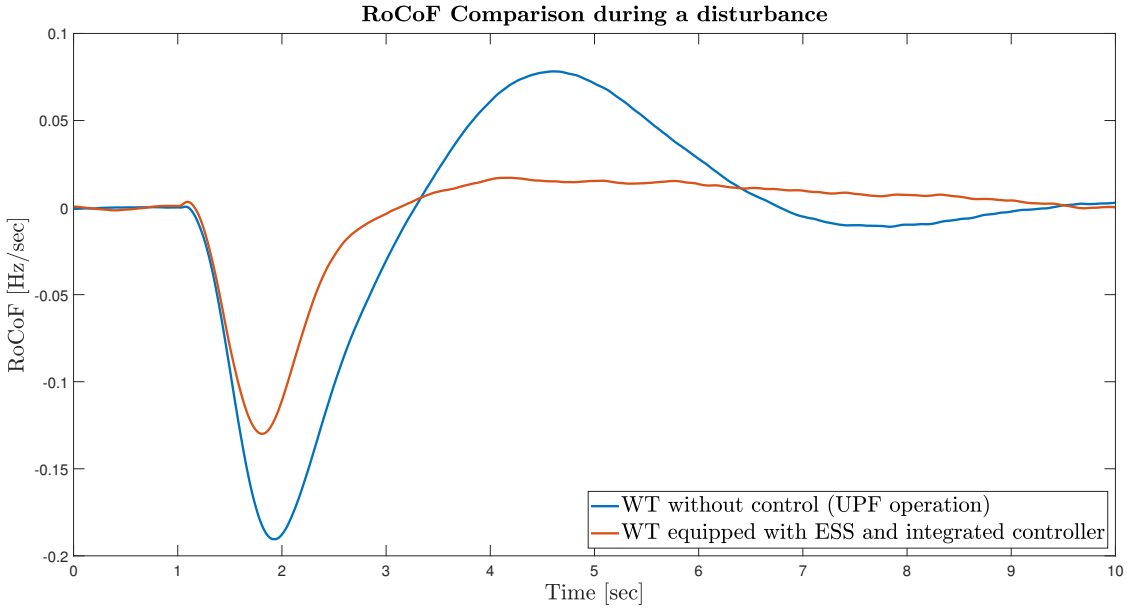

Figure 5.40: RoCoF comparison for simultaneous frequency and voltage disturbance (voltage support provided by GSC).

The results validate how helpful the proposed controller is for the system. Frequency nadir is significantly enhanced, and RoCoF follows the same pattern. Furthermore, regarding primary frequency control capability, it is clear that the settling point of the frequency enhanced with the proposed control system and it is within the allowed limits (50 ± 0.05 Hz).

Since frequency improvement is validated, it is also important to examine the system's voltage deviation. This behaviour, compared to the one when WTs inject exclusively active power to the grid, is shown in Figure 5.41:

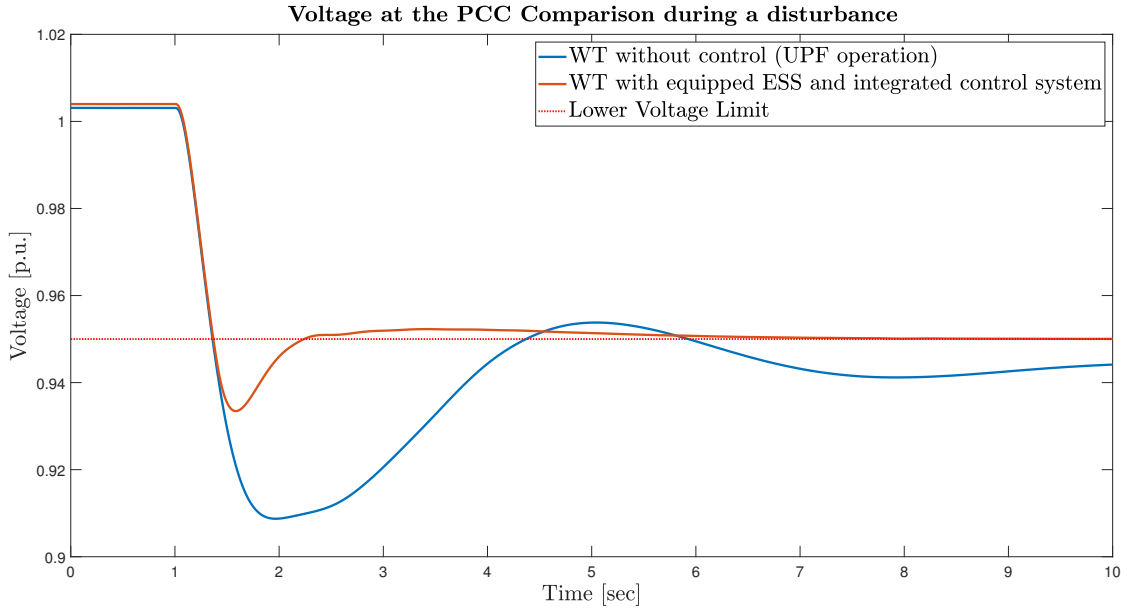

Figure 5.41: Voltage at the PCC (voltage provided by GSC).

It is noted that, when WTs are equipped with the proposed control system, the voltage after a short dip under the lower limit (the red line at the figure) is increasing since it is supported by the DFIG and settles at a point which lays in the allowed voltage range.

From the results shown in Figures 5.39, 5.40 and 5.41, it is unambiguous that the proposed control system and topology are capable of providing the desired Ancillary Services (Inertial Response, Primary

Frequency Control and Voltage Support) to the grid. Both Frequency and Voltage drops were mitigated in comparison with the Base Case, and RoCoF was notably decreased.

It is important to demonstrate the way controller against those deviations, by presenting the output of the respective power electronic topology, in this case, GSC, which diminishes both disturbances by increasing its active and reactive power injection. Those power injections are depicted in Figure 5.42 below:

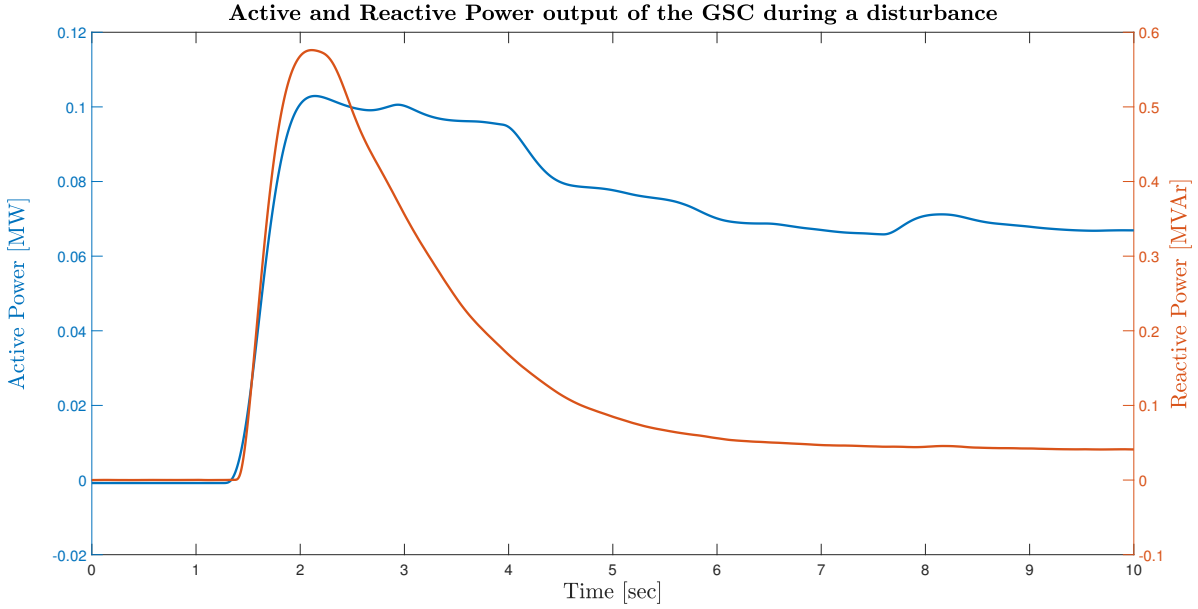

Figure 5.42: Active and reactive output of the GSC (voltage support provided by GSC).

As clearly shown in Figure 5.42 that during steady-state operation, GSC is not injecting any active or reactive power to the grid, which is expected since the generator was operating at synchronous speed; thus rotor's slip power is zero. When the disturbance occurs, and the controlled variables (frequency and voltage) go beyond the allowed limits which are imported to the controller with the help of dead band, active and reactive power injected from the GSC increase in order to support system's frequency and voltage. The controllers, as can be seen, are enabled in a different time. Frequency controller is enabled first and GSC began to inject active power to the grid. After approximately 0.2 seconds, the voltage controller followed, by increasing reactive power reference point.

It was explained in Chapter 2 and specifically in Section 2.2.3 that, one of the biggest advantages of DFIG based WTs is that their cost is reduced, in comparison with Type-4 WTs, due to the fact that power electronic converters are partially rated, since they only need to transfer the slip power of the generator. In order to investigate the loading of the GSC, while providing frequency and voltage support to the grid, GSC's apparent power is depicted in Figure 5.43.

It is considered that "Back to Back" converters are rated at 30% of DFIG's rated power. The simulated DFIG is rated at 2MW; thus power electronic converter rating shall be 0.6 MVA.

From Figure 5.43, it is comprehensible that controller limits are set in a proper way that they protect GSC from overloading risk. This case is the one that stresses GSC most, in terms of power loading and despite that, it is still operating under its limit.

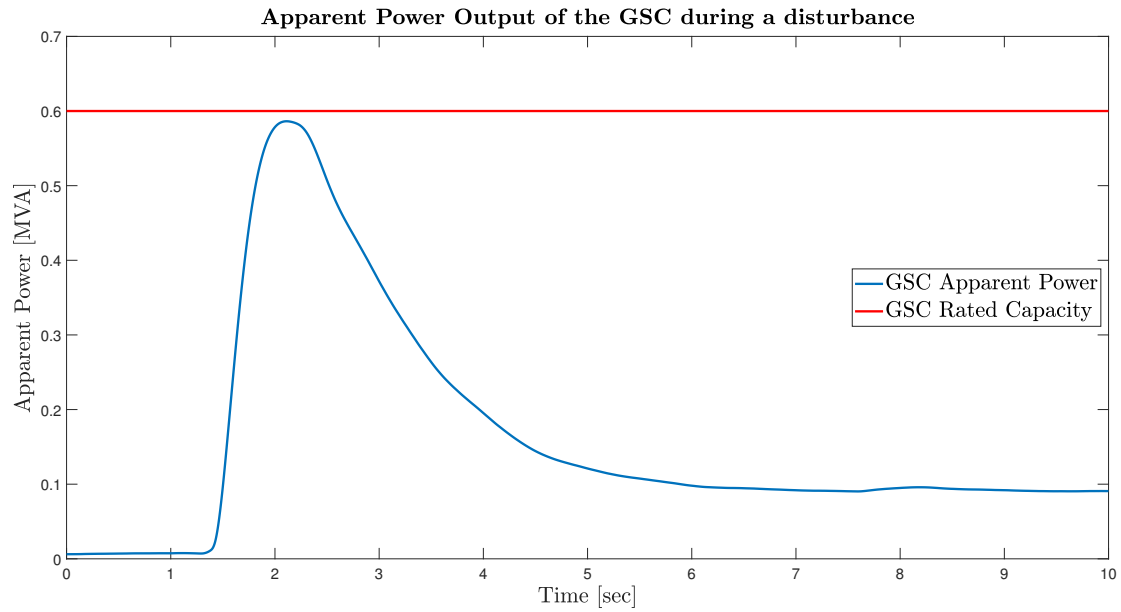

Figure 5.43: Apparent Power output of the GSC (voltage support provided by GSC).

5.3.2. Voltage Support by DFIG's stator

For this operational scenario, like in section 5.2.2, generator speed is considered as 1.2 p.u.. This means that generator is operated at super-synchronous speed and rotor provides slip power (in this case 0.2 p.u.) to the grid via the "Back to Back" converter configuration. This is detected by the proposed control strategy, which will provide reactive power support, when needed, from DFIG's stator with the help of the GSC. With such an operation, overloading power electronic converters is avoided, since stator can be transiently overloaded and provide extra reactive power reserve [6].

Frequency behaviour comparison of the two operational scenarios (DFIG operated under Unity Power Factor and DFIG equipped with the proposed control system) for simultaneous active and reactive power load increase at Bus 2 are shown in Figures 5.44, 5.45 and Table 5.12:

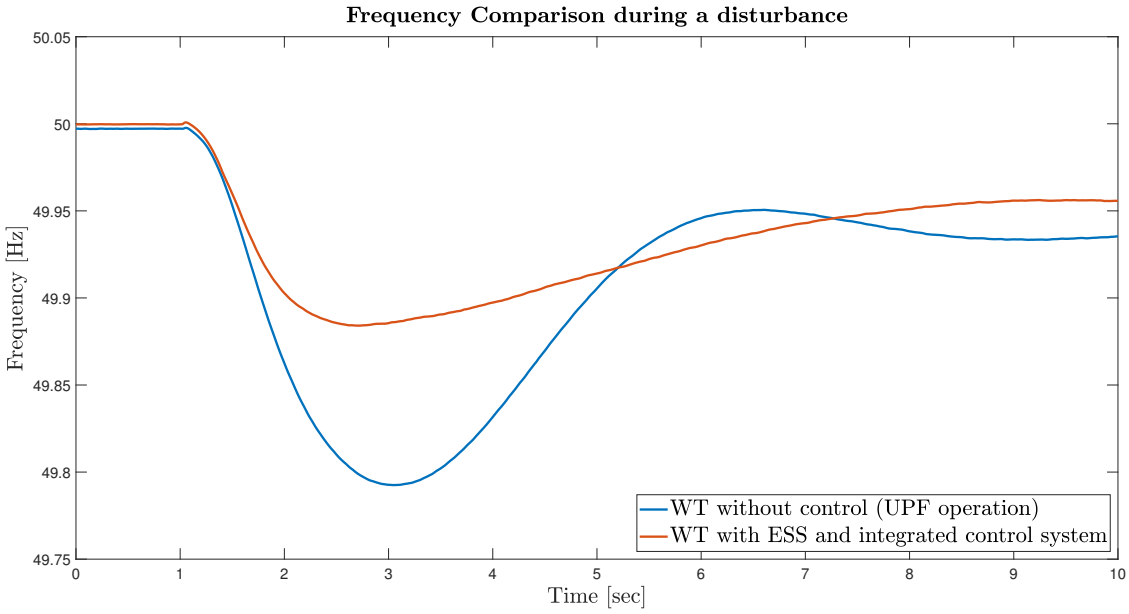

Figure 5.44: Frequency comparison for simultaneous frequency and voltage disturbance (voltage support provided by DFIG's stator).

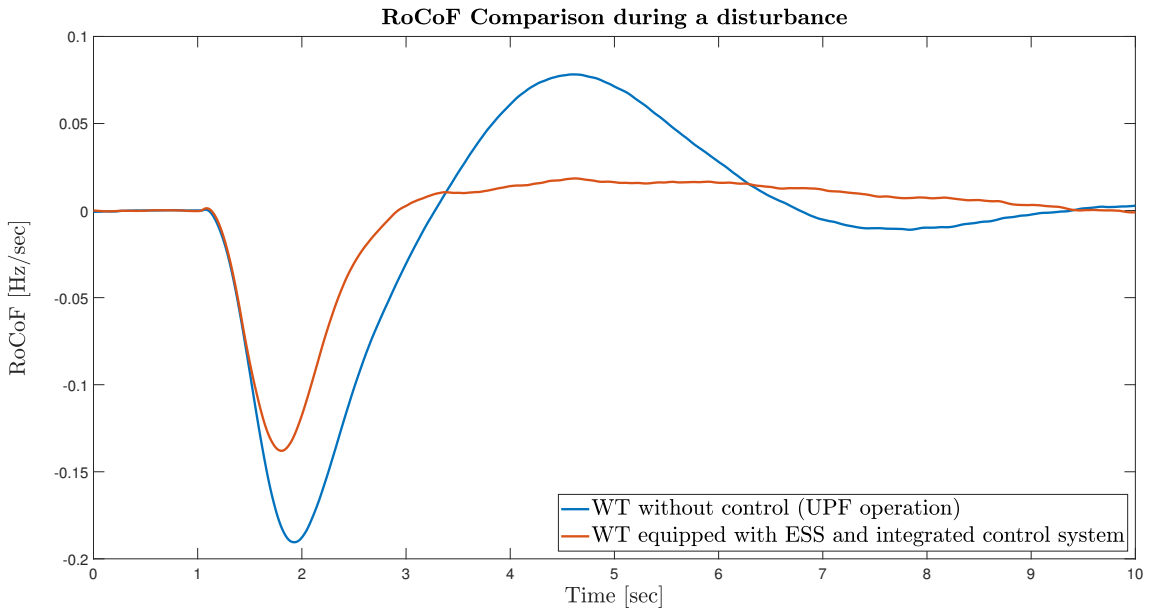

Figure 5.45: RoCoF comparison for simultaneous frequency and voltage disturbance (voltage support provided by DFIG's stator).

Table 5.12: Frequency and RoCoF comparison for simultaneous frequency and voltage disturbance (voltage support provided by DFIG's stator).

Control System	Nadir [Hz]	Max.RoCoF [Hz/sec]
Without Control	49.7925	-0.1905
With Integrated Control	49.8841	-0.1380

Results clearly demonstrate that proposed controller is able to provide inertial response to the grid since RoCoF is significantly decreased the moments after the disturbance, which leads frequency to decline with a less steep slope than the base case when WTs are operated under Unity Power Factor. Furthermore, frequency nadir and settling point are notably enhanced, compared to the base case, and lays in the allowed operational limits (50 ± 0.05 Hz). This means that the proposed controller is successfully providing primary frequency support ancillary service to the grid.

Comparing to the results of the previous subsection 5.3.1, it can be realized that there are not any remarkable differences in frequency behaviour. That was expected since in both cases, frequency support is provided by the GSC; thus frequency is similar for both cases.

Since there is also a reactive power load increase, the voltage is going to be affected. Voltage behaviour when WTs are only injecting active power to the grid compared to the behaviour when the proposed control system is deployed is depicted in Figure 5.46. It is noticed that, when WTs are operated under Unity Power Factor, voltage decline is larger and longer. Moreover, after the transient period, the voltage settling point is lower than the allowed limit.

On the other hand, when integrated control is implemented after the voltage falls below the allowed limit, the controller takes action and supports the voltage, which settles above the lower limit (0.95p.u.).

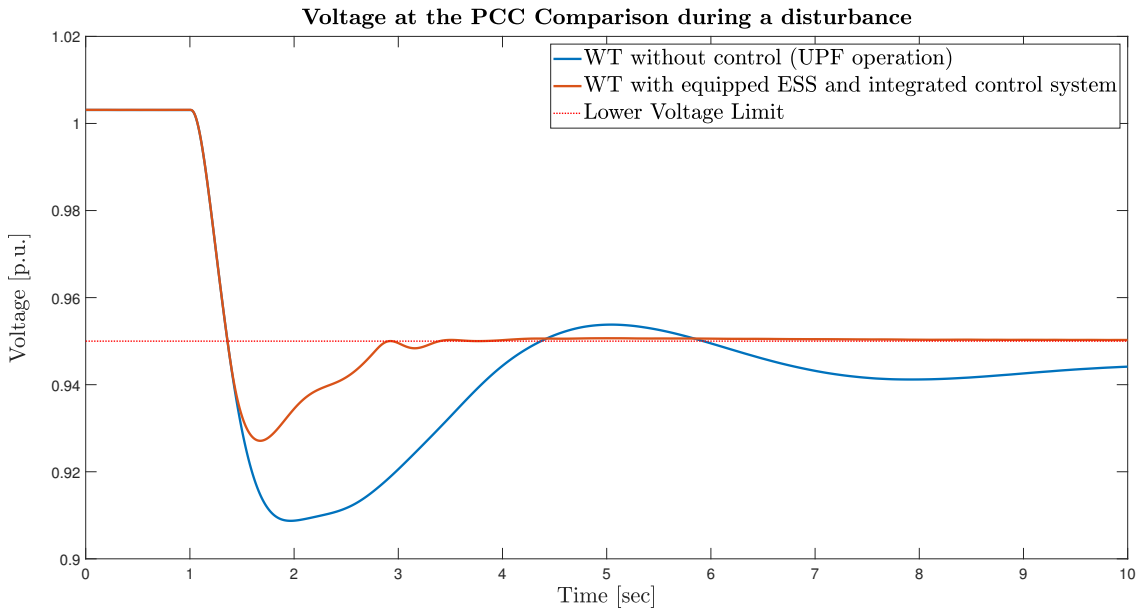

Figure 5.46: Voltage at the PCC comparison between the operational scenarios (voltage support provided by DFIG's stator)..

In order to identify controller's operation, active and reactie power output of DFIG's stator is shown in the following figure:

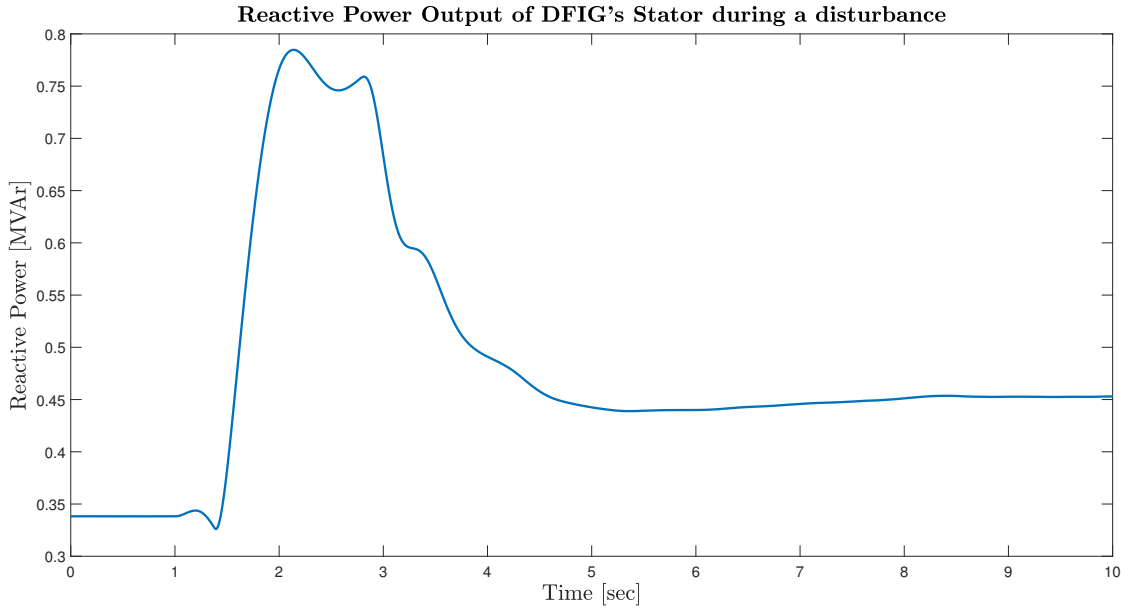

Figure 5.47: DFIG's stator Reactive Power output of the during voltage support.

As shown in Fig.5.47, during steady-state operation, stator's reactive power output is positive. This happens since, at steady state, DFIG is operated under Unity Power Factor; thus, the stator is compensating the reactive power needs of the rotor. After the disturbance, stator's reactive power output is rapidly increasing to support the voltage at the PCC and subsequently at the grid. Active power output is not presented since frequency support is a responsibility of GSC, so stator's injection is not affected by the control action. It is also clear that reactive power output is increased when the voltage drops below the lower voltage limit, which is the time voltage support controller is activated. Stator's apparent power output is depicted in Figure 5.48:

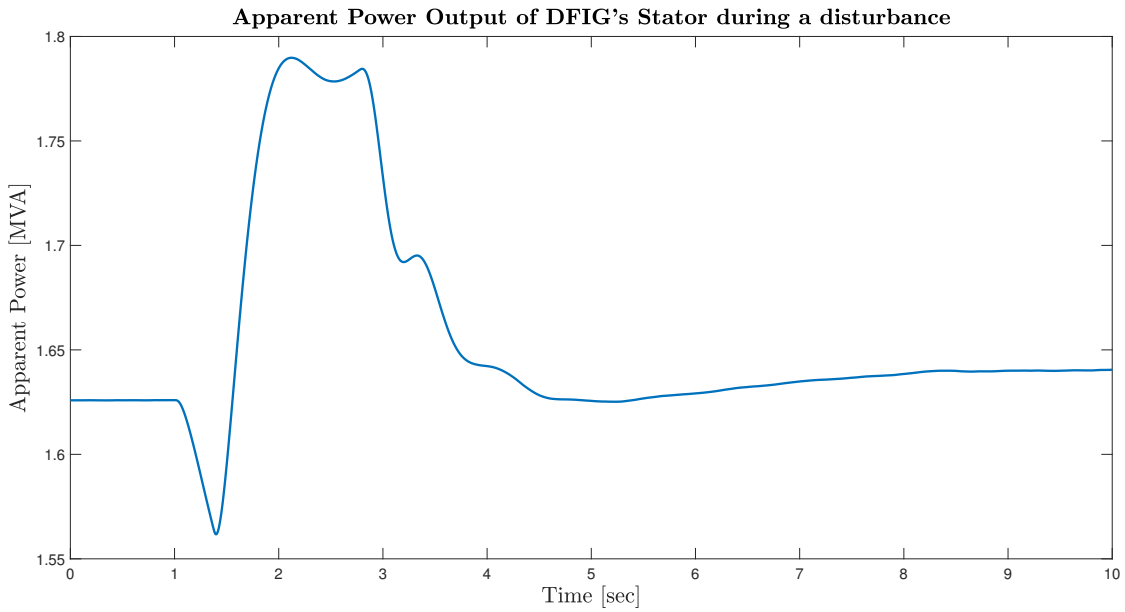

Figure 5.48: DFIG' stator Apparent power output during voltage support.

It was mentioned in Chapter 3, and specifically in subsection 4.3.3, that in order to change the reactive power output of DFIG's stator, rotor excitation currents need to be modified. This change happens with the help of RSC. As mentioned in the previous section, power electronic converters are a sensitive piece of equipment which needs to be operated into specific limits.

Since "Back to Back" converters are partially rated, it needs to be investigated if those limits are breached during the disturbance. GSC is operating within the limits, if it is considered that converters are rated at 30% of DFIG's rated power (see Figure 5.43). For this operational scenario, since RSC has to change the excitation currents, it is also important to examine if its limits are breached. Figure 5.49 shows the Apparent Power which is transferred by the RSC.

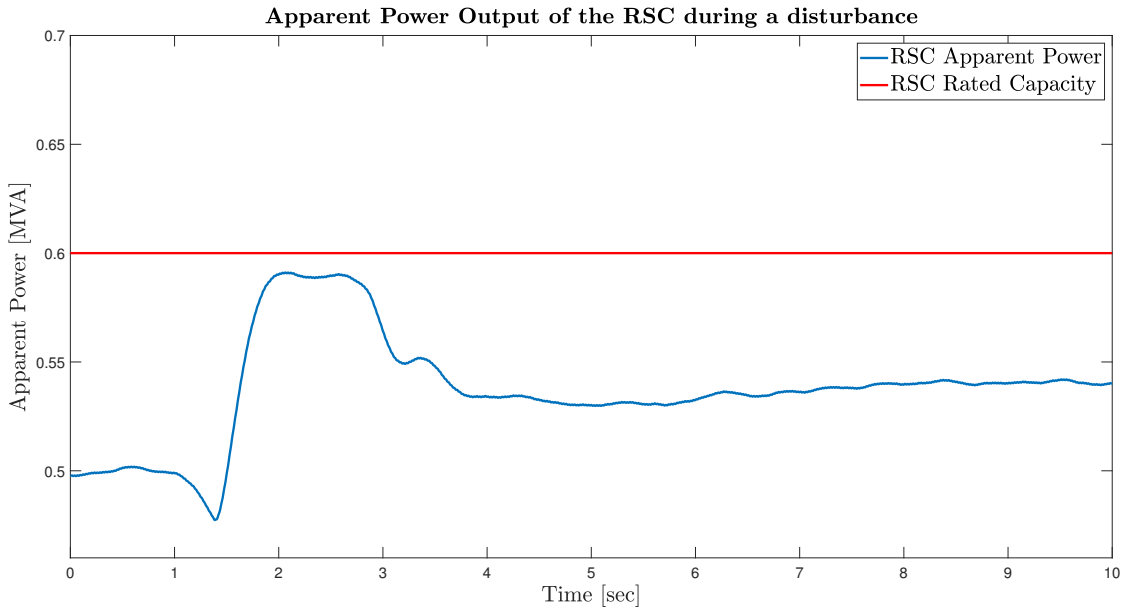

Figure 5.49: Apparent Power output of the RSC (voltage support provided by DFIG's stator).

Before the disturbance, RSC provides the reactive power needs of the rotor. Those are covered by the stator, in order to operate the WT under Unity Power Factor. This means that strictly active power is injected at the PCC. After the disturbance, reactive power transferred by the RSC is increased in order

to properly change the excitation currents of the rotor. Despite that, the converter always operates within its power limits, which means that the controller is appropriately saturated, in order to protect RSC from overloading.

6

Conclusion and Discussion

At Chapter 5, frequency and voltage behaviour was demonstrated under different scenarios and modes of operation. For this purpose, the DFIG with the proposed control and topology additions were modelled with the help of RSCAD software. This model was implemented at the IEEE 14-Bus Benchmark system in order to identify its impact on the system's stability. After that, results were provided that show the participation of the DFIG WTs in ancillary services. Moreover, all the components of DFIG (Stator, Rotor and the "Back to Back" converter configuration, combined with the implemented ESS at the DC Link) were monitored and their contribution to frequency and voltage support was explained and analyzed.

This chapter will present the conclusions which can be extracted from the simulation results, the contribution of this thesis is going to be highlighted, and proposals for future research are going to be referred.

6.1. Summary of operational scenarios and results

In this section, the examined scenarios and observations from Chapter 5 are summarized. Those can be recapitulated as:

- The performance of the system with wind penetration was examined when any control system was implemented. It was identified that load changes had a more significant impact on frequency and voltage variations, comparing to a traditional power system which is operating on SGs.
- An integrated controller for frequency support was designed by combining two different control strategies :
  - Inertial Response
  - Primary Frequency Control

  This controller provides the proper Duty Cycle to the Bi-Directional DC-DC Converter which interfaces ESS with the DC Link of the "Back to Back" converter configuration, in order to inject the desired amount of active power, to mitigate frequency disturbance. With that strategy, DFIG WT is always capable of injecting its maximum active power to the grid.
- System's frequency performance with Primary Frequency Control, and integrated primary frequency and inertia response control were examined, for the proposed DFIG with ESS topology compared between the base case and the case with 15% wind penetration. It was validated that integrated control was capable of providing enhanced frequency performance. Frequency nadir was significantly improved and settling point after the disturbance was increased compared to the base case. Furthermore, RoCoF was notably enhanced, which reduces the stress of the remaining SGs.
- System's frequency performance under different rates of WT equipped with ESS and the proposed control is examined, to show the impact of the proposed frequency support approach. Frequency's behaviour is demonstrated, and the findings are reviewed.

- The controller tuning for the integrated frequency controller is presented by trying different values of droop values for :
  - Inertial Response (K_{in})
  - Primary Frequency Response (K_{droop})
- Controller's response when delays in measurements occur is shown and discussed.
- System's frequency performance under different wind penetration scenarios. This study is essential to identify the proposed system performance, in comparison with the traditional RES approach, which does not participate in frequency regulation.
- System's performance during over-frequency disturbances was examined. Frequency and RoCoF behaviour were presented and analyzed.
- A controller for voltage support was designed and implemented in the existing control scheme of the DFIG. This novel controller takes into consideration the generator's speed in order to provide reactive power to the grid, when needed, in a safe way, by not risking overloading DFIG's power electronic converters.
- System's voltage response during a load change event was examined for both cases (voltage support provided by GSC or DFIG's stator with the help of RSC) and assessed.
- System's frequency and voltage response during a simultaneous active and reactive power load change are examined in order to verify if the integrated control strategy is capable of mitigating both disturbances. Also, in this case, both voltage support scenarios (from GSC and stator) are examined.

6.2. Conclusions

In Chapter 5, different results for different modes of operation were demonstrated. Regarding frequency support, it is clearly shown from the results that the integrated control strategy is remarkably better than the individual control strategies. In fact, the integrated controller can significantly decrease RoCoF, which reduces the stress of the remaining SGs during a disturbance, as discussed in Chapter 1. Moreover, frequency nadir, which is an indicative frequency index, is notably improved and frequency settling point is increased. Furthermore, the proposed topology allows WT to constantly operate at its maximum power point, which is beneficial for both WF operator, since active power injection which is rewarded is optimized and TSO which is able to absorb more power which is produced by "green" and sustainable sources. The results also highlight that it is possible only by having a fraction of the installed WT with the proposed topology and control, to achieve similar or even better performance than the one when the system is running only on SG, which is able to tackle one of the biggest drawbacks of RES, the reduced system inertia.

The controller was capable of mitigating the over-frequency by reducing both frequency peak and RoCoF. Another important feature that has to be noted is that during this kind of disturbances, the proposed system is capable of saving a part of the difference between demand and generation. This energy, which is stored at the ESS with the help of Bi-Directional DC-DC converter, is possible to be used in future under-frequency disturbances, which maximizes the benefit of using the proposed topology.

The proposed control strategy is also helpful regarding the grid's voltage stability. It is shown that the traditional integration approach of RES, which means that they are operated under Unity Power Factor, causes voltage fluctuations that breach the limits, dictated by the grid code. On the other hand, the proposed control strategy is capable of mitigating those voltage fluctuations and maintain the voltage between the voltage limits. It also has to be mentioned, that this support happens in a way, that secures the DFIG equipment by utilizing GSC when it is not loaded (for low slip values) and providing support from the stator when GSC is already charged with active power transfer (higher slip values). The results demonstrate that, with proper controller saturation limits, it is possible to maintain the loading of the converters below their maximum rating and avoid the risk of damaging them.

After conducting all those simulations mentioned above, it is now possible to provide answers to the Research Questions, which were stated in Chapter 1.

- **How is the performance of the proposed DFIG combined with ESS is assessed regarding its ancillary services capabilities?**
  From the obtained results for different operational scenarios demonstrated in Chapter 5, it is clearly shown that the proposed control system is capable of limiting and mitigating frequency and voltage deviations, which helps towards grid's stability assurance. Even if those disturbances occur simultaneously, which is the case when system is highly stressed, proposed system with the integrated controller is able to alleviate both frequency and voltage fluctuations such as keep them between the allowed operational limits.

  Moreover, the proposed system with the suitable control strategy is also capable of following TSO's RfG. Specifically, the proposed DFIG WT was tested for all three frequency support modes (LFSM-U, LFSM-O, FSM) defined by the German Grid Code and it was able to comply with them.

- **What is the performance of the proposed system for different penetration scenarios?**
  As stated in Chapters 1 and 2, one of the most significant drawbacks which do not allow high penetration of RES to the existing grid, is their lack of inertia. Thus, when their generation increases, system becomes more volatile to frequency disturbances. This comes in contrast to the results were presented in subsection 5.1.3. From those results, it can be concluded that the proposed topology combined with the integrated controller strategy for frequency support has the potential to enhance nadir and RoCoF indices while penetration increases. This is caused by the addition of an extra energy storage at the WT, which for the aforementioned simulations was rated as 5% of the total DFIG rated power. This fact provides excellent flexibility and enables the higher penetration of wind energy to the existing grid without causing any risks since frequency stability is ensured. Moreover, another useful feature of the proposed system can be deduced. It is observed, from the simulation results at subsection 5.1.2, that it is possible to achieve better performance than the one when the system is based on Synchronous Generators. This fact can leverage wind energy integration to the existing grid and reduce the CO_2 emissions caused by electric power generation.

  When it comes to Voltage Stability, currently RES have a minimum contribution, since operators prefer to utilize them under Unity Power Factor, since they are rewarded based on the active power that WTs inject to the grid. This introduces problems regarding voltage support, if RES become the dominant electric power generation source. In order to tackle this problem, the proposed control strategy is capable of dynamically modifying the reactive power output of the WT, in order to help towards voltage stabilization. Another important feature of the controller is that it takes into consideration the loading of the "Back to Back" converter topology and decide if it is safe to provide reactive power from the GSC or if stator should give this support to the grid. With that control approach, sensitive equipment, such as power electronic converters are protected from overloading damage.

- **How robust is the proposed control scheme, by means of its ability to handle disturbances in power system?**
  From the obtained simulation results, demonstrated in Chapter 5, it is evident that the proposed control scheme can be assessed as robust since it is possible to mitigate both frequency and voltage disturbances. The controller is effectively supporting the grid during disturbances even if delays are introduced in the measurements, The results shown in subsection 5.1.4, demonstrate that measurement delays have a minimum impact to the response of the controller. This observation leads to the conclusion that, regarding measurement delays, the controller is sufficiently robust.

  Moreover, for simultaneous frequency and voltage disturbances, which were the cases that the developed controller was more stresses, the system remained stable and healthy. Controller limits help towards this cause since they limit DFIG output to protect it from overloading. It was demonstrated that, for all disturbances, DFIG equipment was operating within the operational limits and was able to contribute towards the system's frequency and voltage stabilization robustly.

6.3. Contribution to IEPG Research Group

During this thesis project, the existing DFIG model contained in RSCAD library was expanded in order to include the ESS at the DC Link of the "Back to Back" converter configuration. An appropriate Bi-

Directional DC-DC Converter was implemented to this model, in order to interface the ESS with the DC Link and control its power output. After that, the control strategies for all the converter topologies were developed and implemented in RSCAD, in order to enable DFIG to participate in Frequency and Voltage Support Ancillary Services. Thus, the main contribution of this thesis to the IEPG Research Group can be summarized in the following points:

- Proposal, development and implementation in RSCAD of the enhanced DFIG topology (shown in Figure 4.1) with the integrated ESS with its respective Bi-Directional DC-DC Converter. This model is developed in Small Time-Step, which makes it capable of being used for HIL simulation to test and validate actual hardware.
- Proposal, development and implementation of an integrated control strategy in order to enable Type-3 Wind Turbines to participate in Frequency and Voltage Support. Moreover a control strategy for Primary Frequency Support for Grid compliance was developed and implemented.

6.4. Future research proposals

It was mentioned in Chapter 1, that RES and especially Wind Energy will play an important role in the future power system. Thus the impact of Type-3 Wind Turbines needs to be further examined. Some of the future research topics could be the following :

- Examine the behaviour of the system when WTs are distributed in multiple locations. Till now, large power plants were generating energy which was distributed via a centralized grid. This assumption is not going to be valid in a future power system with increased RES penetration. In contrast with the current situation, production is going to be de-centralized which leads to grid transformation. To investigate the impact of the distributed RES, and especially Type 3 WT which is the subject of the presented thesis, it is necessary to develop an average model for the DFIG. The small tiime-step model, which was developed, is suitable for HIL simulations since it models in detail all the components of the system. If this model is used in a larger power system model, in more than one locations it will add high computational burden which is not necessary. In order to investigate the impact of the DFIG in multiple locations, an average model of this system has to be developed. This model shall not investigate in detail power electronics in order to reduce its complexity. This developed model will be capable of implementation in larger systems and multiple locations in order to investigate the effect of the distributed RES in a power system.
- Expand the proposed control system in order to make Type-3 Wind Turbines capable of participating in more Ancillary Services. Except frequency and voltage support, there are also other services, which have to be provided from WT, in order to allow transition to a RES-dominant power system. Power Smoothing is becoming an issue while RES penetration increases. Nowadays, TSOs specify lower and upper limits of active power ramp ups and downs. Thus, it is necessary to expand the proposed control system in order to mitigate those fluctuations with the proper utilization of the ESS which is integrated in the DFIG. Moreover, the ESS is also capable of enhancing Low Voltage Ride-Through capability. Also in this case, it is necessary to study the DFIG and propose an effective control strategy which can provide this service without conflicting with the other controllers.
- The proposed controller is not taking into consideration ESS State-of-Charge. For better system performance, an Energy Management System (EMS) can be developed, and different control strategies can be examined. It was mentioned in the previous proposal, that ESS is capable of mitigating multiple grid disturbances. To this end, it is necessary to build an Energy Management System, which will decide when ESS is able to provide or absorb power from the grid in order to provide support. It is possible to examine energy management control strategies which exist in the literature or develop a new one if they are not capable of allowing ESS to provide (or absorb) the necessary reserve power when needed.
- Analysis of different types of ESS and their impact on Ancillary Services capability. This thesis examined Li-Ion battery as an ESS which provides the reserve active power to mitigate frequency disturbances. Therefore, there are multiple ESS technologies that can be utilized. Supercapacitors for example, which are able to provide rapid charge and discharge cycles, can provide an improved

behavior when it comes to inertial response. Fuel cells can be more green and sustainable solutions since chemicals needed for the battery can be avoided. Moreover, there is an intense ongoing research towards those ESS which can lead to their domination in the market during the following years, when their technology is going to be mature enough. The research on those alternative ESS can be divided in two parts.

First of all, is is important to develop and validate models of those ESS (Supercapacitors, Fuel Cells, Flywheel etc.) in order to use them in simulations. RSCAD only provides the Li-ion Battery Model in its library, thus all the rest have to be developed

After that, since those models are developed and validated, it is possible to substitute battery in the proposed DFIG topology with them and assess their performance. This comparison is going to show, which storage system is the most efficient and capable solution in providing ancillary services to the grid.

Appendices

A

IEEE 14-Bus Benchmark System

A.1. System Topology

The IEEE 14-Bus power system is widely used for voltage as well as frequency stability studies. It represents a simple approximation of the American Electric Power system as of February 1962. The single line diagram of the benchmark system is shown in Figure A.1. It has to be mentioned that Bus 7, which is the middle point of the 3-Winding Transformer is not modelled in RSCAD due to software's limitations.

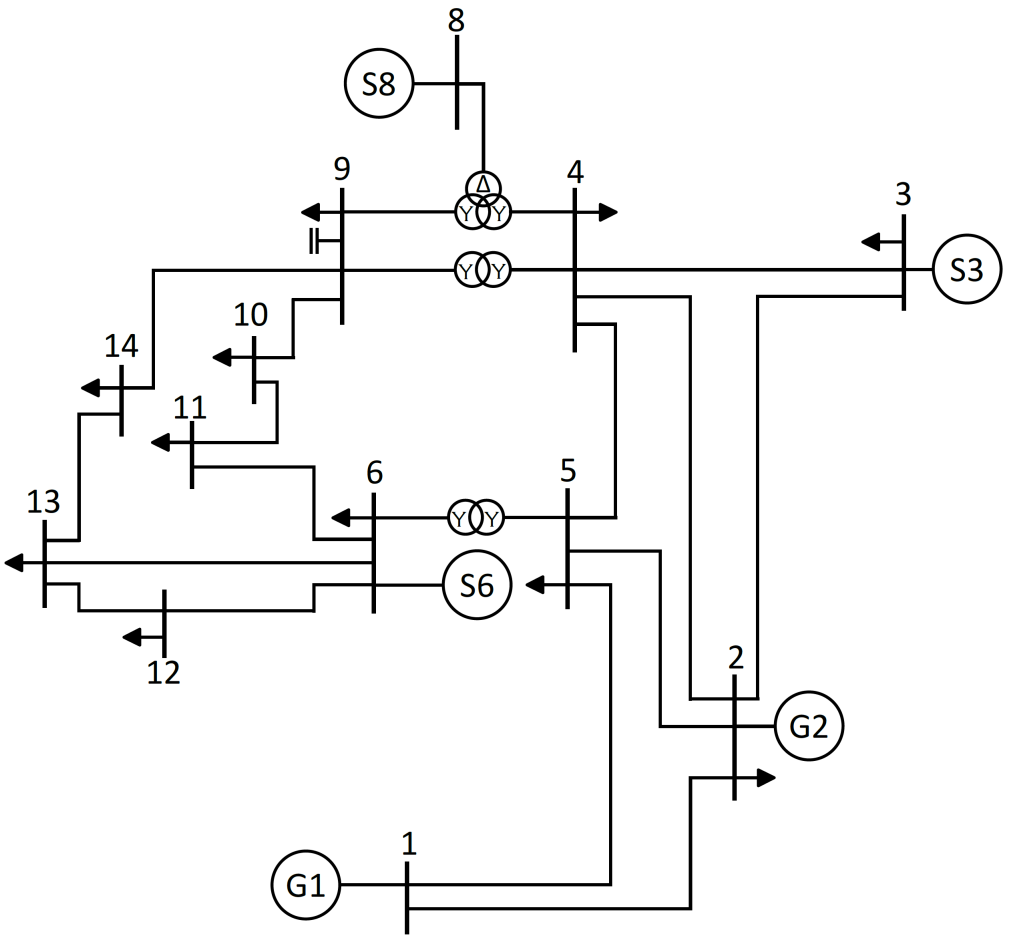

Figure A.1: IEEE 14-Bus Benchmark System Topology.

A.2. System Data

The basic data of the IEEE 14-Bus system are shown in the following table:

Table A.1: IEEE 14-Bus Data.

Bus	Type	|V| (p.u.)	Gen (MW)	Shunt (MVAr)	Loads	
					P (MW)	Q (MVAr)
1	Slack	1.06	-	-	-	-
2	P-V	1.045	40	-	21.7	12.7
3	P-V	1.01	0	-	94.1	19
4	P-V	-	-	-	47.8	3.9
5	P-Q	-	-	-	7.6	1.6
6	P-V	1.07	0	-	11.2	7.5
7	-	-	-	-	-	-
8	P-V	1.09	0	-	-	-
9	P-Q	-	-	190	29.5	16.6
10	P-Q	-	-	-	9	5.8
11	P-Q	-	-	-	3.5	1.8
12	P-Q	-	-	-	6.1	1.6
13	P-Q	-	-	-	13.5	5.8
14	P-Q	-	-	-	14.9	5

Table A.2: Regulated Bus Data.

Bus	|V| (p.u.)	Q_{max} (MVAr)	Q_{min} (MVAr)
2	1.045	-40	50
3	1.01	0	40
6	1.07	-6	24
8	1.09	-6	24

The resistance, reactance and susceptance of each line are enlisted in the following table:

Table A.3: IEEE 14-Bus System Branch Data.

From	To	R (p.u.)	X (p.u.)	B (p.u.)
1	2	0.01938	0.05917	0.0264
1	5	0.05403	0.22304	0.0246
2	3	0.04699	0.19797	0.0219
2	4	0.05811	0.17632	0.0187
2	5	0.05695	0.17388	0.017
3	4	0.06701	0.17103	0.0173
4	5	0.01335	0.04211	0.0064
6	11	0.09498	0.1989	-
6	12	0.12291	0.25581	-
6	13	0.06615	0.13027	-
9	10	0.03181	0.0845	-
9	14	0.12711	0.27038	-
10	11	0.08205	0.19207	-
12	13	0.22092	0.19988	-
13	14	0.17093	0.34802	-

Transformer data are shown in Table A.4:

Table A.4: IEEE 14-Bus System Transformer Data.

From	To	R (p.u.)	X (p.u.)	Tap Ratio
4	7	0	0.20912	0.978
4	9	0	0.55618	0.969
5	6	0	0.25202	0.932
7	8	0	0.17615	1
7	9	0	0.11001	1

The IEEE 14-Bus benchmark system does not provide dynamic data for the generators. For this purpose, typical data for EMT modelling is adopted. Table A.5 shows the data used for the dynamic modeling of the generators.

Table A.5: IEEE 14-Bus Generator Data.

Bus	Base (MVA)	X_a (p.u.)	X_d (p.u.)	$X_d^{'}$ (p.u.)	$X_d^{''}$ (p.u.)	X_q (p.u.)	$X_q^{'}$ (p.u.)	$X_q^{''}$ (p.u.)
1	615	0.145	1.7241	0.2586	0.2029	1.6587	0.4524	0.2029
2	60	0.145	1.7241	0.2586	0.2029	1.6587	0.4524	0.2029
3	60	0.145	1.7241	0.2586	0.2029	1.6587	0.4524	0.2029
6	25	0.145	1.7241	0.2586	0.2029	1.6587	0.4524	0.2029
8	25	0.145	1.7241	0.2586	0.2029	1.6587	0.4524	0.2029

Bus	Base (MVA)	R_a (p.u.)	$T_{d0}^{'}$ (s)	$T_{d0}^{''}$ (s)	$T_{q0}^{'}$ (s)	$T_{q0}^{''}$ (p.u.)	H (s)	D (p.u.)
1	615	0.000125	3.826	0.0225	0.5084	0.0225	3.41	0
2	60	0.000125	3.826	0.0225	0.5084	0.0225	3.41	0
3	60	0.000125	3.826	0.0225	0.5084	0.0225	3.41	0
6	25	0.000125	3.826	0.0225	0.5084	0.0225	3.41	0
8	25	0.000125	3.826	0.0225	0.5084	0.0225	3.41	0

RSCAD provides various build-in exciter and governor models in its library. In this model, **"IEET1"** exciter model and **"TGOV1"** governor model were utilized. The parameters for those two controllers are shown in Tables A.6 and A.7 :

Table A.6: IEEE 14-Bus Generator Exciter Data.

Generator Bus	T_r	K_a	T_a	V_{max}	V_{min}	K_e	T_e	K_f	T_f
1	0	6.2	0.05	5.2	-4.16	1	0.83	0.057	0.5
2	0	6.2	0.05	5.2	-4.16	1	0.83	0.057	0.5
3	0	6.2	0.05	5.2	-4.16	1	0.83	0.057	0.5
6	0	6.2	0.05	5.2	-4.16	1	0.83	0.057	0.5
8	0	6.2	0.05	5.2	-4.16	1	0.83	0.057	0.5

Table A.7: IEEE 14-Bus Generator Governor Data.

Generator Bus	R	T_1	V_{max}	V_{min}	T_2	T_3	D_t
1	0.05	0.49	15	0	2.1	7	0
2	0.05	0.49	15	0	2.1	7	0

B

System Parameters

In this section of the appendix, the various parameters were used for the simulations which provided the results demonstrated in Chapter 6 are presented. This helps towards reproducibility of the presented results from future researchers.

B.1. Asynchronous Machine

The parameters for the Asynchronous Machine, which was implemented in RSCAD can be seen in Table B.1:

Table B.1: Asynchronous Generator Parameters

Parameter	Value	Unit
Saturation Curve	Linear	-
Sets of Rotor Windings	1	-
Rated Stator Voltage	0.69	kV
Turns Ration (Rotor over Stator)	2.6377	p.u.
Rated MVA	2.2	MVA
Rated Frequency	50	Hz
Stator Resistance	0.00462	p.u.
Stator Leakage Reactance	0.102	p.u.
Unsaturated Magnetizing Reactance	4.348	p.u.
First Cage Rotor Resistance	0.0060	p.u.
First Cage Rotor Leakage Inductance	0.08596	p.u.
Inertia Constant	1.5	MWs/MVA

B.2. Bi-directional DC-DC Converter

The parameters for the Bi-directional DC-DC Converter, which was implemented in RSCAD can be identified in Table B.2:

Table B.2: DC-DC Converter Parameters.

Parameter	Value	Unit
DC Link Voltage	1.49	kV
ESS Voltage	760	V
P_{max}	100	kW
L_{dc}	1.67	mH
C	100	mF
$f_{switching}$	1	kHz

B.3. 3-Winding Transformer

The parameters for the 3-Winding Transformer, which was implemented in RSCAD are demonstrated in Table B.3:

Table B.3: 3-Winding Transformer Parameters

Parameter	Value	Unit
Winding 1 Type	Y	-
Winding 2 Type	Y	-
Winding 3 Type	Y	-
Rated Transformer MVA	2.5	MVA
Base Frequency	50	Hz
Rated Winding 1 RMS Voltage (L-L)	22	kV
Rated Winding 2 RMS Voltage (L-L)	0.69	kV
Rated Winding 3 RMS Voltage (L-L)	0.69	kV
Leakage Reactance (Winding 1 - 2)	0.1	p.u.
Leakage Reactance (Winding 2 - 3)	0.1	p.u.
Leakage Reactance (Winding 3 - 1)	0.1	p.u.
Winding 1 Resistance	0	p.u.
Winding 2 Resistance	0	p.u.
Winding 3 Resistance	0.001	p.u.

C

User Manual

C.1. Introduction

The developed model, represents a 2MW DFIG WT equipped with ESS, interfaced with the DC Link of "Back to Back" converters in RSCAD. The model is consisted of two main parts. The first one includes all the electrical parts, like the induction generator, 3-winding interface transofmer, power electronic converters and the second one includes the control systems. This guide is provided, in order to help future users to identify the parts of the model be capable of running different test cases and scenarios.

In order to run this model, RSCAD 5.0 and an IP connection to an RTDS simulator is mandatory.

C.2. Procedure

The following process has to be followed in order to import the model properly and conduct different studies with RSCAD and RTDS.

C.2.1. Loading the Draft File

For this step, project folder shall be copied into RSCAD's `RTDS_USER/fileman` folder, in order to be accessible from RSCAD's Draft Module. After this the following steps are needed:

- Launch the RSCAD software
- Launch the RSCAD's draft module from the file manager window by double-clicking on the relevant model file with ".dft" extension. The model will load as shown in Figure C.1.
- Choose the desired rack and compile the model.

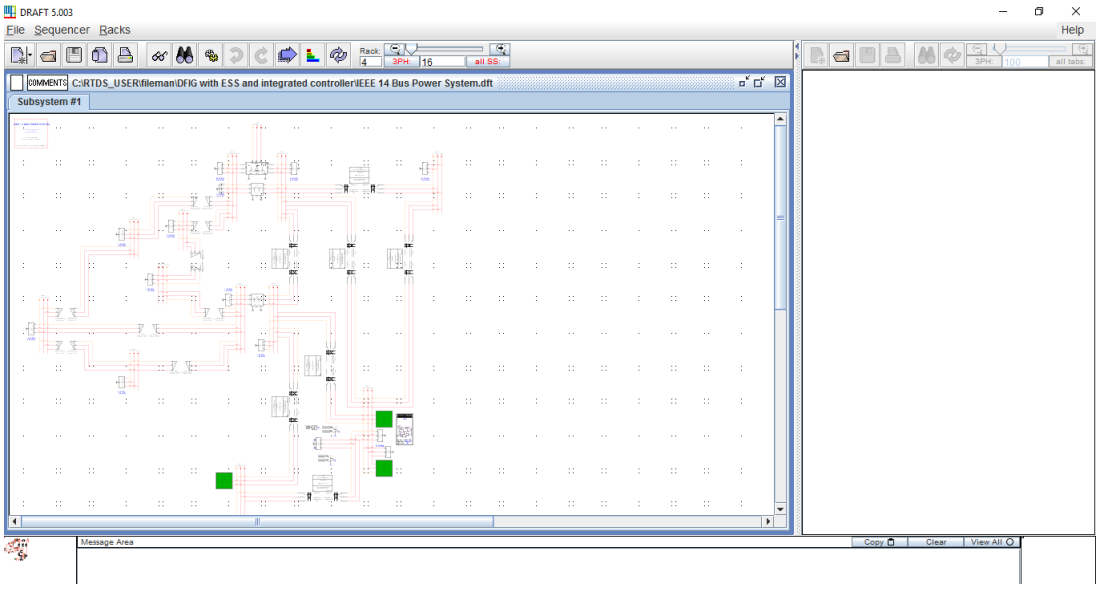

Figure C.1: Benchmark System with WTs in Draft Module.

C.2.2. Running the Simulation

After compiling the model, it is possible to run a real-time simulation and obtain the results. In order to do so, RunTime module is utilized. RunTime module is a complimentary to the Draft module which helps in running the simulation. The different sources and loads can be modified utilizing the sliders and switches in the RunTime module. Moreover, it is also possible to plot different system variables. The RunTime environment is shown in Figure C.2

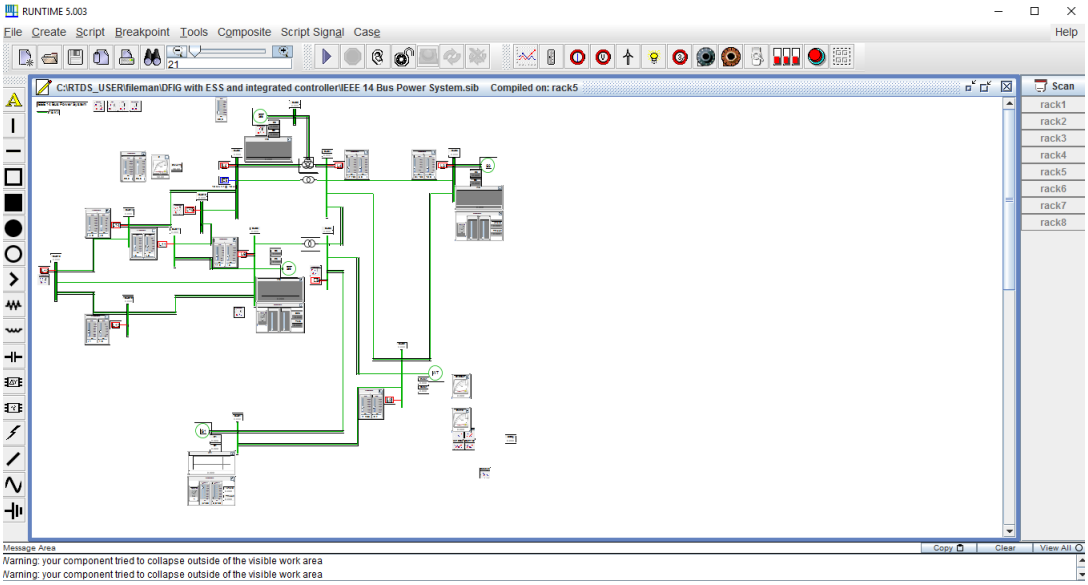

Figure C.2: Model in Rutime Module.

In order to run the desired simulation, it is necessary to open the respective ".sib" file with the RunTime module.

C.2.3. Graphic User Interface

In order to make the model user-friendly, it is necessary to create an interface, which will inform user about the state of the system and the user can change different parameters from it. The GUI can be seen in Figure .

In order to change system's settings, Control Panel It is possible to change the Frequency Control strategy by changing the respective valve. User is immediately informed about the activated control strategy by the indications next to the valve.

Moreover it is also possible to enable and disable the voltage support with the utilization of the respective switch. Again, there is an indication which informs the user if control is enabled or not.

Finally it is possible to change various parameters of the WT and its control system with the help of sliders which are included in the GUI. User is capable of changing the number of the WT, the Wind Speed, the measurement delays and the gains of the controllers. The control Panel GUI can be seen in Figure .

User can find some useful plots about different system's parameters in GUI, as seen in Figure .

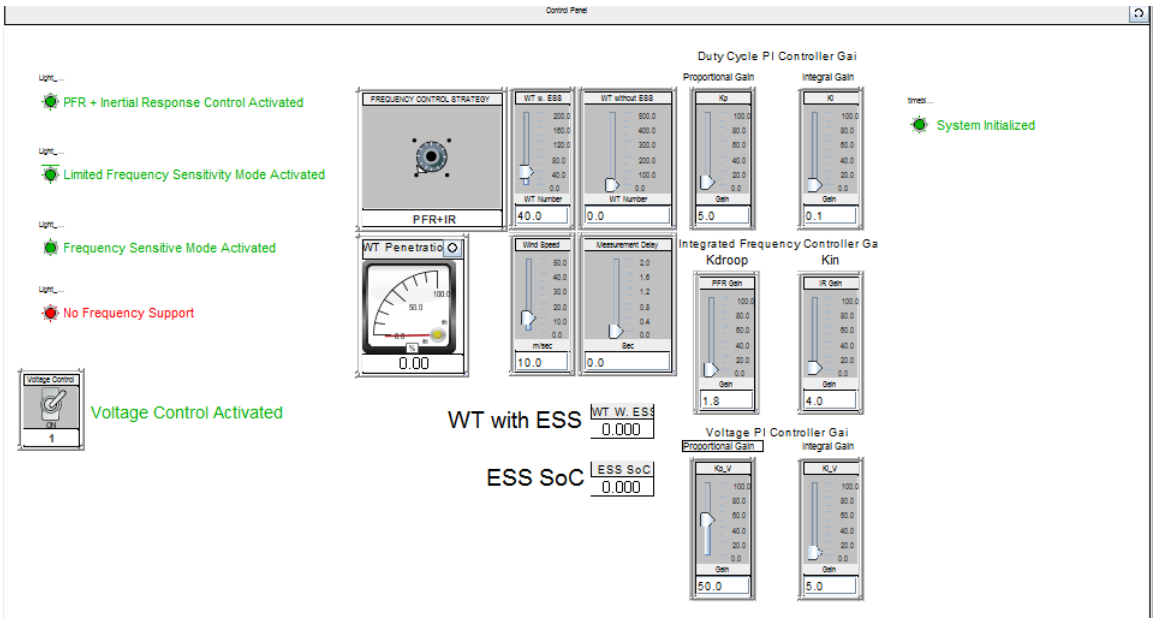

Figure C.3: Control Panel in RunTime Module.

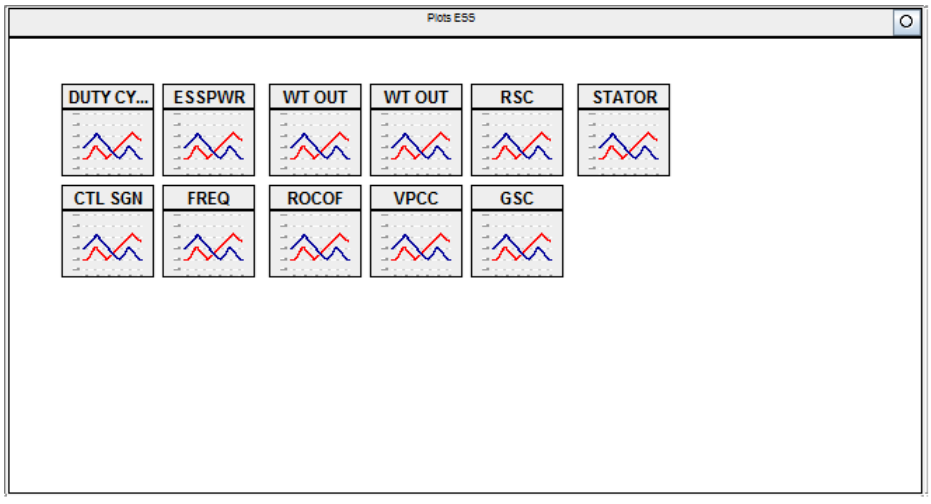

Figure C.4: WT plots in RunTime Module.

D

RTDS Circuit

D.1. Topology

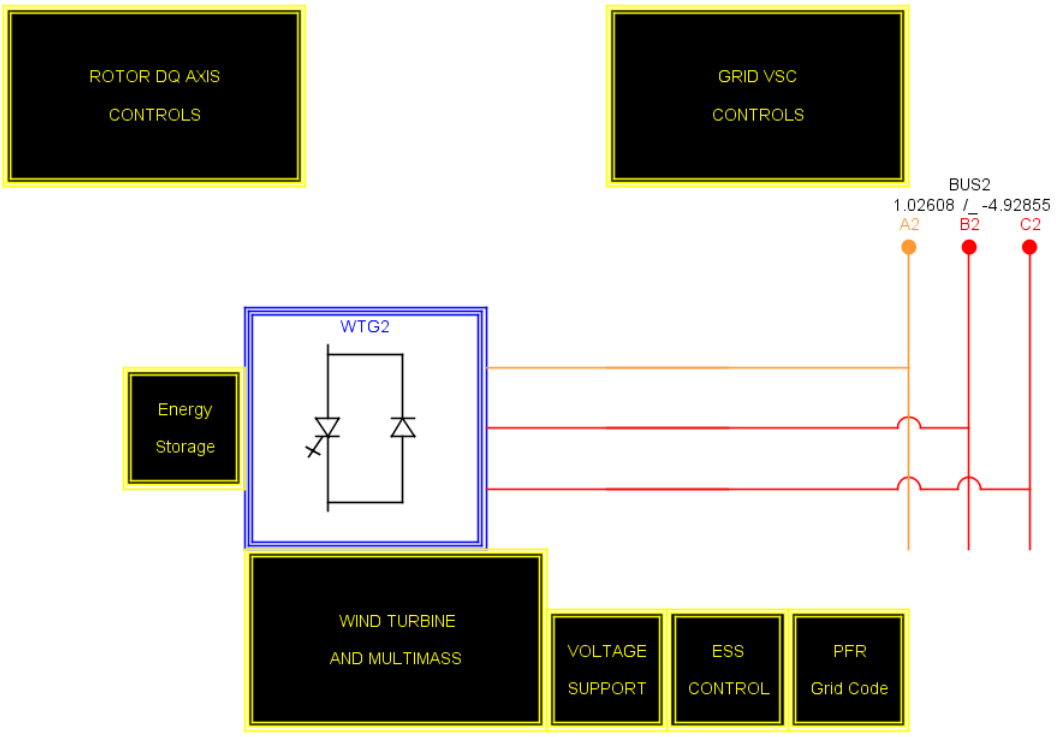

Figure D.1: DFIG with the controller hierarchical boxes connected with the grid model.

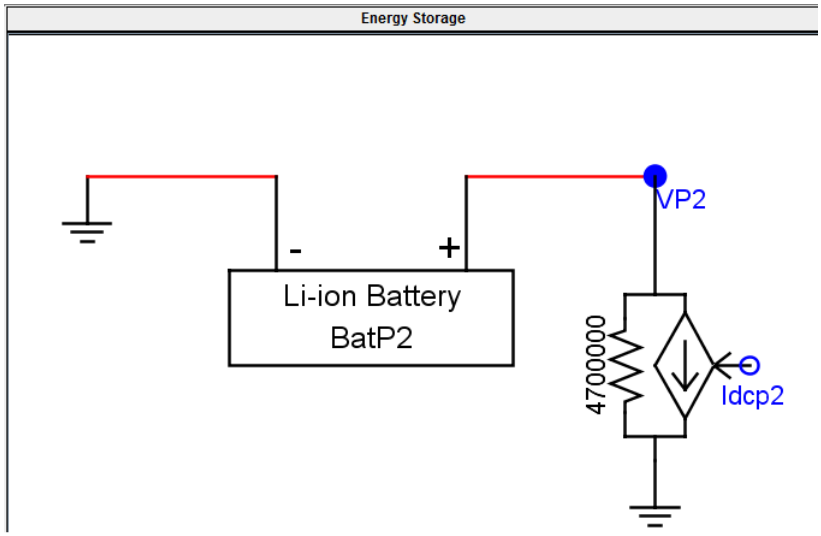

Figure D.2: ESS typical time-step model.

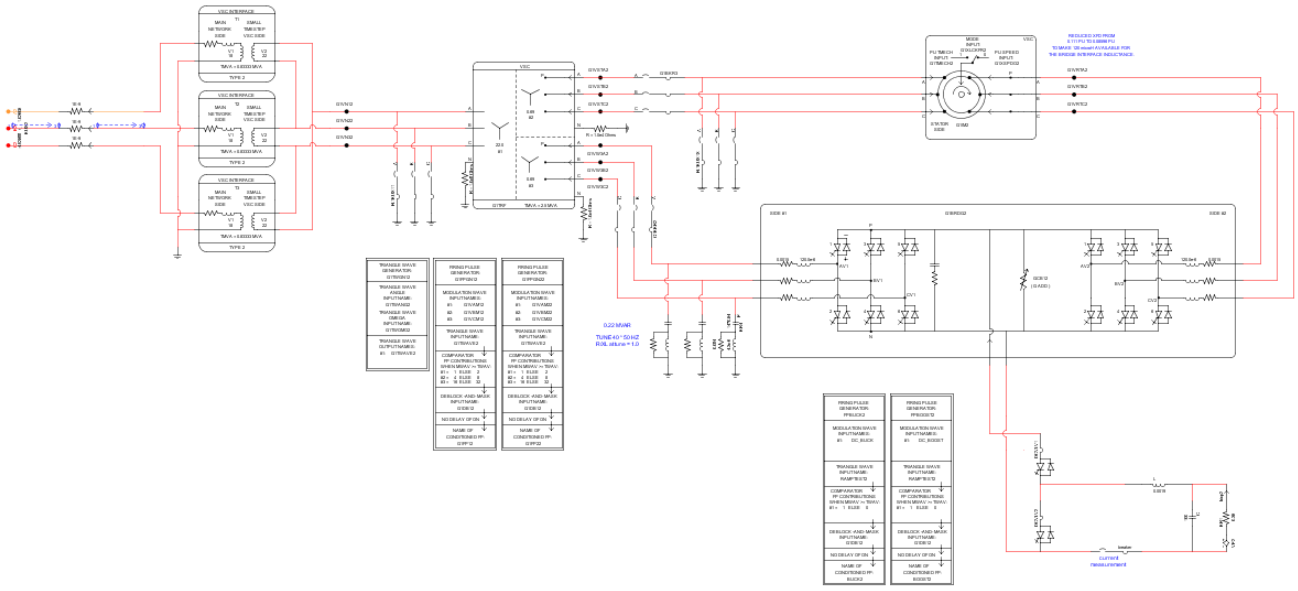

Figure D.3: DFIG small-timestep model.

D.2. Contol Schemes

This section demonstrates the control schemes, as they were implemented in RSCAD software.

D.2.1. Grid Side Converter Control System

In this subsection, the control block diagrams from RSCAD of the GSC are depicted:

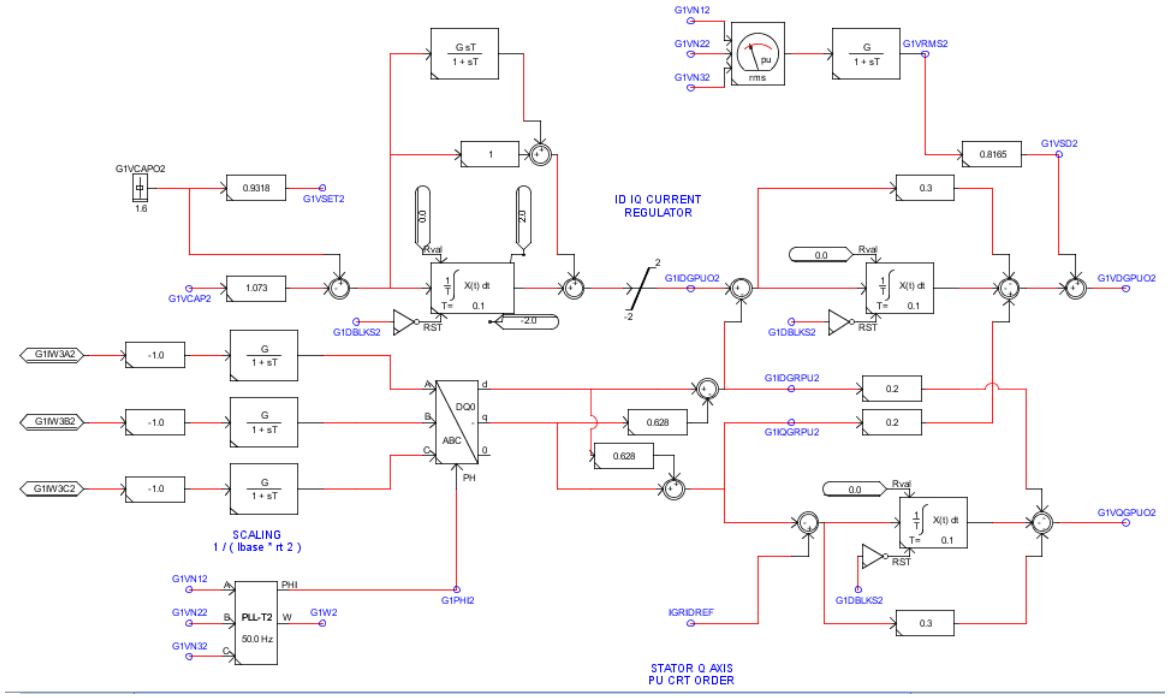

Figure D.4: GSC vector control block diagram.

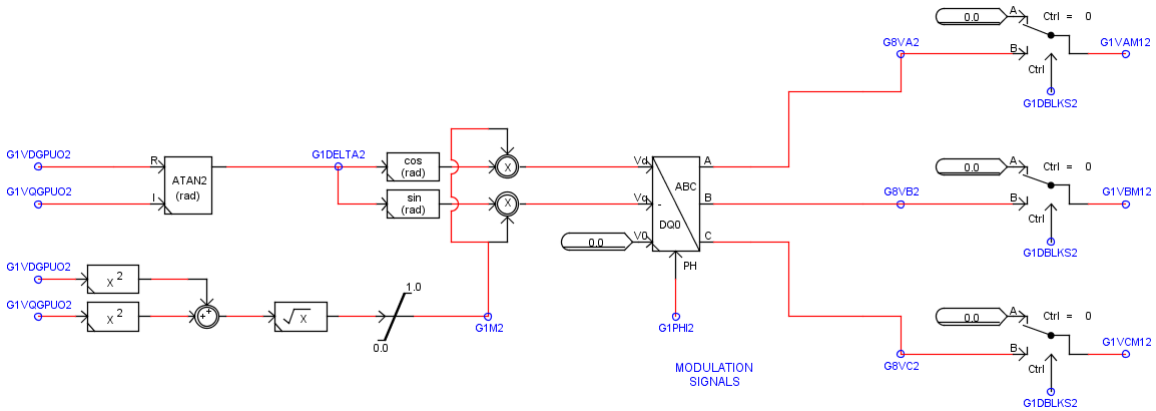

Figure D.5: GSC inverse Park transformation.

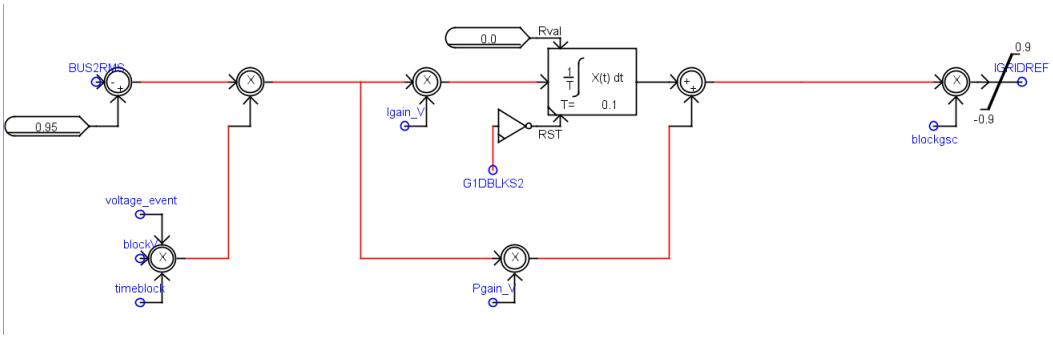

Figure D.6: GSC voltrage control block diagram.

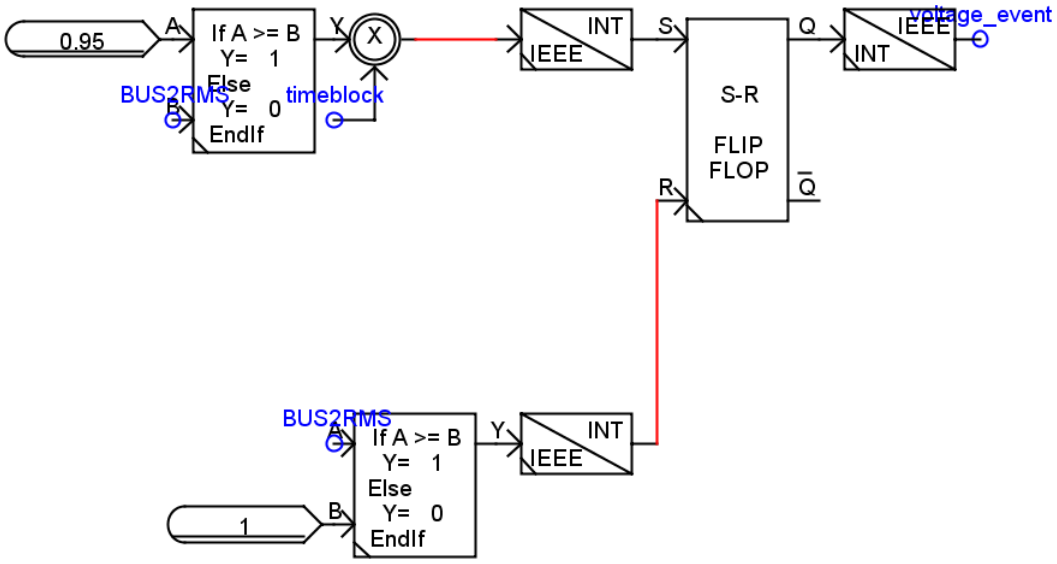

Figure D.7: GSC voltage control enabling logic.

D.2.2. Rotor Side Converter Control System

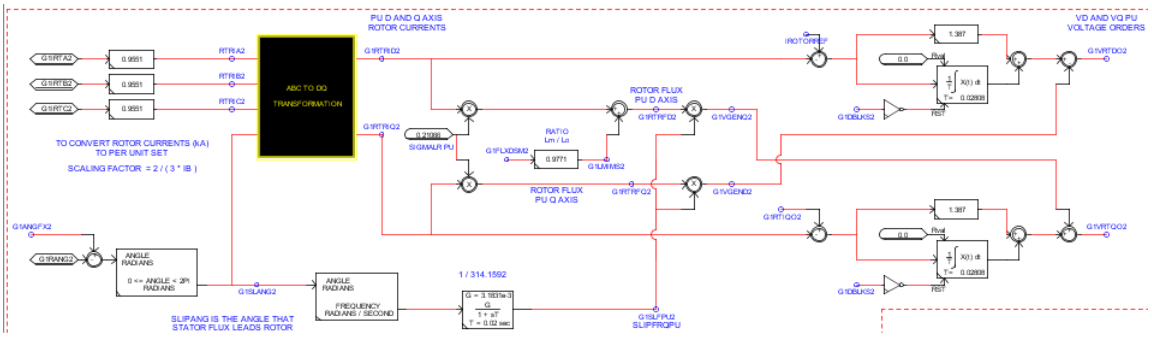

Figure D.8: RSC vector control block diagram.

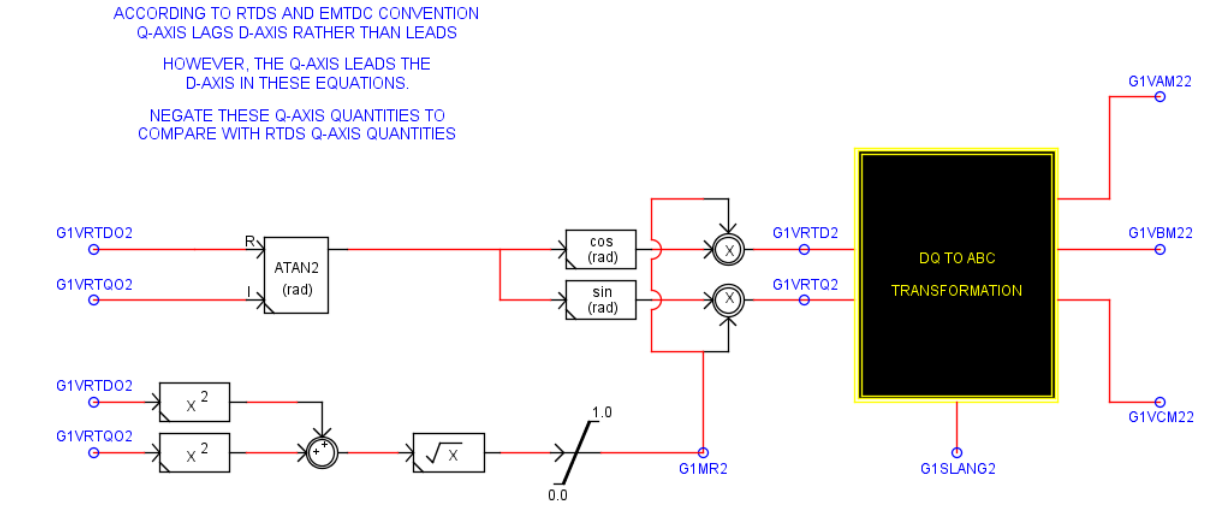

Figure D.9: GSC inverse Park transformation.

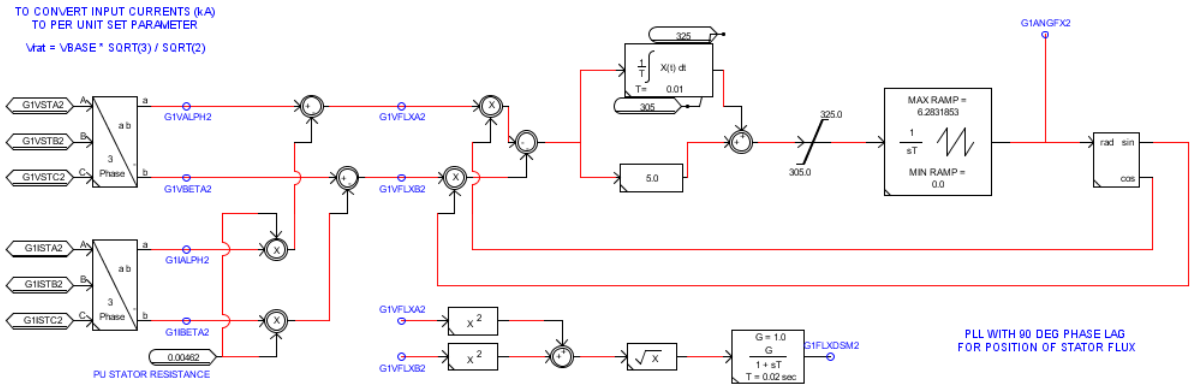

Figure D.10: RSC PLL block diagram

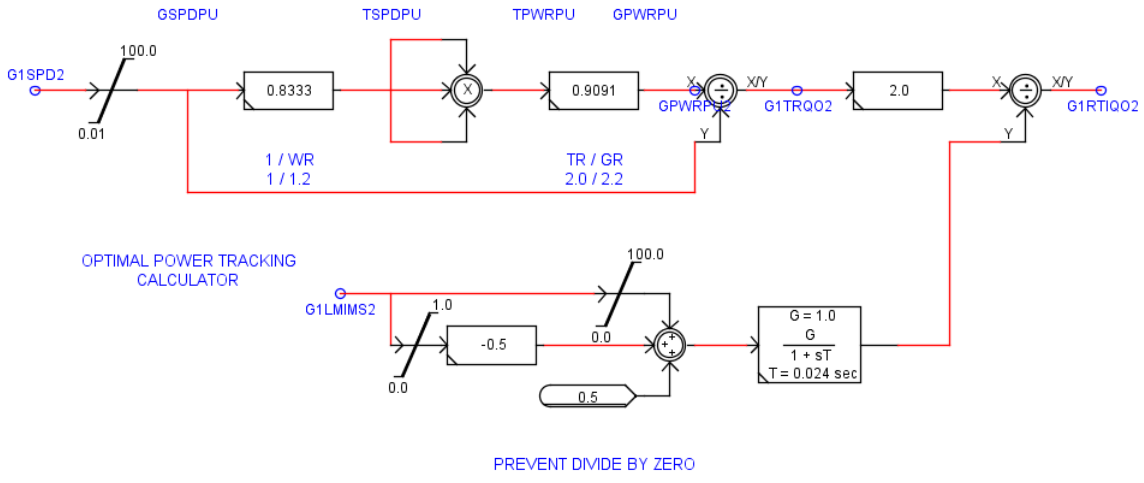

Figure D.11: RSC MPPT block diagram/

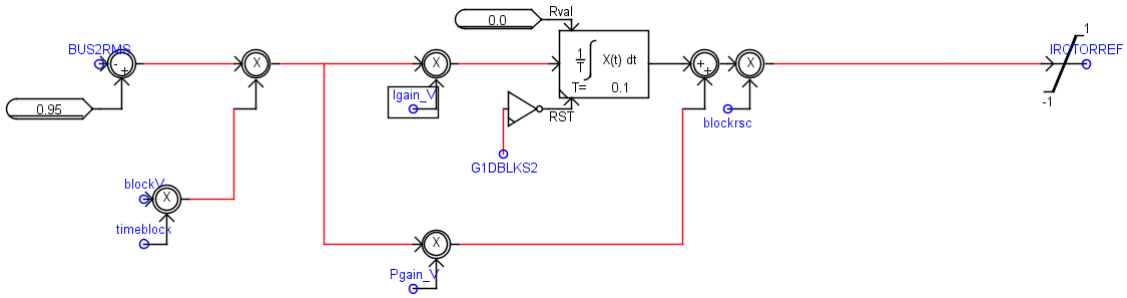

Figure D.12: RSC voltrage control block diagram.

D.2.3. Bi-Directional DC-DC Converter Control System

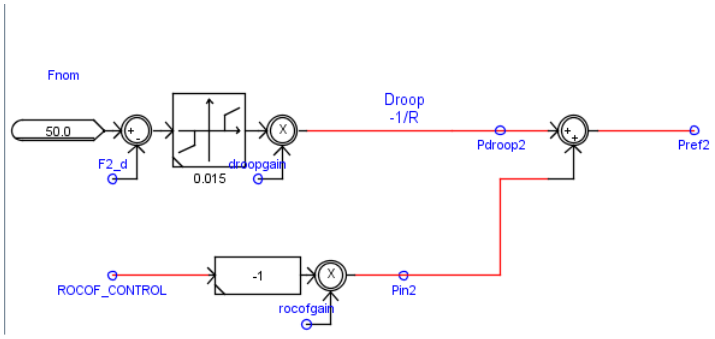

Figure D.13: PFR and Inertial Response integrated controller block diagram.

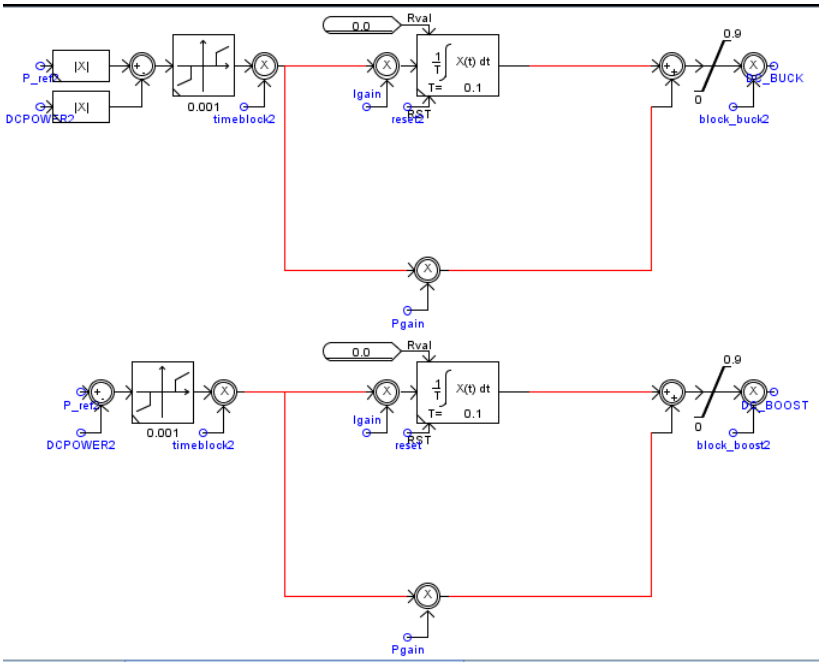

Figure D.14: PI controllers for boost and buck modes of operation.

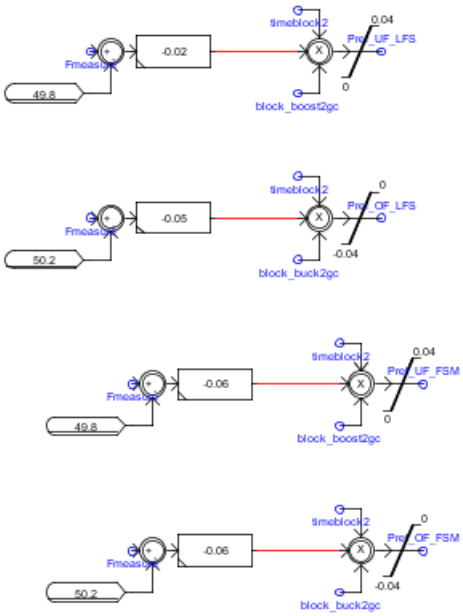

Figure D.15: ESS grid code (FSM,LFSM-U and LFSM-O block diagrams.

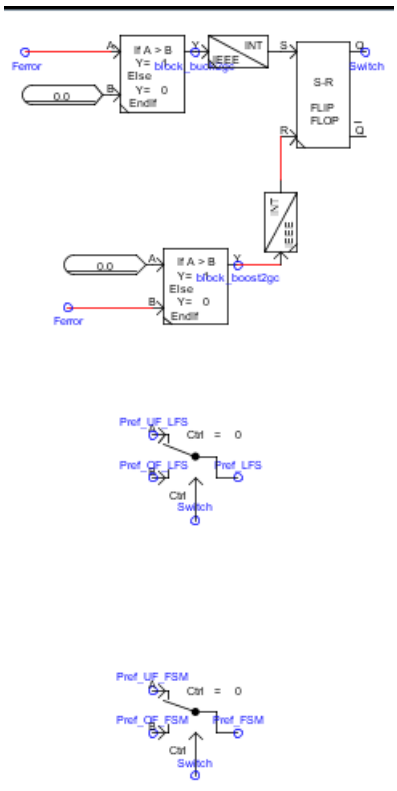

Figure D.16: Control logic block diagram for switching between the different grid code modes.

D.2.4. Measurements and input parameters

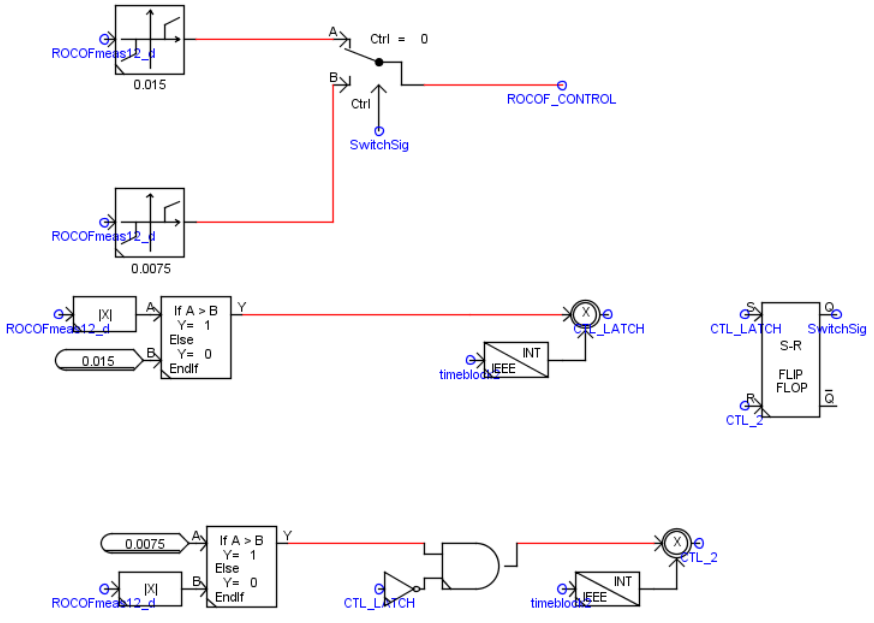

Figure D.17: Control logic block diagram for variable activation and deactivation RoCoF.

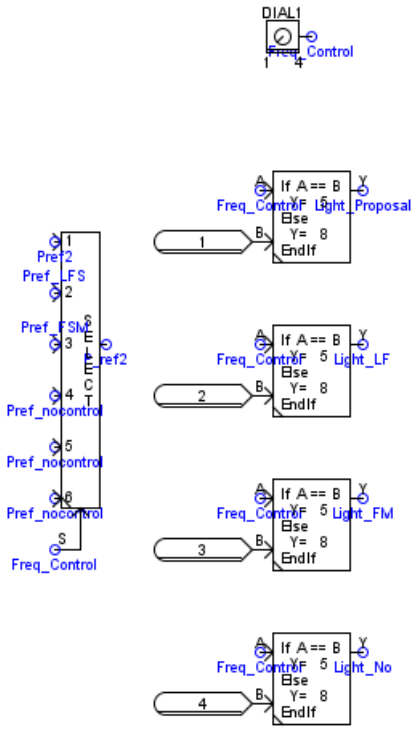

Figure D.18: Control logic block diagram for switching between the different frequency control modes.

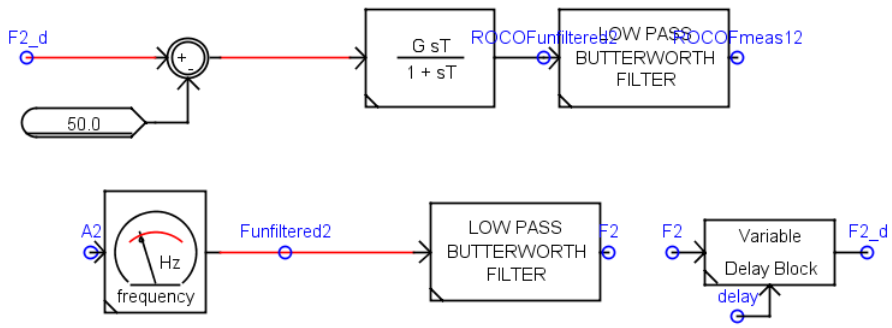

Figure D.19: Frequency and RoCoF measurements in RSCAD.

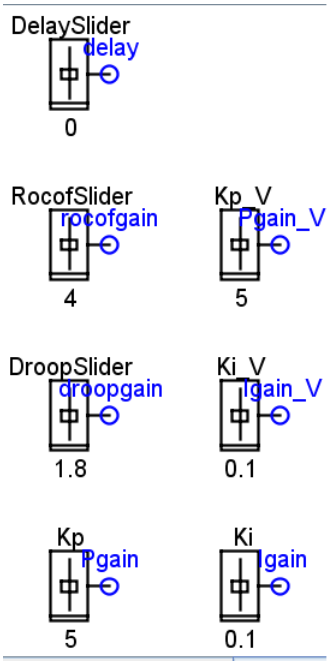

Figure D.20: Sliders for variable control gains in RSCAD.

Bibliography

[1] J. Essletzbichler. Renewable Energy Technology and Path Creation: A Multi-scalar Approach to Energy Transition in the UK. *European Planning Studies*, 20(5):791–816, 2012.

[2] RES21. Renewables 2014. Global status report 2014. Technical report, 2014.

[3] D. Xu, F. Blaabjerg, W. Chen, and N. Zhu. *Advanced Control of Doubly Fed Induction Generator for Wind Power Systems*. John Wiley & Sons, 2018.

[4] S.M Muyeen. *Wind Energy Conversion Systems: Technology and Trends*. Springer, 2012.

[5] ENTSO-E. Rate of change of frequency (ROCOF) withstand capability. ENTSO-E guidance document for national implementation for network codes on grid connection. Technical report, March 2017.

[6] M. Kayikci and J.V Milanovic. Reactive Power Control Strategies for DFIG-Based Plants. *IEEE Transactions on Energy Conversion*, 22(2):389–396, 2007.

[7] J. Van de Vyver, J. De Kooning, B. Meersman, L. Vandevelde, and T. L Vandoorn. Droop Control as an Alternative Inertial Response Strategy for the Synthetic Inertia on Wind Turbines. *IEEE Transactions on Power Systems*, 31(2):1129–1138, 2016.

[8] W. Ziping, G. Wenzhong, G. Tianqi, Y. Weihang, H. Zhang, Y. Shijie, and W. Xiao. State-of-the-art review on frequency response of wind power plants in power systems. *Journal of Modern Power Systems and Clean Energy*, 6(1):1–16, 2018.

[9] L. Chang-Chien, C. Hung, and Y. Yin. Dynamic reserve allocation for system contingency by DFIG wind farms. *IEEE Transactions on Power Systems*, 23(2):729–736, 2008.

[10] J.P Lopes and R. Almeida. Participation of Doubly Fed Induction Wind Generators in System Frequency Regulation. *IEEE Transactions on Power Systems*, 22 (3):944–950, 2007.

[11] H.T Ma, and B.H Chowdhury. Working towards frequency regulation with wind plants: combined control approaches. *IET Renewable Power Generation*, 4(4):308–316, 2010.

[12] A. Žertek, G. Verbič, and M. Pantoš. A Novel Strategy for Variable-Speed Wind Turbines' Participation in Primary Frequency Control. *IEEE Transactions on sustainable energy*, 3(4):791–799, 2012.

[13] A. Žertek, G. Verbič, and M. Pantoš. Optimised control approach for frequency-control contribution of variable speed wind turbines. *IET Renewable Power Generation*, 6(1):17–23, 2012.

[14] D. Wang, H. Wang, J. Jia, and Y. Zhang. Reactive power control of Doubly Fed Induction Generator in wind farm under low grid voltage. In *5th International Conference on Critical Infrastructure (CRIS)*, pages 1–6. IEEE, 2010.

[15] S. Engelhardt, I. Erlich, C. Feltes, J. Kretschmann, and F. Shewarega. Reactive power capability of wind turbines based on Doubly Fed Induction Generators. *IEEE Transactions on Energy Conversion*, 26(1):364–372, 2010.

[16] D.Y.C Leung and Y. Yang. Wind energy development and its environmental impact: A review. *Renewable and sustainable energy reviews*, 16(1):1031–1039, 2012.

[17] M. Pacesila, S.G Burcea, and S.E. Colesca. Analysis of renewable energies in European Union. *Renewable and Sustainable Energy Reviews*, 56:156–170, 2016.

[18] T.J Price. James Blyth—Britain's first modern wind power pioneer. *Wind Engineering*, 29(3): 191–200, 2005.

[19] F. Blaabjerg and K. Ma. Wind Energy Systems. *Proceedings of the IEEE*, 105(11):2116–2131, Nov 2017. ISSN 0018-9219.

[20] Wind Europe. Wind energy in Europe in 2018, trends and statistics. Technical report, 2019.

[21] L.D Kirsch and H. Singh. Pricing ancillary electric power services. *The Electricity Journal*, 8(8): 28–36, 1995.

[22] J. Fletcher and J. Yang. Introduction to the Doubly-Fed Induction Generator for Wind Power Applications. *Paths to Sustainable Energy*, pages 259–278, 2010.

[23] M. Ndreko. *Offshore wind power plants with VSC-HVDC transmission: Grid code compliance optimization and the effect on high voltage ac transmission system*. PhD thesis, Delft University of Technology, 2017.

[24] F. Caricchi, F. Crescimbini, G. Noia, and D. Pirolo. Experimental study of a bidirectional DC-DC Converter for the DC link voltage control and the regenerative braking in pm motor drives devoted to electrical vehicles. In *Proceedings of 1994 IEEE Applied Power Electronics Conference and Exposition-ASPEC'94*, pages 381–386. IEEE, 1994.

[25] H.R. Karshenas, H. Daneshpajooh, A. Safaee, P. Jain, and A.R. Bakhshai. Bidirectional DC-DC converters for energy storage systems. In *Energy Storage in the Emerging Era of Smart Grids*, 2011.

[26] ENTSO-E. Frequency Sensitive Mode. ENTSO-E Guidance document for national implementation for network codes on grid connection. Technical report, November 2017.

[27] ENTSO-E. Limited Frequency Sensitive Mode. ENTSO-E Guidance document for national implementation for network codes on grid connection. Technical report, November 2017.

[28] E. Nycanderand and L. Söder. Review of European Grid Codes for Wind Farms and Their Implications for Wind Power Curtailments. In *17th International Wind Integration Workshop Stockholm Sweden*, 2018.

[29] H. Ali and D. Dasgupta. Effects of time delays in the electric power grid. In *International Conference on Critical Infrastructure Protection*, pages 139–154. Springer, 2012.

[30] Y. Teng, F. Tang, H. Zhang, and L. Ding. Risk of over frequency-overvoltage and its suppression strategies after the separation of small grid in remote areas from the main grid. In *2014 International Conference on Power System Technology*, pages 537–542. IEEE, 2014.

[31] ENTSO-E. Network code for requirements for grid connection applicable to all generators (NG RFG). Technical report, March 2013.